# UNDERSTANDING HOW BACTERIA MANAGE COSTS AND BENEFITS OF COOPERATIVE BEHAVIOR.

A Dissertation

Presented to the Faculty of the Weill Cornell Graduate School

of Medical Sciences

in Partial Fulfillment of the Requirements for the Degree of

Doctor of Philosophy

by

Kerry Eileen Boyle

May 2016

# UNDERSTANDING HOW BACTERIA MANAGE COSTS AND BENEFITS OF COOPERATIVE BEHAVIOR.

Kerry Eileen Boyle, Ph.D.

Cornell University 2016

Cooperation plays a key role in the lives of unicellular and multicellular organisms. However, the molecular mechanisms that stabilize cooperative behavior are still largely unknown. We use a model bacterial system of social behavior to investigate molecular mechanisms that regulate and stabilize cooperative traits. This model system is swarming motility in the opportunistic pathogen, *Pseudomonas aeruginosa*. Using this system in combination with computational techniques and quantitative systems biology approaches we studied the production dynamics of a public good, rhamnolipids.

Through studying the native regulation of rhamnolipids synthesis in the wild-type strain of *P. aeruginosa* we found that quorum sensing signals are integrated with internal metabolic signals in a non-digital manner to determine the level of rhamnolipid synthesis gene expression. Starvation by different nutrients induced radically different expression patterns of the rhamnolipid synthesis operon *rhlAB* suggesting that the internal metabolic state of the cell plays a large role in determining the expression level of this cooperative trait.

To further understand how metabolism affects the stability of cooperative behavior, we used experimental evolution in swarming colonies starting with an engineered metabolic mutant, which lacked the gene Δ*cbrA*. This study revealed that cooperative behavior can be recovered after significant perturbation, but recovery to a stable cooperative state was associated with a metabolic profile distinct from the wild-type.

As a whole this work supports that metabolism is intimately linked with the social behavior of an organism. The quantitative assays, computational models and data from this work provide a foundation for the continued investigation of the link between cooperative traits and metabolism in *P. aeruginosa* and other organisms.

## Biographical Sketch

Kerry Eileen Boyle began her research career as an undergraduate student at the University of California, Berkeley in the College of Natural Resources. In Dr. Richard Stephen's lab she studied the process of chlamydia infection in an in vitro cell culture system. In 2010, Kerry graduated with a Bachelors of Science with honors in Microbial Biology.

After graduation Kerry enrolled in the Immunology and Microbial Pathogenesis PhD program at Weill Cornell Graduate School of Medical Sciences and moved to New York City. There she joined the lab of João Xavier and continued work on dissecting molecular decision-making in a model system of social behavior, swarming in *Pseudomonas aeruginosa*. To further her education in microbial genetics Kerry completed the Advanced Bacterial Genetics course at Cold Spring Harbor in 2012. Kerry authored a paper investigating the integration of multiple signals into the molecular decision to cooperate through rhamnolipid production. In addition to this original research article Kerry also authored a review.

## Acknowledgements

I would like to begin by thanking my husband, Eric Liu, who has been a never-ending source of support throughout this entire process. He has helped me gain invaluable confidence in all of my work and has been my cheerleader, voice of reason and adventure companion over the years. Eric has continually reminded me to have fun and curiosity in life, which has kept my sense of wonder in the laboratory alive. Thank you for never failing to pick me up even when I was determined to stay down.

I would also like to thank my parents James and Patricia Boyle for all of the love and support that they have given me. They have put up with many surprises throughout my scientific journey, which they have nurtured for as long as I can remember. They truly instilled in me the idea that I could do anything and to never give up on searching for answers. I cannot ever repay them for the encouragement they have given me or for the damage I did to their kitchen with 'experiments' when I was growing up. I would like to thank my brother, Robert Boyle. He has been a source of inspiration and the most wonderful example of a dedicated compassionate human being. I know I am a better person and a better scientist because of him. To all of my family, sisters-in-law, parents-in-law, cousins, aunts and uncles, thank you for all of your love and support.

Of course I would not have been able to achieve this without the expertise, mentorship and guidance of my thesis advisor, João Xavier. The diverse and stimulating environment João has created within his lab was a remarkable place to work in as a graduate student. Thank you João, for taking a chance on me as a first year graduate student who didn't even know what Matlab was until I rotated in your lab. João has taught me how to work scientifically and to always care about the details no matter how small. The many conversations I have had with him over the years not only shaped the way I thought about my project, but also the way I think about the world.

Thanks to all of my lab members that I had the great pleasure of working with: Hilary Monaco, for always having my back in and out of lab, bringing my coding to a new level, and never forgetting to grab me a bagel. Dave van Ditmarsch, for many invaluable tips and techniques for working with *Pseudomonas* and for keeping the lab running like clockwork. Carlos Carmona Fontaine, for never failing to make me laugh while simultaneously inspiring me to raise the bar of my scientific work. Laura de Vargas Roditi, for teaching me my very first line of code and for continuing to send support across the Atlantic. William Chang, for always asking the questions that no one else has thought of. Jinyuan Yan, for walking me through whole genome sequencing and for helping me get one of my last experiments working when I was absolutely stuck. Silja Heilmann, for always being game to talk abstractly about bacterial cooperation. Maxime Deforet, for constantly amazing me with what people are capable of creating. Vanni Bucci, for welcoming me to the lab and for being a great travel companion after American Airlines stranded us and João in Philadelphia. And to all of the other members of the Xavier lab and all those who have visited, collaborated or stopped by over the years.

Finally, I would also like to thank the NIH for funding the research that I performed and *Pseudomonas aeruginosa* for being a resourceful bacterium that filled years of research with surprises, frustration and delight.

# TABLE OF CONTENTS

# LIST OF FIGURES

## Chapter 1



## Chapter 2

## Chapter 3

# LIST OF TABLES

## Chapter 1



## Chapter 2



## Chapter 3

# Chapter 1 Introduction

# 1.1 - General Introduction

**Evolution of Cooperation**

Let us consider a population of cells. What will determine if these cells will work together and cooperate or work against each other and compete? If cells within a population are able to cooperate with each other they can achieve population level benefits and access resources that they could not as individuals or resist environmental conditions they would succumb to if acting alone [1-3]. However, cooperation requires the commitment of resources to the population, which has the potential to be costly to individual organisms [4].

Cooperation is of fundamental interest because it is required for the evolution of multicellularity and multicellular organisms [5]. The somatic cells of a multicellular organism coordinate and cooperate in large numbers sometimes across very long distances to form the organs, tissues, and in some cases the immune system of the organism. The somatic cells in a multicellular organism are able to cooperate without conflict, because they are not competing with each other to pass on their DNA. The passing of genes to the next generation is taken care of solely by the germ line cells. For populations of bacterial cells the situation is radically different. A single bacterial cell is the unit of the organism, and is the exact same cell that is going to be competing to pass on its DNA. This situation introduces a fundamental conflict when it comes to cooperation, because now each bacterial cell has to decide whether it is going to commit resources only to producing its own progeny or will it cooperate with other cells in the population but also divert costly resources towards producing shared products that will benefit the population as a whole [3, 6].

Since evolution by natural selection is survival of the fittest, we might assume that we would see bacteria solely devoting resources towards their own survival and reproduction, because diverting any resources towards the population could impair their individual fitness and therefore could never be selected for. Cooperation is indeed under constant threat of exploitation [3, 7, 8]. Cheaters, individuals that use, but do not produce a shared product, do not pay any cost for shared product production and therefore have the potential to exploit a social trait and outcompete cooperators [3, 9]. However, even with the potential hurdles that cooperation faces to be evolutionarily stable, we now greatly appreciate that bacteria spend perhaps the majority of their time in multicellular communities that require individuals to cooperate [10]. In recent decades microbiology has undergone a large shift from thinking about bacteria as freestanding individuals to members of social communities [11]. In addition to opening the door for understanding fundamental aspects of social behavior, microbial social traits and communities have also been shown to be incredibly important for understanding bacterial virulence and environmental survival [1, 10, 12].

Bacteria have clearly found a way to resolve the conflict between self-interest and population interest and are able to cooperate in an evolutionarily stable manner, but what mechanisms stabilize bacterial cooperation? Formal theory on cooperation has been extensively developed, originally to explain animal social behavior. Kin selection theory was developed by W. D. Hamilton to describe the genetic basis for the existence of altruism among social insects [4]. In altruism, one individual performs a behavior that benefits another at a cost or no benefit to itself. Hamilton's theory proposed that related individuals cooperate with one another because of their shared genes. For example, a parental altruistic behavior towards its offspring is evolutionarily favored because the parent is in fact helping his or her own genes to be passed on. However, Hamilton went

further to state that the relationship between kin is not a unique one, only one that has a high degree of close relatedness [4] and therefore a higher chance of having cooperative genes in common compared to the rest of the population. Therefore this formal theory on social behavior and the stability of cooperation can be applied to any social behavior. A key rule from this theory that predicts when cooperation will be favored is Hamilton's rule:

$$br > c$$

Where $c$ is the fitness cost to the actor, $b$ is the fitness benefit to the recipient and $r$ is the correlation between the genotypes of actors and recipients, also called relatedness. It is important to note that fitness here is the increase of gene frequency within the population [4]. If the benefit and relatedness outweigh the costs then cooperation will be favored. Conversely selfish behaviors can always be selected for given a low enough relatedness, which happens for example when cheaters and cooperators are highly intermixed and there is no mechanism for kin discrimination. In higher organisms Hamilton's rule can be satisfied by increasing the amount of relatedness between the individuals receiving benefit. Social insects such as ants or honeybees live in colonies where the individuals of a community are able to stay in very close proximity, making the relatedness of the community very high. Thus when a worker bee is helping a queen produce more progeny they are helping to pass on more of their own genes [13]. For bacteria, horizontal gene transfer, high mutations rates, and environmental mixing make it difficult for individuals to ensure that they will remain with their progeny in the long-term and decreases the ability of bacteria to satisfying Hamilton's rule through high relatedness.

**Bacterial social traits**

Although bacteria are not able to ensure high relatedness within a population, they can determine how much a behavior costs through molecular regulation. Behaviors that benefit the actor and the recipient, termed mutualistic behaviors, can be selected for, even between species, if the behavior carries no energetic cost [14]. Regulatory strategies that reduce the cost of a social behavior offer a direct method for bacterial genes to stabilize cooperation [15].

These regulatory systems that reduce cooperation costs in bacteria are fundamentally interesting as they give us a window into understanding how cooperation among unicellular organisms led to the evolution of multicellularity [5]. In addition to understanding evolutionary principles and the development of multicellularity, the study of bacterial social behavior also provides a novel way to disrupt bacterial populations in medical settings such as infections or industrial settings such as bio fouling. Current antibiotic treatments target individual cells, which rapidly selects for resistance to the antibiotic [16]. Targeting social traits rather than individual cells is predicted to be a more stable antibiotic method [1, 12] and since social traits are known to be key to bacterial survival and virulence [12, 17] these social "antibiotics" could be quite effective.

In the following chapters of this thesis the native regulation of shared product in wild-type *Pseudomonas aeruginosa*, an opportunistic pathogen is quantitatively analyzed and this data is then used to parameterize a mathematical model of growth and shared product gene expression. By studying the regulation of social traits we can begin to understand what molecular inputs are required to make molecular decisions that stabilize cooperation. Social trait regulation is studied further by analyzing the recovery of stable regulation after significant metabolic perturbation. This recovery is seen through experimental

evolution allowing us to gain insight into the recovery of social trait regulation across evolutionary time scales. Together this work can allow us to identify components of these molecular decision making processes and learn about the fundamental stability of cooperative behavior.

## References


1. Foster, K.R., *Hamiltonian Medicine-Why the Social Lives of Pathogens Matter.* Science, 2005. **308**: p. 1269-1270.
2. Hoiby, N., et al., *Antibiotic resistance of bacterial biofilms.* Int J Antimicrob Agents, 2010. **35**(4): p. 322-32.
3. West, S.A., et al., *Social evolution theory for microorganisms.* Nat Rev Microbiol, 2006. **4**(8): p. 597-607.
4. Hamilton, W.D., *The Genetical Evolution of Social Behavior. I.* Journal of Theoretical Biology, 1964. **7**: p. 1-16.
5. Smith, J., *The major transitions in evolution*. 1997: Oxford University Press.
6. Nadell, C.D., et al., *Cutting through the complexity of cell collectives.* Proc Biol Sci, 2013. **280**(1755): p. 20122770.
7. Régis Ferriere, J.L.B., Sergio Rinaldi, Richard Law, Mathias Gauduchon, *Cheating and the evolutionary stability of mutualisms.* Proceedings of the Royal Society B, 2002.
8. Strassmann, J.E. and D.C. Queller, *Evolution of cooperation and control of cheating in a social microbe.* Proc Natl Acad Sci U S A, 2011. **108 Suppl 2**: p. 10855-62.
9. Foster, K.R., K. Parkinson, and C.R. Thompson, *What can microbial genetics teach sociobiology?* Trends Genet, 2007. **23**(2): p. 74-80.
10. J. W. Costerton, P.S.S., E. P. Greenberg, *Bacterial Biofilms: A Common Cause of Persistent Infections.* Science, 1999. **284**(1318-1322).
11. Greenberg, E., *Sociomicrobiology: a personal perspective on an emerging research area.* Microbe Mag, 2010. **ASC**.
12. Rutherford, S.T. and B.L. Bassler, *Bacterial quorum sensing: its role in virulence and possibilities for its control.* Cold Spring Harb Perspect Med, 2012. **2**(11).
13. Hamilton, W.D., *Altruism and related phenomena, mainly in social insects.* Annu. Rev. Ecol. Syst., 1972. **3**: p. 193–232.
14. Connor, R.C., *Pseudo-reciprocity: Investing in Mutualism*. Animal Behavior, 1986. **34**: p. 1562-1584.
15. Xavier, J.B., W. Kim, and K.R. Foster, *A molecular mechanism that stabilizes cooperative secretions in Pseudomonas aeruginosa.* Mol Microbiol, 2011. **79**(1): p. 166-79.

16. Davies, J. and D. Davies, *Origins and evolution of antibiotic resistance.* Microbiol Mol Biol Rev, 2010. **74**(3): p. 417-33.
17. West, S.A. and A. Buckling, *Cooperation, virulence and siderophore production in bacterial parasites.* Proc Biol Sci, 2003. **270**(1510): p. 37-44.

# 1.2 - Exploiting social evolution in biofilms*

*Published as: K. E. Boyle, S. Heilmann, D. van Ditmarsch and J. B. Xavier (2013). "Exploiting social evolution in biofilms." Curr Opin Microbiol **16**(2): 207-212.

**Abstract**

Bacteria are highly social organisms that communicate via signaling molecules, move collectively over surfaces and make biofilm communities. Nonetheless, our main line of defense against pathogenic bacteria consists of antibiotics–drugs that target individual-level traits of bacterial cells and thus, regrettably, select for resistance against their own action. A possible solution lies in targeting the mechanisms by which bacteria interact with each other within biofilms. The emerging field of microbial social evolution combines molecular microbiology with evolutionary theory to dissect the molecular mechanisms and the evolutionary pressures underpinning bacterial sociality. This exciting new research can ultimately lead to new therapies against biofilm infections that exploit evolutionary cheating or the trade-off between biofilm formation and dispersal.

**Introduction**

The past few decades have witnessed a major change in the way microbiologists view bacteria. Rather than being solitary organisms, many bacteria live in biofilm communities, share nutrient scavenging molecules, communicate by cell–cell signaling, form fruiting bodies and migrate collectively by swarming motility (Figure 1.1). Biofilms, in particular, may be the norm rather than the exception: an often cited number is that 60% of all human bacterial infections involve biofilms [1]. Even though our view of bacteria has undergone a dramatic change [2], the concepts of microbial sociality have only in rare instances been translated into therapies. Antibiotics, which are nonetheless our main line of defense against infectious bacteria, target individual-level traits such as cell wall

assembly or DNA replication and therefore select for resistance against their own action [3] (Figure 1.2A). In contrast, innovative therapeutics that disrupt population level traits such as quorum sensing [4] or phage-based therapies that disperse biofilms [5,6] can potentially be used to reduce virulence while avoiding selection for resistance. Here we discuss recent results in the field of microbial social evolution and how this emerging field can open up new therapeutic avenues against biofilm related infections. We focus on the opportunistic pathogen *Pseudomonas aeruginosa*, a well-known biofilm pathogen. The principles of social evolution are general and they should be applicable to all biofilm-forming microbes as well as other microbial social traits [7–9].

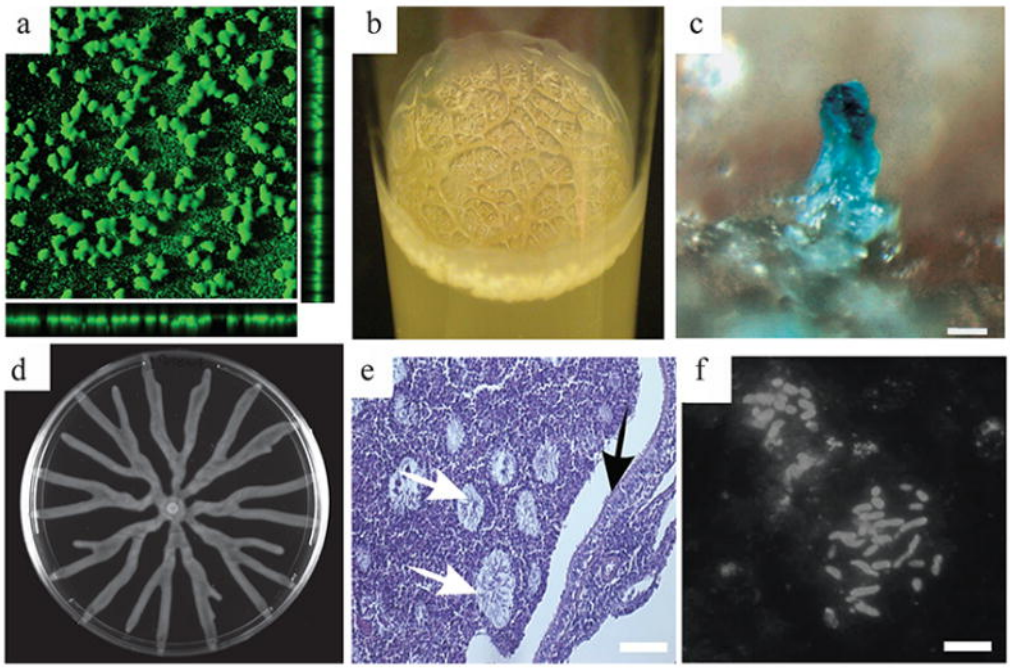


**Figure 1.1 Microbial social traits.**

(A) Vibrio cholera wild type rugose biofilm (10x magnification). (B) V. cholera wild type rugose pellicle (a and b images contributed by Yildiz laboratory, UC Santa Cruz). (C) A fruiting body in Bacillus subtilis (reprinted with permission from [37]). (D) A Pseudomonas aeruginosa swarming colony (9 cm wide). (E) P. aeruginosa macrocolonies in obstructed cystic fibrosis bronchus (reprinted with permission from [38]). (F) Cystic fibrosis lung P. aeruginosa macrocolonies stained with antibodies against P. aeruginosa (reprinted with permission from [38]) (scale: c — 50mm, e — 100mm, f — 10mm).

**Public good cooperation**

*P. aeruginosa* is a gram-negative bacterium notorious for causing diverse infections in multiple anatomic niches, including wounds, chronic lung infections in cystic fibrosis, septicemia, bacterial keratitis and urinary tract infections. This opportunistic pathogen is also a highly social organism. *P. aeruginosa* lives in close interaction with microbial strains of the same and other species and is becoming a model system for microbial social evolution. Much of the social activity of *P. aeruginosa* involves cooperation through the secretion of public goods. 'Public good' is an umbrella term used in the microbial social evolution literature to refer to a resource, such as a secondary metabolite, that is secreted by bacteria and becomes publically available to other cells within a population [8]. Many public goods are costly to produce, making them susceptible to exploitation by cheater strains that benefit from the public good without producing it themselves. For example, the siderophores of *P. aeruginosa* are iron-scavenging molecules that are costly to produce but are necessary for colonization of iron-limited environments such as eukaryotic tissues [10,11]. The potential for cheater exploitation makes public good production an attractive target for therapies that select against resistance. The prediction on the basis of social evolutionary theory is that in contrast to antibiotic-resistant mutants, mutants that resist a drug to prevent public good production would not be favored by natural selection. Because drug-sensitive bacteria would get a small initial growth advantage due to not producing costly public goods when the drug is present, drug-sensitive cheaters would eventually outcompete the drug-resistant producers. In the case of siderophores, a cheater population would be weakened without iron and more easily cleared by the host (Figure 1.2B). This conceptual example illustrates how a drug targeting a microbial social trait may succeed where antibiotics fail by enabling cheaters to outcompete more virulent strains.

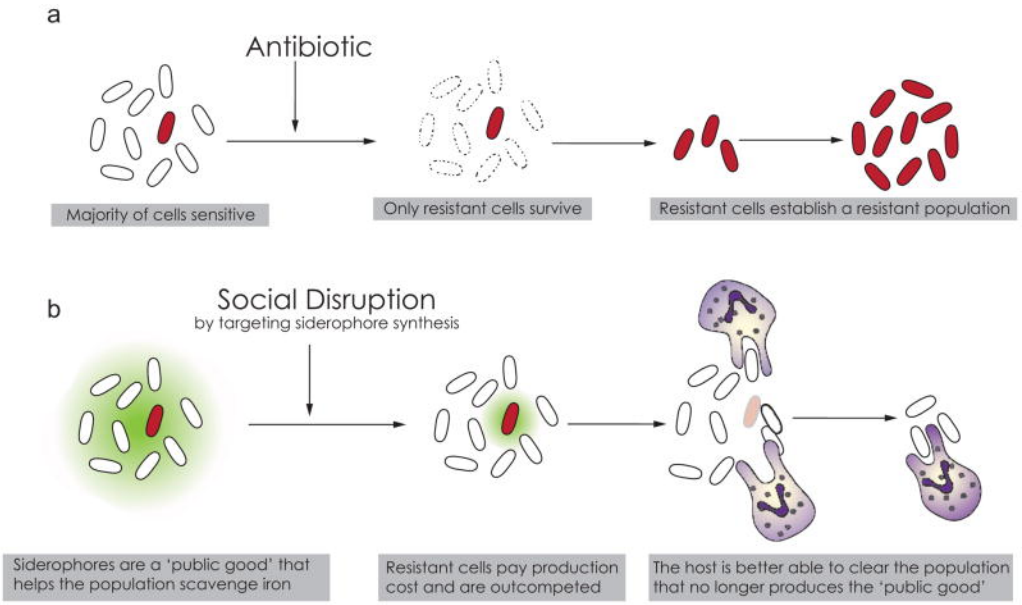


**Figure 1.2 Antibiotics versus social disruption.**

Traditional antibiotic approaches (A) are prone to emergence of resistance. Strategies on the basis of social evolutionary theory (B) can shift selection away from resistance allowing the immune system to clear the weakened infection.

However, the reality can be more complex. For example, social evolutionary experiments have shown that less virulent quorum sensing signal-blind mutants, which do not produce a range of public goods, outcompete virulent *P. aeruginosa* strains in vitro [12–14]. The selective advantage may explain why signal-blind mutants are often found in long-term chronic cystic fibrosis infections [15] and suggests that quorum sensing inhibitors would be a suitable therapy targeting population-level traits [13]. Nevertheless, another recent study tested a quorum sensing inhibitor in patients and the results were quite the opposite: instead of attenuating the *P. aeruginosa* infection the quorum sensing inhibitor aggravated infection by decreasing the relative advantage of cheaters [16]. The exact selective pressures involved in social disruptions should be thoroughly investigated.

**Social evolution in biofilms**

Biofilms are a continuing problem in the clinic because biofilm bacteria are often more robust against antibiotic and metabolic stresses than planktonic bacteria [17]. Biofilm formation is itself a social trait that requires the production and secretion of shared substances. For example, extracellular polymeric substances, (EPS) that encase bacteria in biofilms [18] are shared products, which, like siderophores, are potentially available to neighboring cells after they have been secreted. Unlike siderophores EPS production seems not to be exploited by cheaters. A mechanism for this protection was recently proposed on the basis of computer simulations that modeled the dynamics of EPS production and nutrient diffusion in biofilms [19]. The model showed that even when EPS-producers pay a large cost of EPS production, EPS producers are capable of outcompeting EPS non-producers in the same biofilm. EPS-producers are able to overcome their growth disadvantage because daughter cells of EPS-producers (unlike daughter cells of non producers) are pushed up above the focal cell in the EPS matrix, allowing the EPS-producer cells to access superior nutrient conditions such as higher oxygen levels. As the cells grow, divide and secrete EPS, EPS-producers form high, tower-like structures within the biofilm, smothering the neighboring non-producer cells, which remain close to the substrate (Figure 1.3).

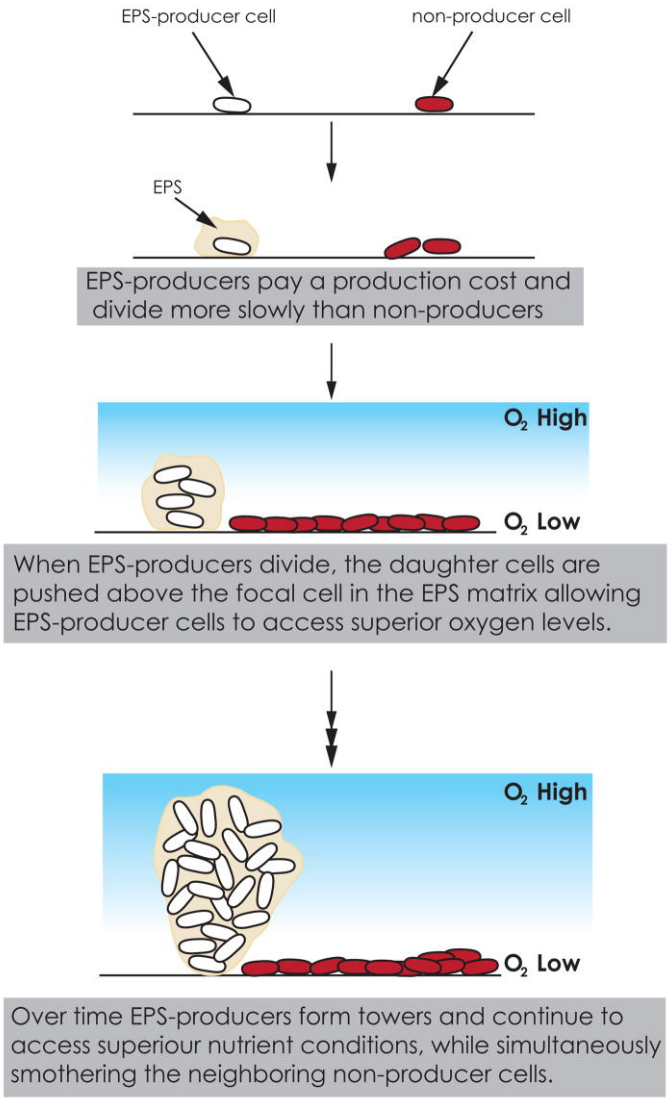


**Figure 1.3 EPS-producers in biofilm competition with non-producers.**

Even when EPS-producers have a significantly slower growth rate than non- producers because of costly EPS production, they are able to win in direct competitions with non-producers due to their ability to access superior nutrient conditions [19,21].

Nutrient limitation is key to the EPS-producer advantage. In simulations where there is no nutrient gradient, the non-producers win due to their higher growth rate. However, conditions without nutrient gradients are unrealistic as nutrients are transported into the biofilm by diffusion, which can be a slow process compared with the fast rates of nutrient uptake by bacteria [20]. As a consequence, biofilm bacteria rarely grow in conditions where nutrients or oxygen levels are non-limiting. In realistic conditions, EPS-producers are able to overcome the cost of production and outcompete cheaters by their ability to take a more advantageous location within the biofilm [19]. While the computer simulations were originally conducted with *P. aeruginosa* in mind [19], the proposed role of EPS in the competition between cell lineages within a biofilm was confirmed by experiments in *Vibrio cholerae* [21]. In these experiments, the EPS-producers (Δ*flaA*Δ*hapR*) were more competitive and increased in population fraction during the course of co-culture competitions with non-producers (Δ*flaA*Δ*hapR*Δ*vpsL*), even though EPS producers pay a substantial production cost and have a slower maximum growth rate compared to non-producers. As seen in the in silico study, *V. cholerae* EPS-producers formed high towers in the biofilm while the non-producers remained in a flat layer [21]. Taken together, these studies demonstrate the importance of social interaction for the success of bacterial strains in a community and illustrate that rather than being the result of a purely cooperative process, the formation of complex biofilms can involve a balance between cooperative and competitive interactions [22]. Another recent study investigated the role of quorum sensing cheaters on *P. aeruginosa* biofilm stability. The experimentalists demonstrated that cheaters reduce the overall productivity of a biofilm and render biofilms more susceptible to antibiotics [23 ]. Importantly, the effects of cheaters were more severe in biofilms than in planktonic populations, suggesting that biofilm infections are particularly susceptible to social disruption strategies. With both competitive and cooperative traits playing important roles for biofilm stability, the next question is which social traits are appropriate targets for biofilm disruption therapies.

**Inducing biofilm dispersal**

Inducing dispersal of unwanted biofilms is an appealing strategy [17,24]. However, the use of extrinsic detachment promoting agents can be limited by a slow diffusion of the agent into the biofilm [25]. An alternative is to manipulate the bacterial regulatory mechanisms for different modes of growth to make bacteria less successful at forming biofilms or even disperse established biofilms. In *P. aeruginosa*, biofilm formation and motility behaviors are inversely regulated [26,27]. The *sad* genes, chemotaxis genes and intracellular c-di-GMP levels have been shown to play roles in this inverse relationship between biofilms and motility [27]. As more molecular mechanisms are uncovered (Table 1.1), such systems could be manipulated to direct cells away from forming a stable biofilm. *P. aeruginosa* produces rhamnolipid biosurfactants that promote detachment of its own biofilms [28]. The ability to secrete the right amount of rhamnolipids is crucial for proper biofilm architecture and stability. Therefore, strains that overproduce rhamnolipids are deficient in biofilm formation, forming thin, flat biofilms compared to the wild type's voluminous towers. Artificially induced production of rhamnolipids, on the other hand, leads to detachment of cells within the biofilm [28]. Rhamnolipid-induced dispersal is not limited to *P. aeruginosa* making these biosurfactants appealing candidates for dispersal of multi-species biofilms in both medical and industrial settings [29]. Rhamnolipid secretion has the potential to induce biofilm dispersal in vivo and make bacteria more vulnerable to clearing by the host or by traditional antibiotics. Here, again, proper caution must be taken. The rhamnolipids of *P. aeruginosa* have detrimental effects on eukaryotic cells, lysing red blood cells and causing necrotic cell death in polymorphonuclear leukocytes (PMNs) and macrophages [30]. This function may have an important role in protecting biofilms from the host immune cells such as PMNs, which are critical to clearing *P. aeruginosa* in vivo [31]. Biofilms of rhamnolipid-deficient

strains cause significantly less necrosis in PMNs [30]. Additionally, experiments using implants colonized by *P. aeruginosa* in mice showed that robust implant colonization requires biosurfactant production [31,32]. Rhamnolipid deficient strains can be phagocytosed and cleared by predating PMNs, thereby failing to form biofilms comparable to those of wild type rhamnolipid-producing strains. The role of *P. aeruginosa* rhamnolipids is therefore multifactorial and their use as a therapeutic target requires further investigation.

**Table 1.1 Examples of intrinsic mechanisms for dispersal of bacterial biofilms**

| | |
|---|---|
| *Bacillus subtilis* — D-amino acids | D-Amino acids naturally produced by *B. subtillis* induce biofilm dispersal by inducing release of amyloid fibers from cells within the biofilm [39]. |
| *Pseudomonas aeruginosa* — rhamnolipids | Rhamnolipid biosurfactants naturally produced by *P. aeruginosa* induce detachment of *P. aeruginosa* cells from the biofilm and disperse biofilms of other species [ 28 and 29]. |
| *Staphylococcus aureus* — extracellular proteases | Extracellular proteases regulated by the *S. aureus* agr quorum sensing system mediate detachment of mature biofilms. Dispersed cells have increased sensitivity to antibiotic treatment [40]. |
| Bacteriophage engineered delivery of dispersal enzymes | Biofilms of *E. coli* can be dispersed by expression of the active biofilm-degrading enzyme, Dispersin B, introduced by an engineered bacteriophage [6]. |

Rhamnolipid-targeting drugs may take advantage of a complex transcriptional regulation of rhamnolipid synthesis that integrates metabolic and quorum sensing signals. Rhamnolipids are produced by the action of three sequentially functioning enzymes: RhlA, RhlB and RhlC [33]. RhlA is required for any rhamnolipid synthesis in the cell and catalyzes the initial conversion of b-hydroxyacylACP to 3-(3-hydroxyalkanoyloxy) alconoic acids (HAAs) [34]. After this conversion, RhlB and RhlC are sequentially required to add rhamnose units, producing mono-rhamnolipid and di-rhamnolipids, respectively. Quorum sensing signals are necessary but not sufficient for the expression

of the *rhlAB* operon, the rate-controlling step for rhamnolipid production. New studies suggest that bacteria require excess carbon in addition to quorum sensing signals to trigger the synthesis of rhamnolipids [35]. Thus, the bacterial cells carry out an integration of metabolic and quorum sensing signals in order to initiate rhamnolipid production (Figure 1.4). The mechanism of metabolic and quorum sensing integration is called metabolic prudence, since it prevents wild type strains from being outcompeted by cheaters even though rhamnolipid production requires significant metabolic resources [35 ,36]. Through metabolic prudence, rhamnolipid synthesis is delayed until other nutrients such as nitrogen have been depleted and excess carbon used in rhamnolipid synthesis is free to be diverted away from the production of biomass. In addition to biofilm dispersal, targeting rhamnolipid production with social disruption strategies could have substantial impacts on the ability of bacteria to compete successfully in a biofilm or infection. Engineered rhamnolipid-producer strains, which have rhamnolipid synthesis under an inducible promoter and therefore lack metabolic prudence, are highly susceptible to cheaters and are quickly outcompeted in co-culture swarming colonies [35 ]. Manipulating rhamnolipid secretion will require a more complete understanding of the system, as key molecular details of the integration between quorum sensing and metabolic sensing are still unknown. Further study into the molecular basis of metabolic prudence may reveal new avenues to exploit the intrinsic mechanism of biofilm dispersal of *P. aeruginosa*.

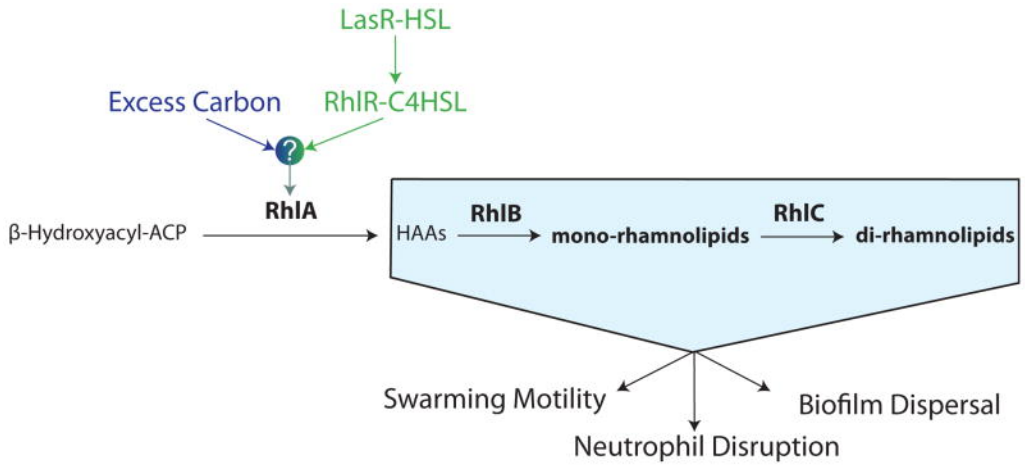


**Figure 1.4 The pathway for synthesis of rhamnolipid biosurfactants in P. aeruginosa**.

Expression of the enzyme RhlA is the rate-limiting step for rhamnolipid synthesis [34] and implements a molecular decision-making process by which bacteria start producing rhamnolipids. The process requires the integration of quorum sensing (Las and Rhl systems) and metabolic cues [35]. The molecular details of the integration, represented here by a question mark, remain unknown.

## Conclusion

There is a pressing need for alternatives to antibiotics, our main defense against bacterial pathogens that is increasingly threatened by the emergence of resistance. The solution may come from targeting population-level traits such as biofilm formation and quorum sensing. Microbial social evolution can help identify novel therapeutic targets and assist in the rational design of therapies that avoid selection for resistance. The coming years are sure to bring more insights from the fascinating interface between molecular microbiology and social evolution theory.

## References

Papers of particular interest, published within the period of review, have been highlighted as: of special interest • of outstanding interest ••


1. Costerton JW: Bacterial biofilms: a common cause of persistent infections. Science 1999, 284:1318-1322.
2. Greenberg EP: Sociomicrobiology: a personal perspective on an emerging research area. Microbe Mag 2010, ASC.
3. Bérdy J: Thoughts and facts about antibiotics — where we are now and where we are heading. J Antibiot 2012, 65:441.
4. Jimenez PN, Koch G, Thompson JA, Xavier KB, Cool RH, Quax WJ: The multiple signaling systems regulating virulence in Pseudomonas aeruginosa. Microbiol Mol Biol Rev 2012, 76:46-65.
5. Khalil AS, Collins JJ: Synthetic biology: applications come of age. Nat Rev Genet 2010, 11:367-379.
6. Lu TK, Collins JJ: Dispersing biofilms with engineered enzymatic bacteriophage. Proc Natl Acad Sci U S A 2007, 104:11197-11202.
7. Foster KR: The sociobiology of molecular systems. Nat Rev Genet 2011, 12:193-203.
8. Xavier JB: Social interaction in synthetic and natural microbial communities. Mol Syst Biol 2011, 7.
9. Nadell CD, Xavier JB, Foster KR: The sociobiology of biofilms. FEMS Microbiol Rev 2009, 33:206-224.
10. Jiricny N, Diggle SP, West SA, Evans BA, Ballantyne G, Ross- Gillespie A, Griffin AS: Fitness correlates with the extent of cheating in a bacterium. J Evol Biol 2010, 23:738-747.
11. Griffin AS, West SA, Buckling A: Cooperation and competition in pathogenic bacteria. Nature 2004, 430:1024-1027.
12. Diggle SP, Griffin AS, Campbell GS, West SA: Cooperation and conflict in quorum-sensing bacterial populations. Nature 2007, 450:411-414.
13. Mellbye B, Schuster M: The sociomicrobiology of antivirulence drug resistance: a proof of concept. mBio 2011, 2.
14. Sandoz KM, Mitzimberg SM, Schuster M: Social cheating in Pseudomonas aeruginosa quorum sensing. Proc Natl Acad Sci U S A 2007, 104:15876-15881.

15. Bjarnsholt T, Jensen P.Ø., Jakobsen TH, Phipps R, Nielsen AK, Rybtke MT, Tolker-Nielsen T, Givskov M, Høiby N, Ciofu O et al.: Quorum sensing and virulence of Pseudomonas aeruginosa during lung infection of cystic fibrosis patients. PLoS ONE 2010, 5:e10115.

16. Kohler T, Perron GG, Buckling A, van Delden C: Quorum sensing inhibition selects for virulence and cooperation in Pseudomonas aeruginosa. PLoS Pathog 2010, 6:e1000883.

•• This study tested the quorum sensing inhibiting drug, azxithromycin, to reduce pathogenesis of infecting P. aeruginosa. Instead, the drug decreased the advantage quorum sensing cheaters giving an advantage to the virulent wild type bacteria. The paper highlights the importance of thoroughly understanding the selective pressures involved.

17. Høiby N, Bjarnsholt T, Givskov M, Molin S, Ciofu O: Antibiotic resistance of bacterial biofilms. Int J Antimicrob Agents 2010, 35:322-332.

18. Flemming HC, Wingender J: The biofilm matrix. Nat Rev Microbiol 2010, 8:623-633.

19. Xavier JB, Foster KR: Cooperation and conflict in microbial biofilms. Proc Natl Acad Sci U S A 2007, 104:876-881.

20. Nadell CD, Foster KR, Xavier JB: Emergence of spatial structure in cell groups and the evolution of cooperation. PLoS Comput Biol 2010, 6:e1000716.

21. Nadell CD, Bassler BL: A fitness trade-off between local competition and dispersal in Vibrio cholerae biofilms. Proc Natl Acad Sci U S A 2011, 108:14181-14185.

•• This paper demonstrates that, similar to in silico models, V. cholera EPS-producers outcompete non-producers in biofilms. The paper goes on to show that the advantage has a trade-off: EPS-producers depart from the biofilm and seed new areas at a lower rate than they increase in the biofilm.

22. Dandekar AA, Chugani S, Greenberg EP: Bacterial quorum sensing and metabolic incentives to cooperate. Science 2012, 338:264-266.

23. Popat R, Crusz SA, Messina M, Williams P, West SA, Diggle SP: Quorum-sensing and cheating in bacterial biofilms. Proc Biol Sci 2012, 279:4765-4771.

• This paper shows that P. aeruginosa quorum sensing cheaters reduce growth of a population and that this reduction is more pronounced in biofilms. Biofilms are also more susceptible to antibiotic treatment when cheaters are present.

24. Brindle ER, Miller DA, Stewart PS: Hydrodynamic deformation and removal of Staphylococcus epidermidis biofilms treated with urea, chlorhexidine, iron chloride, or Dispersin B. Biotechnol Bioeng 2011, 108:2968-2977.

25. Xavier JB, Picioreanu C, Rani SA, van Loosdrecht MC, Stewart PS: Biofilm-control strategies based on enzymic disruption of the extracellular polymeric substance matrix — a modelling study. Microbiology 2005, 151(Pt 12):3817-3832.

26. Caiazza NC, Merritt JH, Brothers KM, O'Toole GA: Inverse regulation of biofilm formation and swarming motility by *Pseudomonas aeruginosa* PA14. J Bacteriol 2007, 189:3603-3612.

27. O'Toole GA: At surfaces, these bacteria either form biofilms or swarm, a regulated behavior with important consequences for pathogenesis. ASM Microbe Mag 2008, 3:65-71.

28. Boles BR, Thoendel M, Singh PK: Rhamnolipids mediate detachment of Pseudomonas aeruginosa from biofilms. Mol Microbiol 2005, 57:1210-1223.

29. Zeraik AE, Nitschke M: Biosurfactants as agents to reduce adhesion of pathogenic bacteria to polystyrene surfaces: effect of temperature and hydrophobicity. Curr Microbiol 2010, 61:554-559.

30. Jensen PO, Bjarnsholt T, Phipps R, Rasmussen TB, Calum H, Christoffersen L, Moser C, Williams P, Pressler T, Givskov M et al.: Rapid necrotic killing of polymorphonuclear leukocytes is caused by quorum-sensing-controlled production of rhamnolipid by Pseudomonas aeruginosa. Microbiology 2007, 153(Pt 5):1329-1338.

31. Van Gennip M, Christensen LD, Alhede M, Phipps R, Jensen PO, Christophersen L, Pamp SJ, Moser C, Mikkelsen PJ, Koh AY et al.: Inactivation of the rhlA gene in Pseudomonas aeruginosa prevents rhamnolipid production, disabling the protection against polymorphonuclear leukocytes. APMIS 2009, 117:537-546.

32. van Gennip M, Christensen LD, Alhede M, Qvortrup K, Jensen PO, Hoiby N, Givskov M, Bjarnsholt T: Interactions between polymorphonuclear leukocytes and Pseudomonas aeruginosa biofilms on silicone implants in vivo. Infect Immun 2012, 80:2601-2607.

33. Abdel-Mawgoud AM, Lepine F, Deziel E: Rhamnolipids: diversity of structures, microbial origins and roles. Appl Microbiol Biotechnol 2010, 86:1323-1336.

34. Zhu K, Rock CO: RhlA converts beta-hydroxyacyl-acyl carrier protein intermediates in fatty acid synthesis to the beta- hydroxydecanoyl-beta-hydroxydecanoate component of rhamnolipids in Pseudomonas aeruginosa. J Bacteriol 2008, 190:3147-3154.

35. Xavier JB, Kim W, Foster KR: Mol Microbiol 2011, 79:166-179. A molecular mechanism that stabilizes cooperative secretions in Pseudomonas aeruginosa.

•• This paper shows that P. aeruginosa uses a mechanism of metabolic prudence to delay production of rhamnolipid biosurfactants, a public good required for swarming migration,

until nitrogen is depleted and growth has slowed. Metabolic prudence reduces the cost of producing the public good, making the wild type more competitive against cheaters.

36. van Ditmarsch D, Xavier J: High-resolution time series of Pseudomonas aeruginosa gene expression and rhamnolipid secretion through growth curve synchronization. BMC Microbiol 2011, 11:140.

37. Branda SS, Gonzalez-Pastor JE, Ben-Yehuda S, Losick R, Kolter R: Fruiting body formation by Bacillus subtilis. Proc Natl Acad Sci U S A 2001, 98:11621-11626.

38. Worlitzsch D, Tarran R, Ulrich M, Schwab U, Cekici A, Meyer KC, Birrer P, Bellon G, Berger J, Weiss T et al.: Effects of reduced mucus oxygen concentration in airway Pseudomonas infections of cystic fibrosis patients. J Clin Investig 2002, 109:317-325.

39. Kolodkin-Gal I, Romero D, Cao S, Clardy J, Kolter R, Losick R: D-amino acids trigger biofilm disassembly. Science 2010, 328:627-629.

40. Blaise R, Boles ARH: agr-Mediated dispersal of Staphylococcus aureus biofilms. PLoS Pathog 2008, 4:e1000052.

# 1.3 - Understanding Cooperative Behavior Through Swarming Motility, and Multilevel Selection*

*Data Published in:
de Vargas Roditi, L., K.E. Boyle, and J.B. Xavier, *Multilevel selection analysis of a microbial social trait.* Mol Syst Biol, 2013. **9**: p. 684.
van Ditmarsch, D., et al., *Convergent evolution of hyperswarming leads to impaired biofilm formation in pathogenic bacteria.* Cell Rep, 2013. **4**(4): p. 697-708.

In order to study the regulation of social traits in bacteria we need to have a social phenotype that we can observe and manipulate in a laboratory setting. Swarming motility in the opportunistic pathogen *Pseudomonas aeruginosa*, is a model social trait and a remarkable surface based social motility that allows bacteria to move out from the inoculation site at the center of the plate and form large colonies agar petri dishes (Fig 1.5) [1]. By doing this behavior the bacteria are able to forage more nutrients and grow to a much larger population size than they would if they had stayed in the center of the plate and not moved [2, 3]. To perform swarming motility *P. aeruginosa* needs at least three things: (1) flagella to move, (2) the density dependent signaling system in bacteria (quorum sensing), and (3) to produce massive amounts of a natural biosurfactant know as rhamnolipids [1, 4]. Rhamnolipids that provide lubrication for the bacteria to perform swarming motility are the same molecules capable of dispersing biofilms [5]. In a swarming agar plate, secreted rhamnolipids act as a biosurfactant and draw water out of the agar in the petri dish allowing the bacteria to swim into new un-colonized areas of the plate. Rhamnolipids behave as 'public goods,' and once secreted outside of the cell they are available not only to the cell that produced them, but also surrounding cells. The public good nature of rhamnolipids makes their production susceptible to cheating [2, 6].

**Figure 1.5 Wild-type *P. aeruginosa* swarming colony**

Wild-type swarming colony of *P. aeruginosa* formed after 24 hours of incubation in on 9cm soft agar petri dish. The branched tendril formation allows the colony to access additional nutrients.

## Cheating the system

Rhamnolipids are publically available within a swarm, and in line with predictions, an engineered cheater strain Δ*rhlA*, which lacks the essential enzyme for rhamnolipid production, RhlA, is capable of free-riding on the rhamnolipids produced by another strain [2]. Interestingly, this cheater strain does not have a fitness advantage over the wild-type in mixed swarming colonies [2]. This indicates that the metabolic prudence regulation in the wild-type reduces the cost of rhamnolipid production to levels below detection or eliminates cost entirely. In fact, when the wild-type is mixed with a Δ*rhlA* cheater in a swarming colony there is a mild benefit to the wild-type, where the wild-type actually increases in frequency in the population relative to the non-producer (Fig 1.6)[3].

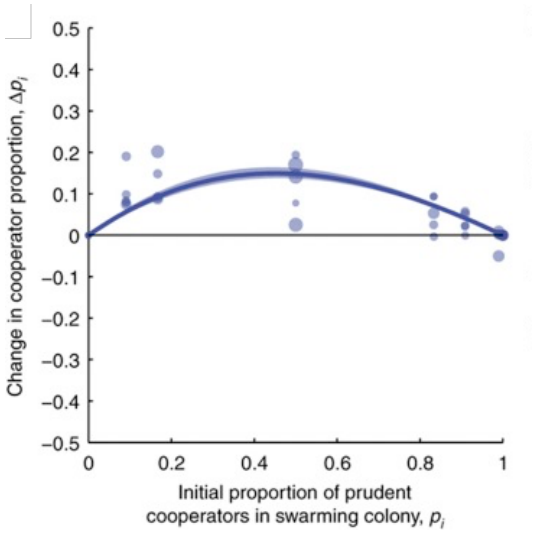


**Figure 1.6 Wild-type does not lose in competition with cheaters***

The change in wild-type (prudent cooperator) proportion due in swarming competitions with the Δ*rhlA* cheater strain. Results show a marginal individual-level advantage of prudent cooperators.
*Published in Mol Syst Biol, 2013. **9**: p. 684.

The metabolically prudent regulation of expression of a cooperative trait appears to be an elegant solution to stabilize cooperative secretions. Indeed prudent regulation has been found as a general regulatory strategy governing several shared products in *P. aeruginosa* [7] and other bacteria [8, 9]. The native prudent regulation present in wild-type *P. aeruginosa* elicits questions about the origin of such a regulatory system and how it might have evolved. In wild-type *P. aeruginosa* rhamnolipids are under the control of two nested quorum sensing systems and metabolic prudence [2, 10]. What advantages does such a complex regulatory system convey? An approach to answering this question is to strip down rhamnolipid regulation and compare how a simplified regulatory system performs relative to the native wild-type regulation.

**Optimal Constitutive Production of Rhamnolipids**

A simple regulation of a secreted product is constitutive expression at an ideal level. Constitutive regulation cannot dynamically adapt to changing environments, but theoretically can be stable under the correct conditions even if the constitutive production comes at a cost [11]. Understanding how costly constitutive production can be favored in a mixed population requires the use of multilevel selection theory. Multilevel (or group) selection theory proposes a mechanism where natural selection occurs at the level of an individual actor as well as the level of the actor's social group [12]. A global population can be made up of many smaller local populations, which are then made up of individuals. Within these local populations the costly production of a public good could be beneficial at the population level, such that populations with more cooperators will have an increased carrying capacity or grow at a faster rate. Although the trait is costly at the individual level the benefit it provides to the population can cause local populations with more cooperators to comprise a greater fraction of the global population (Fig 1.7) [3, 11]. Under certain conditions of cost and benefit this can allow the cooperators to increase globally even though they decrease in every local population.

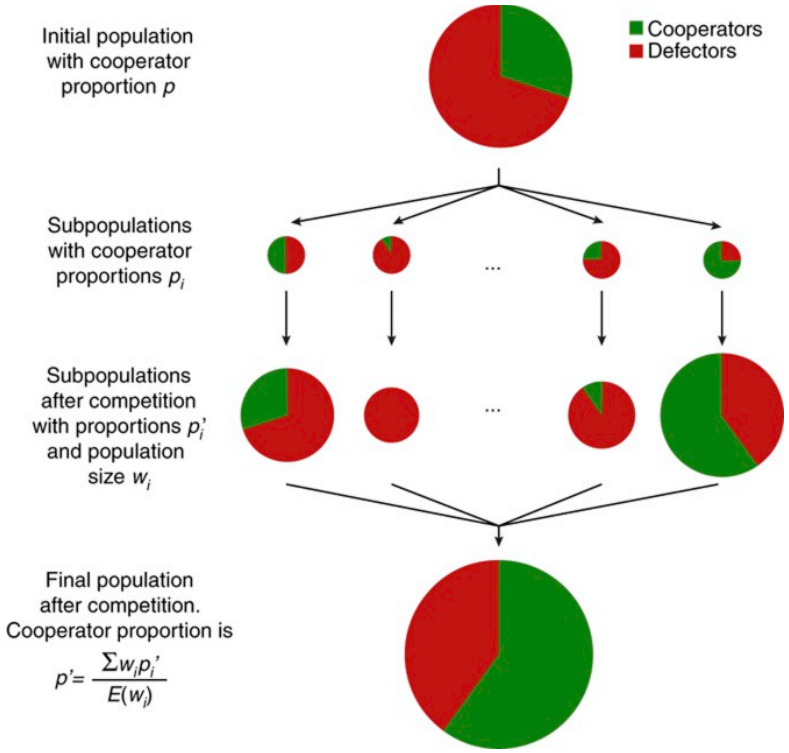


**Figure 1.7 The theoretical scenario used in multilevel selection analysis.***

A global population with an initial proportion of cooperators p is sampled to seed several subpopulations each with an initial local cooperator proportion $p_i$ (the average across all populations being p). Each subpopulation is allowed to compete for 24 h and at the end of the competition the proportion of cooperators has changed to $p_i'$. In swarming motility, the subpopulations seeded with higher initial proportions of cooperators tend to produce larger colonies ($w_i$ increases with $p_i$ ), and thus will contribute more to the global pool. After competition, all subpopulations are pooled together and the final proportion of cooperators is assessed, $p' = \sum_i (w_i p_i)/\overline{w}$. Cooperation is favored by multilevel selection when $\Delta p = p - p' > 0$.
*Published in Mol Syst Biol, 2013. **9**: p. 684.

Costly, constitutive production was examined in *P. aeruginosa* swarming colonies using an engineered strain, where rhamnolipid synthesis is under the control of a tunable promoter, $P_{BAD}$, which increases expression of the gene with increasing concentrations of the molecule L-arabinose (PA14 Δ*rhlA*:$P_{BAD}$-*rhlAB*) [13]. This system allows the production level of rhamnolipids to be set at an optimal constitutive level for swarming where the expression of *rhlAB* is sufficient to produce enough rhamnolipids for swarming but not so high that it becomes detrimental to fitness and impairs swarming motility (Fig

1.8) [3].

However, even at an optimal level of *rhlAB* expression the constitutive cooperator loses in direct competition with an engineered Δ*rhlA* cheater that does not produce any rhamnolipids, demonstrating an individual level cost. The population benefits from the rhamnolipids produced by cooperators in the swarming colony and this benefit increases proportionally with the fraction of cooperators in the initial inoculation until a point of saturation (~0.5 initial proportion cooperators).

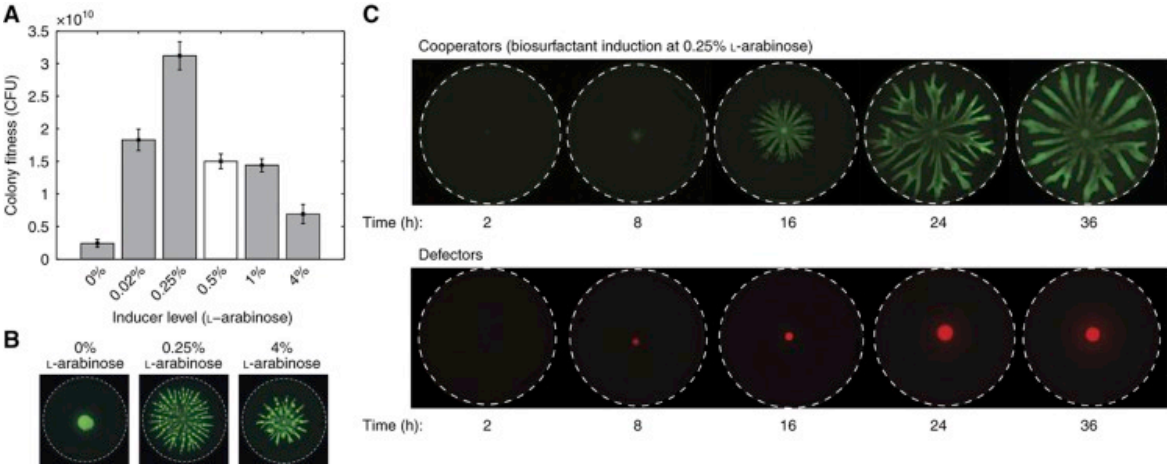


**Figure 1.8 Cooperative swarming allows Pseudomonas aeruginosa colonies to expand over large areas.***

(A) In colonies of the inducible ($P_{BAD}$-*rhlAB*) cooperator, fitness peaks at L-arabinose 0.25%. At this level biosurfactant production is high enough for swarming expansion but low enough that its costs do not overwhelm the benefit of swarming colony expansions. The data point at 0.5% L-arabinose (white bar) comes from a previous study (Xavier, 2011a); all other data (gray bars) were acquired in de Vargas Roditi, 2013. (B) Images of swarming colonies. Dashed line represents the edge of 9cm Petri dish. (C) Cooperators (biosurfactant producers induced by 0.25% L-arabinose) expand over the entire Petri dish. Defectors (Δ*rhlAB*) are incapable of swarming and the colonies grow less.
*Published Mol Syst Biol, 2013. **9**: p. 684.

Wet lab experiments measuring growth rate, swarming colony size, and frequency of constitutive cooperators and Δ*rhlA* cheaters demonstrated that increased cooperation benefited the group in single strain swarming colonies (Fig 1.9) [3]. The constitutive cooperator colonies were able to reach much larger population sizes compared to their cheating Δ*rhlAB* counterparts. The data from the wet lab experiments were used to parameterize a mathematical model. The model analyzes the outcomes of mixing cooperators with cheaters using multilevel selection theory [12] and predicts that although optimal constitutive cooperation could be evolutionarily stable, this only occurs at levels of very high relatedness that are not likely to occur in natural microbial environments [3]. In contrast the native, metabolically prudent, regulation of the wild-type is always favored. The production of rhamnolipids by the wild-type improves the outcome for the population at either no cost to the individual or even a minor benefit. This highlights the importance of prudent regulation in the stability of cooperative rhamnolipid secretion in natural mixed populations and indicates that mechanics of the complex rhamnolipid regulatory system in the wild-type are crucial to maintaining cooperative behavior.

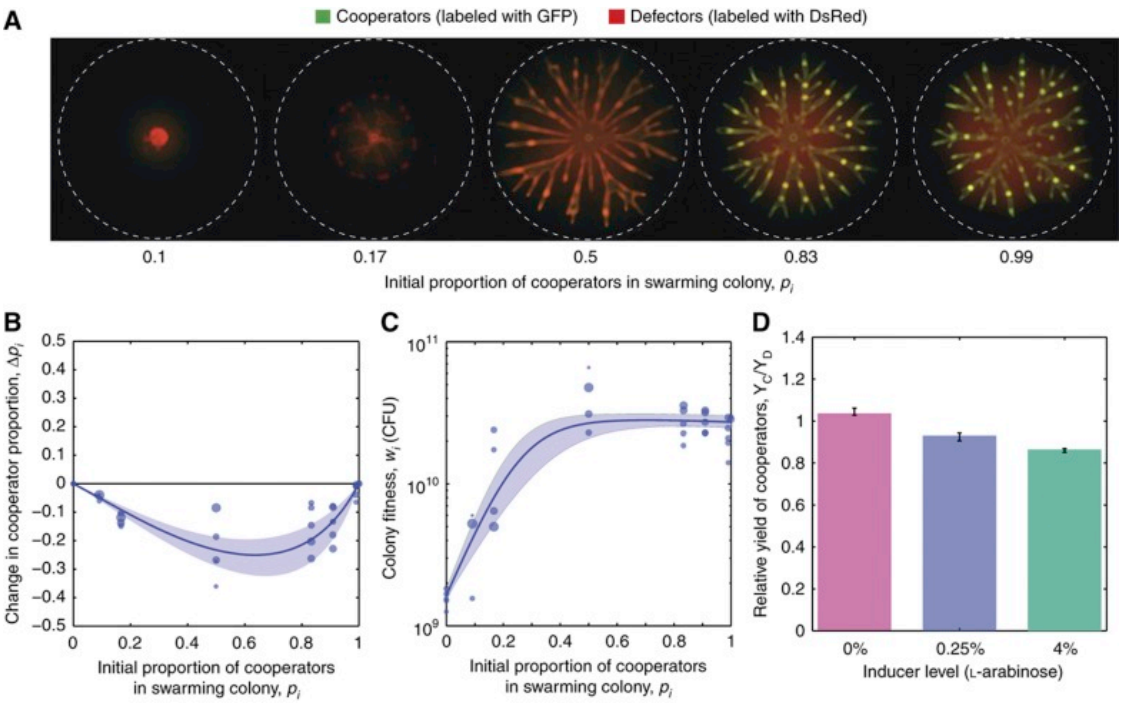


**Figure 1.9 Individual-level selection disfavors cooperation: induced cooperators increase population size but lose to defectors. ***

(A) Competitions between cooperators and defectors mixed at varying mixing proportions (L-arabinose at 0.25% for all competitions). Cooperators are labeled with GFP and defectors are labeled with DsRed-Express. (B) The change in cooperator proportion due to competition reveals that induced cooperation is strongly selected against. Lines represent best fit for mathematical model and shaded areas represent confidence levels from bootstrapping. Size of data points is proportional to the weight of the data point in the parameter fitting. (C) Colony fitness increases with the proportion of cooperators but shows diminishing returns. (D) The growth yield of cooperators relative to the yield of defectors decreases with increasing levels of biosurfactant induction. Error bars represent minimum and maximum parameter value obtained from bootstrapping.

*Published in Mol Syst Biol, 2013. **9**: p. 684.

## Experimental Evolution in Swarming Conditions

As previously demonstrated, cooperation in swarming motility can have a large benefit at the group level [2, 3]. Another approach to understanding a prudent regulatory system is to perturb it and then use experimental evolution [14] to allow the bacterial system to evolve naturally, in this case swarming motility in *P. aeruginosa*. This has the advantage of not making any assumptions about what type of regulatory strategy should be engineered to govern a particular trait, but can be more difficult to interpret and the exact selection pressure can be challenging to determine. Short generation times, genetically malleable systems and relatively small genomes make bacteria an incredibly tractable system for experimental evolution.

## Experimental Evolution of Wild-type *P. aeruginosa* in Swarming Colonies Leads to Hyperswarmers

Experimental evolution in swarming conditions starting from wild-type *P. aeruginosa* resulted in the convergent parallel evolution of multi-flagellated bacteria, termed hyperswarmers, as the swarming colonies of these mutants cover the entire plate without branched tendrils (Fig 1.10) [15]. The hyperswarmer mutants are significantly more fit in swarming colonies. Hyperswarmers are capable of reaching the edge of the swarm and accessing better nutrient conditions leading them to outcompete their wild-type ancestor (Fig 1.11). Although the hyperswarmers have a clear fitness advantage in swarming conditions, these strains are poor at biofilm formation, which is an essential part of the survival of *P. aeruginosa* in the environment (Fig 1.12). *P. aeruginosa* mutants that acquire multiple flagella in the environment are likely strongly selected against due to an inability to form biofilms and therefore do not reach fixation.

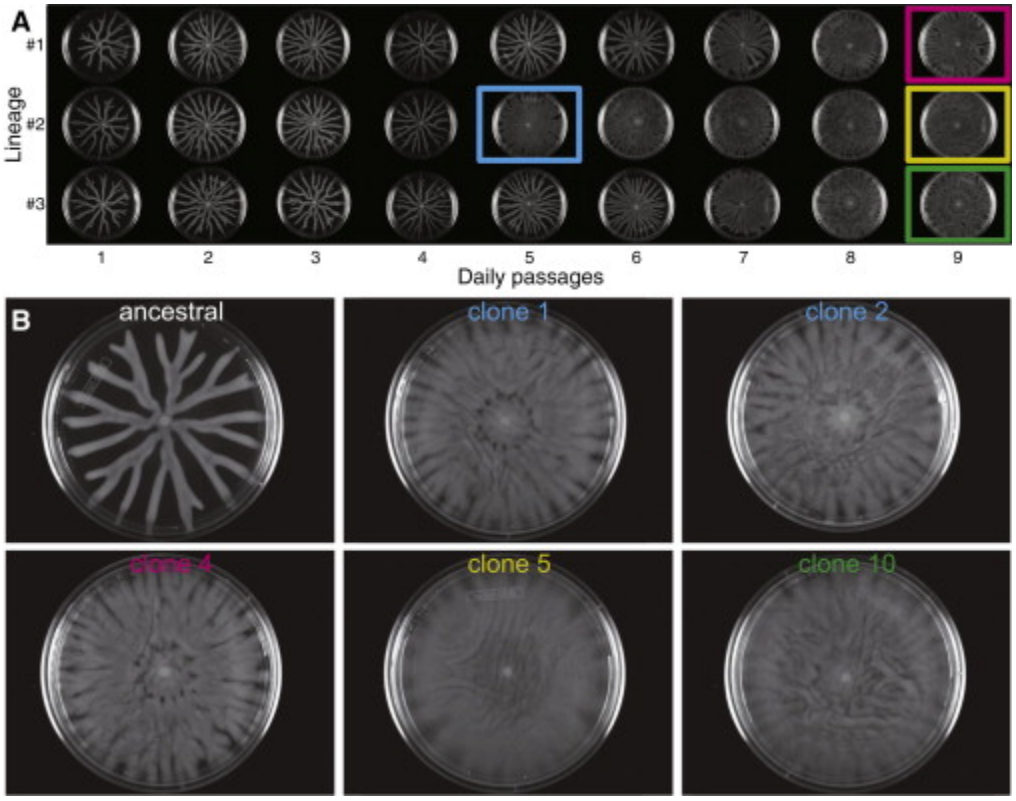


**Figure 1.10 Experimental Evolution of Swarming Motility Produces a Stable and Heritable Hyperswarmer Phenotype ***

(A) Three independent lineages (1–3) were subjected to experimental evolution by sequential passages of growth in swarming media. After each 24 hr swarming interval, the entire colony was flushed off the plate, and a 1/1,500 fraction (2$\mu$L) of the recovered population was inoculated onto a fresh swarming plate. Lineage #2 acquired a hyperswarming phenotype at day 5, whereas lineages #1 and #3 only did so at day 7. The colonies outlined in color were selected for clonal isolation procedures. (B) Hyperswarming is stable and heritable. Swarming colonies of the ancestral strain and clones isolated from each of the colonies outlined in (A) are shown.
*Published in Cell Rep, 2013. **4**(4): p. 697-708.

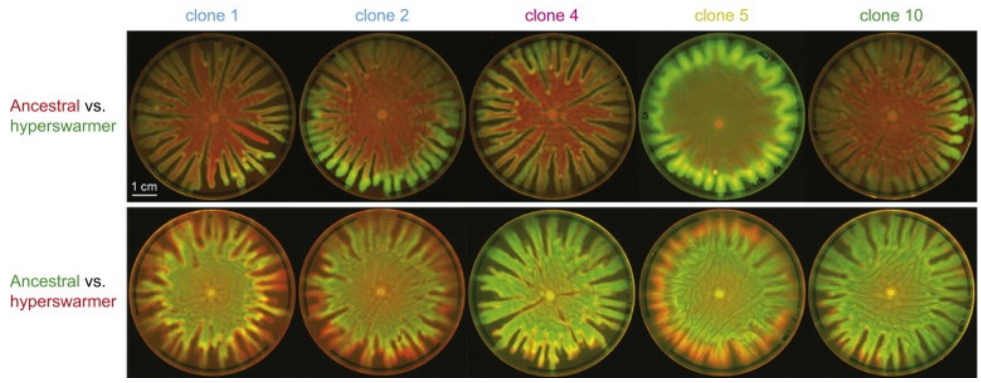


**Figure 1.11 Hyperswarmers Prevail in Swarming Competitions by Segregating at the Leading Edges of Expanding Swarming Colonies***
Hyperswarmers are enriched at the leading edge of swarming colonies. Fluorescence scans of swarms initiated with a 10:1 ratio of ancestral in green to hyperswarmer in red (top row) or the inverse (bottom row) are presented.
*Published in: Cell Rep, 2013. **4**(4): p. 697-708.

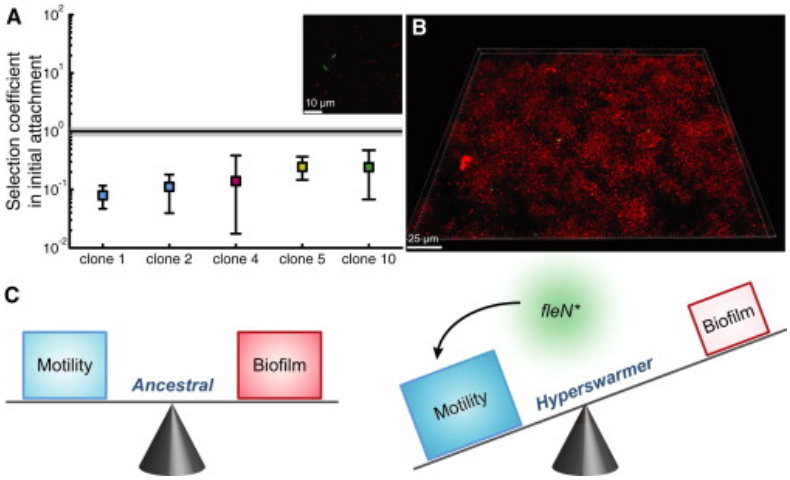


**Figure 1.12 Hyperswarmers Lose Biofilm Competitions against the Ancestral Strain, Indicating an Evolutionary Trade-Off between Motility and Biofilm Formation ***
(A) Hyperswarmer clones lose against the ancestral strain already at the phase of initial attachment to a biofilm substratum. Slide biofilms were inoculated at a 1:1 ratio and incubated for 6 hr before imaging the attached cells (see inset where ancestral is red, and clone 4 is green). The black line indicates the neutral selection coefficient of 1. These experiments were performed in duplicate (also for the neutral selection coefficient). The 95% confidence intervals (both for neutral and actual selection coefficients) were determined through the probability density functions of the counts. (B) Full-grown, flow cell biofilm of clone 4 (green) and ancestral (red) is presented. The biofilm was inoculated at a 1:1 ratio and then grown for 24 hr before imaging. The image is a deconvolved 3D projection of the biofilm.
*Published in Cell Rep, 2013. **4**(4): p. 697-708.

In each experimental evolution lineage using the wild-type *P. aeruginosa* in swarming colonies, multi-flagellated hyperswarming mutants emerged [15]. No mutants with altered rhamnolipid regulation were isolated in this study, suggesting that the prudent regulation of wild-type *P. aeruginosa* is already well optimized for swarming conditions. The striking parallel convergent evolution in the hyperswarmer experimental evolution study also prompts questions about what conditions lead to convergent evolution versus divergent evolution. This remains an open question in evolutionary biology and utilizing swarming motility as a model system allows for the investigation of cooperative regulation and evolutionary dynamics.

The multilevel selection work in conjunction with the hyperswarmer experimental evolution study sets the stage for further investigating how prudent regulation stabilizes cooperation in dynamic social groups. The native regulation of the wild-type has been demonstrated to be well optimized for laboratory swarming conditions and critical for the stability of cooperation through rhamnolipid secretion [3, 15]. However, the way in which prudent regulation integrates with quorum sensing signals and the dynamics and consequences of these mechanisms are not understood. Likewise, the evolution and adaptation of rhamnolipid regulation in swarming colonies has not yet been investigated and could provide insight into evolutionary dynamics as well as molecular mechanisms that stabilize cooperative secretion.

**References**


1. Thilo Kohler, L.K.C., Francisco Barja, Christian van Delden, *Swarming of Pseudomonas aeruginosa Is Dependent on Cell-to-Cell Signaling and Requires Flagella and Pili.* JOURNAL OF BACTERIOLOGY, 2000. **182**(21): p. 5990–5996.
2. Xavier, J.B., W. Kim, and K.R. Foster, *A molecular mechanism that stabilizes cooperative secretions in Pseudomonas aeruginosa.* Mol Microbiol, 2011. **79**(1): p. 166-79.

3. de Vargas Roditi, L., K.E. Boyle, and J.B. Xavier, *Multilevel selection analysis of a microbial social trait.* Mol Syst Biol, 2013. **9**: p. 684.
4. Deziel, E., et al., *rhlA is required for the production of a novel biosurfactant promoting swarming motility in Pseudomonas aeruginosa: 3-(3-hydroxyalkanoyloxy)alkanoic acids (HAAs), the precursors of rhamnolipids.* Microbiology, 2003. **149**(Pt 8): p. 2005-13.
5. Zeraik AE, N.M., *Biosurfactants as agents to reduce adhesion of pathogenic bacteria to polystyrene surfaces: effect of temperature and hydrophobicity.* Curr Microbiol 2010. **61**: p. 554-559.
6. West, S.A., et al., *Social evolution theory for microorganisms.* Nat Rev Microbiol, 2006. **4**(8): p. 597-607.
7. Mellbye, B. and M. Schuster, *Physiological framework for the regulation of quorum sensing-dependent public goods in Pseudomonas aeruginosa.* J Bacteriol, 2014. **196**(6): p. 1155-64.
8. Martin Schuster, D.J.S., Stephen P. Diggle, and E. Peter Greenberg, *Acyl-Homoserine Lactone Quorum Sensing: From Evolution to Application.* Annual Review of Microbiology, 2013. **67**: p. 43-63.
9. Bruger, E. and C. Waters, *Sharing the sandbox: Evolutionary mechanisms that maintain bacterial cooperation.* F1000Res, 2015. **4**.
10. Latifi, M.F., K.Tanaka, P.Williams and A. Lazdunski', *A hierarchical quorum-sensing cascade in Pseudomonas aeruginosa links the transcriptional activators LasR and RhlR (VsmR) to expression of the stationary-phase sigma factor RpoS.* Molecular Microbiology, 1996. **21**(6): p. 1137-1 146
11. John S. Chuang, O.R., Stanislas Leibler, *Simpson's Paradox in a Synthetic Microbial System.* Science, 2009. **323**: p. 272-275.
12. Wright, S., Ecology, 1945. **26**: p. 415–419.
13. Boles, B.R., M. Thoendel, and P.K. Singh, *Rhamnolipids mediate detachment of Pseudomonas aeruginosa from biofilms.* Mol Microbiol, 2005. **57**(5): p. 1210-23.
14. Richard E. Lenski, M.R.R., Suzanne C. Simpson and Scott C. Tadler, *Long-Term Experimental Evolution in Escherichia coli. I. Adaptation and Divergence During 2,000 Generations.* The American Naturalist, 1991. **138**(6): p. 1315-1341.
15. van Ditmarsch, D., et al., *Convergent evolution of hyperswarming leads to impaired biofilm formation in pathogenic bacteria.* Cell Rep, 2013. **4**(4): p. 697-708.

# Chapter 2 - Integration of Metabolic and Quorum Sensing Signals Governing the Decision to Cooperate in a Bacterial Social Trait*

Boyle, K. E., H. Monaco, D. van Ditmarsch, M. Deforet and J. B. Xavier

*Published in: PLoS Comput Biol **11**(5): e1004279

**Abstract**

Many unicellular organisms live in multicellular communities that rely on cooperation between cells. However, cooperative traits are vulnerable to exploitation by non-cooperators (cheaters). We expand our understanding of the molecular mechanisms that allow multicellular systems to remain robust in the face of cheating by dissecting the dynamic regulation of cooperative rhamnolipids required for swarming in *Pseudomonas aeruginosa*. We combine mathematical modeling and experiments to quantitatively characterize the integration of metabolic and population density signals (quorum sensing) governing expression of the rhamnolipid synthesis operon *rhlAB*. The combined computational/experimental analysis reveals that when nutrients are abundant, *rhlAB* promoter activity increases gradually in a density dependent way. When growth slows down due to nutrient limitation, *rhlAB* promoter activity can stop abruptly, decrease gradually or even increase depending on whether the growth-limiting nutrient is the carbon source, nitrogen source or iron. Starvation by specific nutrients drives growth on intracellular nutrient pools as well as the qualitative *rhlAB* promoter response, which itself is modulated by quorum sensing. Our quantitative analysis suggests a supply-driven activation that integrates metabolic prudence with quorum sensing in a non-digital manner and allows *P.aeruginosa* cells to invest in cooperation only when the population size is large enough (quorum sensing) and individual cells have enough metabolic resources to do so (metabolic prudence). Thus, the quantitative description of *rhlAB* regulatory dynamics brings a greater understating to the regulation required to make swarming cooperation stable.

**Author Summary**

Although bacteria are not multicellular organisms, they commonly live in large communities and engage in many cooperative behaviors. Cooperation can allow bacteria

to access additional nutrients, but it requires the secretion of products that will be shared by the community. How bacteria make the molecular decision to cooperate within a community is still not completely understood. The bacterium *Pseudomonas aeruginosa* regulates the secretion of one of these shared products, rhamnolipids, using information about population density and nutrient availability in its environment. Expression of the operon *rhlAB* is required for the bacteria to produce rhamnolipids. We use a combined computational and experimental approach to investigate how *P. aeruginosa* continually combines current information of population density and nutrient availability to determine if it should express *rhlAB*. We find that when conditions are nutrient rich, *P. aeruginosa* uses population density to modulate the amount *rhlAB* expression, however when the bacteria are starved for nutrients the starvation condition largely determines how the bacteria will express *rhlAB*. Because the bacteria continually adjust expression based on the current conditions, the molecular decision to produce rhamnolipids can be adjusted if either population density or nutrient conditions change. Our combined computational and experimental approach sheds new light on the rich regulatory dynamics that govern a cellular decision to cooperate.

## Introduction

Cells can cooperate as multicellular populations and impact their environment in ways that would not be possible for an individual cell. This strength in numbers is observed in many natural populations of unicellular microbes and can be leveraged in engineered systems for synthetic biology [1]. While cooperation helps a population as a whole, natural selection acts at the level of individual cells, which makes cooperation susceptible to cheating [2]. The potential exploitation by non-cooperator cells (cheaters) that benefit from cooperation without participating in it threatens the robustness of multicellular systems both natural and synthetic [3–7]. However, the potential for cheating can drive

the evolution of molecular mechanisms capable of effectively regulating cooperative traits [8]. Investigating the natural mechanisms that prevent cheating can reveal design principles underlying the robustness of multicellular systems.

In bacteria, the expression of cooperative genes is often regulated by density-dependent signaling systems, called quorum sensing, that detect the transition from a unicellular to a multicellular state [9–11]. Quorum sensing works by the secretion of small signaling molecules, called autoinducers, which accumulate in the extracellular space in a density-dependent manner. Cells sense the extracellular concentration of these molecules and use it as a proxy for population density. Quorum sensing is used to regulate the expression of cooperative multicellular traits such as bioluminescence [9], biofilm formation [12] and virulence factors [13–16]. The ubiquity of quorum sensing across bacterial species suggests a range of applications for this circuitry as a design principle [1,17]. Although quorum sensing can provide a robust benefit in changing conditions [18], it is vulnerable to cheating. Cheater cells can take advantage of quorum sensing autoinducers or public goods that are regulated by quorum sensing [3,19,20].

Cooperative genes regulated by quorum sensing can also be sensitive to nutrient conditions, suggesting that metabolic information is integrated into the decision to cooperate [21–28]. Integrating metabolic information with quorum sensing offers a possible mechanism to prevent cheating, as cells can only cooperate when they have the appropriate nutritional resources to do so, reducing the cost of cooperation to the individual cell. The opportunistic pathogen*Pseudomonas aeruginosa* secretes massive amounts of rhamnolipid biosurfactants in order to move collectively over surfaces, a phenomenon known as swarming [29–33]. Swarming provides a benefit at the population level, enabling cells in a colony to disperse over wide areas and grow to large numbers. However, rhamnolipid production can be a significant cost to the individual cell since it

requires an investment of carbon that might otherwise be used for cell growth and division. Non-producing cells can exploit secreted rhamnolipids, which makes the trait vulnerable to cheating. Appropriate regulation of rhamnolipid synthesis is therefore crucial to prevent cheating and make cooperation stable.

The rhamnolipid synthesis operon *rhlAB* is regulated by a quorum-sensing cascade composed of *lasI*/lasR followed by *rhlI/rhlR* [34,35]. Although quorum-sensing regulation is necessary for*rhlAB* expression, it is not sufficient. Expression only occurs when the bacteria have carbon in excess of that needed for growth [23,36]. The use of metabolic signals to trigger expression of cooperative genes, in this case excess carbon triggering expression of *rhAB*, is termed metabolic prudence. This native regulation of quorum sensing and metabolic prudence prevents exploitation by cheaters and stabilizes cooperation [36,37].

The production of both mono- and di-rhamnolipids requires the function of three enzymes RhlA, RhlB and RhlC. RhlA converts B-hydroxyacl-ACP, an intermediate from fatty acid biosynthesis, into B-hydroxyalkanoyl-B-hydeoxyalkanoyl (HAA) [31]. RhlB and RhlC are required for the addition of rhamnose groups to produce mono- and di-rhamnolipids, respectively. RhlA is the rate-limiting enzyme and is required for any rhamnolipid production by the cell [38]. Tracking the activity of the *rhlAB* promoter therefore serves as a reporter for when a cell has made the decision to commit carbon to rhamnolipid production.

Although synthetic constitutive expression of *rhlAB* can result in rhamnolipid production and enable swarming, this synthetic rhamnolipid regulation severely impacts *P. aeruginosa* fitness and makes cooperation cheatable [36,37]. To understand how the native circuitry allows *P.aeruginosa* to produce rhamnolipids without compromising

fitness we construct a quantitative picture of *rhlAB* regulatory dynamics. We combine quantitative experiments with mathematical modeling to systematically probe *P. aeruginosa* growth behavior and *rhlAB* promoter activity as a population transitions between different nutrient levels and population densities. We find that a classical Monod model cannot explain growth under starvation of nitrogen or iron and that internal pools of these nutrients sustain growth during starvation. Utilizing our understanding of growth in different nutrient limitations we quantitatively analyze *rhlAB* promoter activity and find that there are sufficient signals of excess carbon during exponential phase to trigger *rhlAB*expression in a density-dependent manner. We also find that although the limiting nutrient governs the qualitative behavior of promoter activity during starvation, starvation-induced activity is also scaled by population density. Together these results suggest a supply-driven activation that continually integrates metabolic prudence with quorum sensing in a non-digital manner. These results support the view that *P. aeruginosa* cells express rhamnolipids prudently to reduce fitness costs and prevent cheating and add details about the nuances of this regulation under different conditions.

## Results

### Expression of *rhlAB* Depends on Growth Phase

We analyzed the timing of *rhlAB* promoter activity directly in swarming colonies using fluorescent imaging and time-lapse video using a $P_{rhlAB}$-*gfp* reporter strain (Fig 2.1A) [39]. A colony of *P. aeruginosa* inoculated on a swarming plate first grows without moving until it reaches a certain critical size at ~5 h (Fig 2.1B). During the 2–5 h period expression at the colony center coincides with a decrease in growth rate that could be due to local nutrient depletion (Fig 2.1C and 2.1D). GFP levels continue to increase until ~5 h when we can observe a translucent ring of secreted rhamnolipids around the colony by

eye. This is followed by the appearance of motile swarming tendrils shooting out from the colony. The secreted rhamnolipids lubricate the agar surface and allow the colony to slide over it.

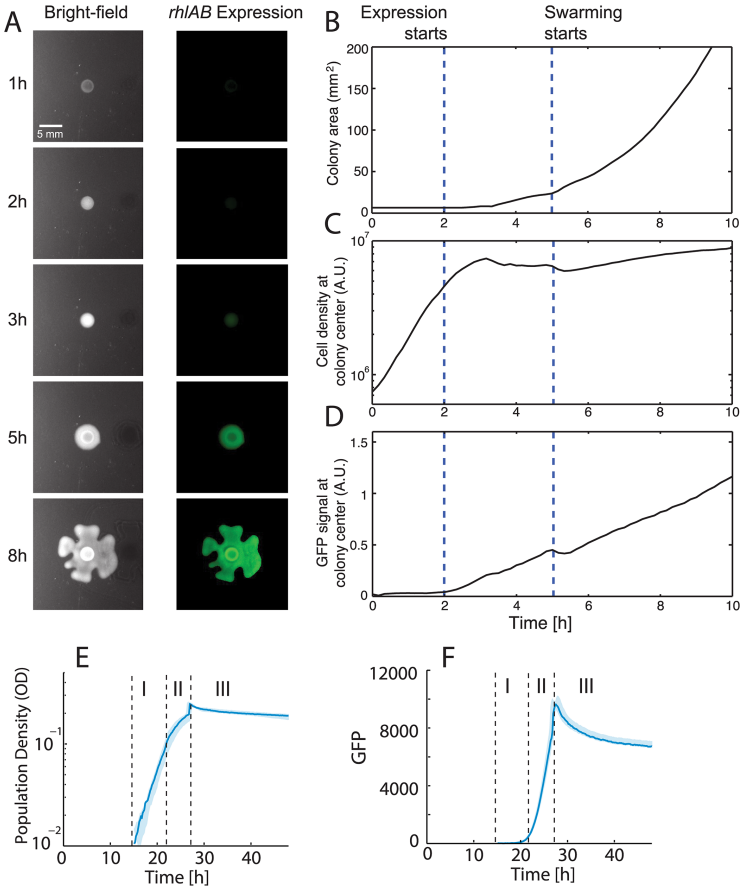


**Figure 2.1 Expression of *rhlAB* coincides with a slowdown in growth.**
(A) Time-lapse imaging of swarming and GFP fluorescence driven by the P*rhlAB* promoter. The colony grows until it reaches a critical size at ~5h and subsequently begins tendril formation. Before tendril formation, *rhlAB* expression is observed. B-D The time points where *rhlAB* expression starts and swarming motility starts are indicated by dashed vertical lines. (B) The increase in total area of the swarming colony shows that swarming starts at ~5h. (C) Cell density at the center of the colony increases exponentially until t = ~2h then growth rate slows down (D) The *rhlAB* expression (GFP signal) at the center of the colony was normalized by cell density. *rhlAB* expression revealed that expression of biosurfactant synthesis genes starts ~3h before the onset of swarming. (E) Growth curve of a P. aeruginosa population in synthetic liquid media (see Synthetic Growth Media) where all three growth phases occur. Phases I, II, and III are indicated with dashed lines. (F) P*rhlAB–gfp* expression of the population shown in E. over time. The majority of GFP production occurs during phase II, when the population growth rate has slowed. GFP measurements shown are corrected for autofluorescence (see Correction of Autofluoresence in the *gfp* Signal).

In order to probe *rhlAB* expression more systematically, we turned to a batch culture system using shaken liquid media in a microtiter-based assay. This way we can simultaneously assess population density and gene expression using OD (optical density) and the $P_{rhlAB}$-*gfp* reporter respectively. Bacterial growth curves are typically described by four phases: lag phase, exponential phase (sometimes called "log" phase), stationary phase, and death phase. The definition of stationary phase often includes qualitatively distinct sub-phases of slowed growth and no growth, which can make analyzing responses to nutrient starvation difficult. To facilitate our analysis, we separate time series into three phases after lag phase. Phase I begins when the population becomes detectable by absorbance at 600 nm (OD, for optical density; detectable at 0.01 OD in this study) and grows exponentially at its maximum rate, $\mu_{max}$. During this initial period, the cells have all nutrients required for biomass synthesis and thus achieve balanced growth. The start of phase II is defined by growth limitation, where an essential nutrient runs out and the population growth rate has slowed below $\mu_{max}$. Phase III is when population density stops increasing and may actually decay. Fig 2.1E shows a representative growth curve with all three growth phases. The $P_{rhlAB}$-*gfp* construct enables tracking of *rhlAB*expression throughout the different phases of growth with high time resolution (Fig 2.1F). We corrected for *P. aeruginosa* secreted products that fluoresce in the GFP detection wavelengths, thus generating a compensated GFP signal from the $P_{rhlAB}$ promoter over time (Fig 2.2 and Correction of Autofluoresence in the *gfp* Signal). Using population density and population level measurements of GFP assumes that *rhlAB* expression is homogenous across the population. To test if this assumption is valid, we used microscopy to measure single-cell expression levels at different stages of growth (Fig 2.3). The up-regulation of *rhlAB* was simultaneous across the population rather than bimodal. Therefore, we concluded that the population-level measurements could be used to probe expression dynamics.

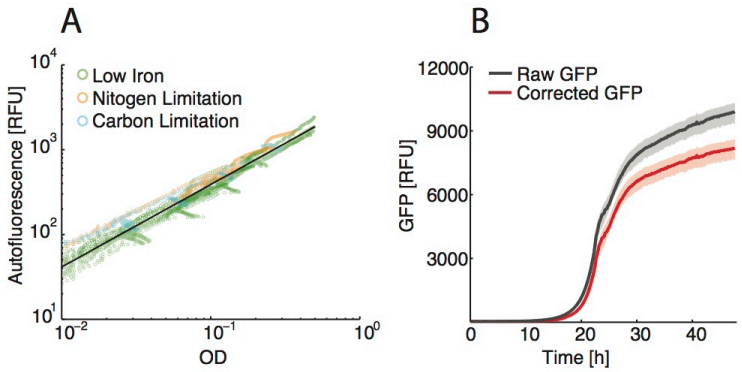


**Figure 2.2 Autofluorescence correction**

(A) Data used to in the linear regression that is used to correct the PrhlAB signal. All data is from the WT strain that expresses no fluorescent proteins under different nutrient limitations. Low iron data is from media where iron alone or iron and carbon or iron and nitrogen are limiting throughout growth. Autofluorescence has a similar relationship to OD across all limitations. (B) Population level GFP raw data (black) and after correction for autofluorescence (red). SeePromoter Activity Calculation for calculation. The correction for autofluorescence in the GFP channel significantly changes the observed GFP.

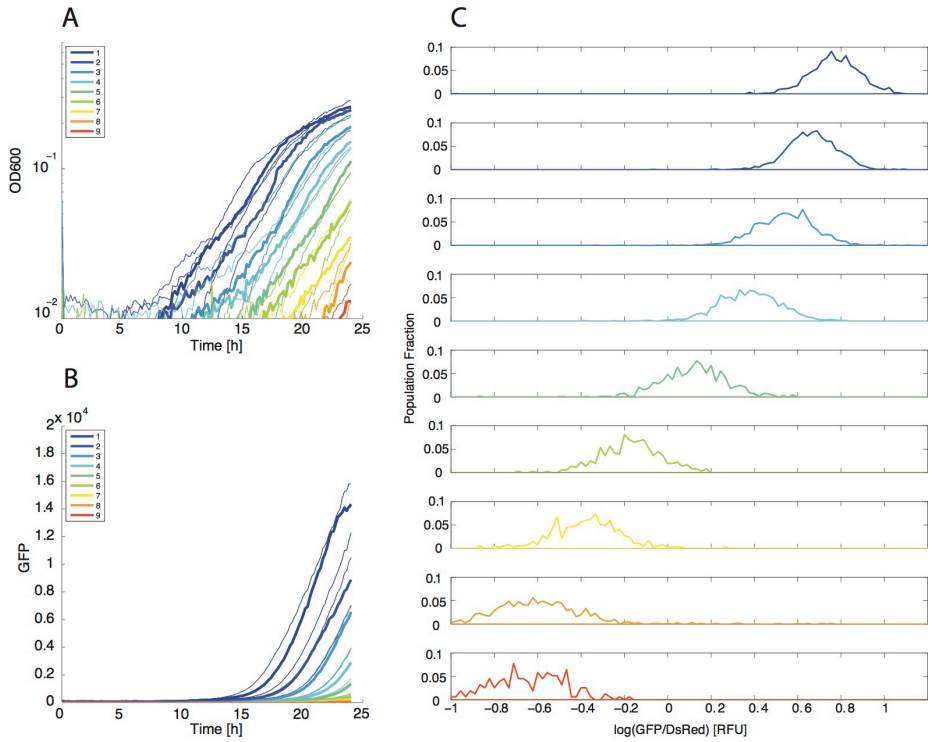


**Figure 2.3 Single cell gene expression analysis.**

(A) OD of P. aeruginosa populations in synthetic media using growth curve synchronization method of inoculation [33]. #1–9 are a dilution series of initial inoculum with 1 being the highest initial inoculum (OD 0.01) and then two-fold dilutions were used to create 2–9. Population with a higher initial inoculum are at a more advanced growth stage at the time of harvesting (B) Total GFP from PrhlAB-gfp promoter of populations in A. Populations further along in growth have higher levels of GFP expression (C) Histograms of log(GFP/DSRED) ratio for each population in A. DSRED is expressed from a constitutive promoter inserted in the genome and is used as a proxy for cell size. The expression of rhlAB is not bimodal, but increases as a single peak as growth progresses. Colors correspond to populations #1–9 in A and B.

## Growth Response to Nutrient Limitation

To better understand how a population responds to the entry into starvation we first analyze growth behavior in different limiting conditions. Our first growth limitation experiments set carbon as the growth-limiting nutrient in the media. We used varying concentrations of the carbon source (glycerol) and added a nitrogen source (ammonium sulfate) and iron (iron(II) sulfate) in excess. In these conditions, the population density

and the length of phase I have a dose dependency with the initial amount of carbon, confirming that carbon is indeed the limiting nutrient (Fig 2.4A). Each growth curve follows the same phase I (exponential growth) with identical $\mu_{max}$ values (0.33 $h^{-1}$). We observed that once the carbon in the media is fully consumed, cell growth stops abruptly and the population shifts sharply from phase I to phase III (decay) without going through a period of slowed growth (phase II). We carried out additional growth experiments, now in limiting concentrations of nitrogen. As before, population density and phase I time scale with initial nitrogen concentration, confirming that nitrogen is the limiting nutrient (Fig 2.4B). In nitrogen starvation the growth rate drops at the end of phase I but, unlike carbon starvation, population density continues to increase until the end of our observation period (approximately 45 hours). Throughout this period of slowed growth (phase II), the growth rate is continually decreasing.

Finally, we conducted experiments with iron as the growth-limiting nutrient. Increasing the amount of supplemented iron in the media increases both the population density and phase I, confirming that iron is the limiting nutrient (Fig 2.4C). Interestingly, the behavior under iron-limiting conditions was qualitatively distinct from both carbon and nitrogen limitation. In iron-limited growth there is still a transition from phase I to phase II, however this transition is gradual. The growth rate continually slows from $\mu_{max}$, unlike the abrupt transition to phase II seen in nitrogen limitation. In the iron limitation titration, there is an uneven spacing between the curves; doubling the supplemented iron did not result in a doubling of total population density. This can be explained by a constant yield for iron ($Y_{Fe}$) and the presence of trace iron in the growth media. If trace iron is present then doubling the amount of supplemented iron will not double the total amount of iron in the system, but rather add to the trace amount already present. To test this explanation, we used the population density data from the iron titrations (Fig 2.4C), which fell on a line with slope $Y_{Fe}$ (Fig 2.5), to calculate the level of trace iron present in our non-iron

supplemented media, $Fe_0 = 1.4 \times 10^{-5}$ gFe/L. To additionally confirm the presence of trace iron in the media, we grew bacteria in media with no iron supplemented. As expected, the population was able to sustain a phase I (Fig 2.6) in this medium and grew to the population density predicted by our trace iron calculation (Fig 2.5C). See Table 2.1 for information regarding biological and technical replicates.

**Figure 2.4 Bacterial growth behavior under different limiting conditions in batch culture.** All growth curves are aligned to OD = 0.01 at 10 hours. See Table 2.2 for lag phase times. Shaded area represents full range; data lines represent the median. (A) Growth of P. aeruginosa populations limited by carbon. The population transitions from phase I immediately to phase III when carbon is depleted with no observed period of slow growth. (B) Growth behavior of populations limited by nitrogen. The populations abruptly transition from phase I to phase II when nitrogen is depleted. (C) Growth behavior of populations grown in limiting concentrations of iron. The populations gradually transitions from phase I to phase II when iron is depleted from the media. For D-F the model is in thick lines and the data in thin lines. (D) Mathematical model of growth in carbon-limited media. Growth halts when carbon is depleted from the media. (E) Mathematical model of growth in nitrogen-limited media. Phase II growth is driven by an intracellular pool of nitrogen. (F) Mathematical model of growth in iron-limited media. Phase II growth is driven by an intracellular pool of iron. (G) Experimental scheme for testing growth behavior in the absence of extracellular carbon or nitrogen. (H) Growth of the population that will be used in the depletion experiment. The population was grown to exponential phase in synthetic media rich in carbon, nitrogen and iron. I. Cells harvested from the population in H were washed and placed in one of the limiting media. The population without extracellular nitrogen is able to grow and increase in OD, while the population without extracellular carbon decays in OD. The data displayed is from a representative experiment from the biological replicates listed in Table 2.1. The number of technical replicates is listed in Table 2.1.

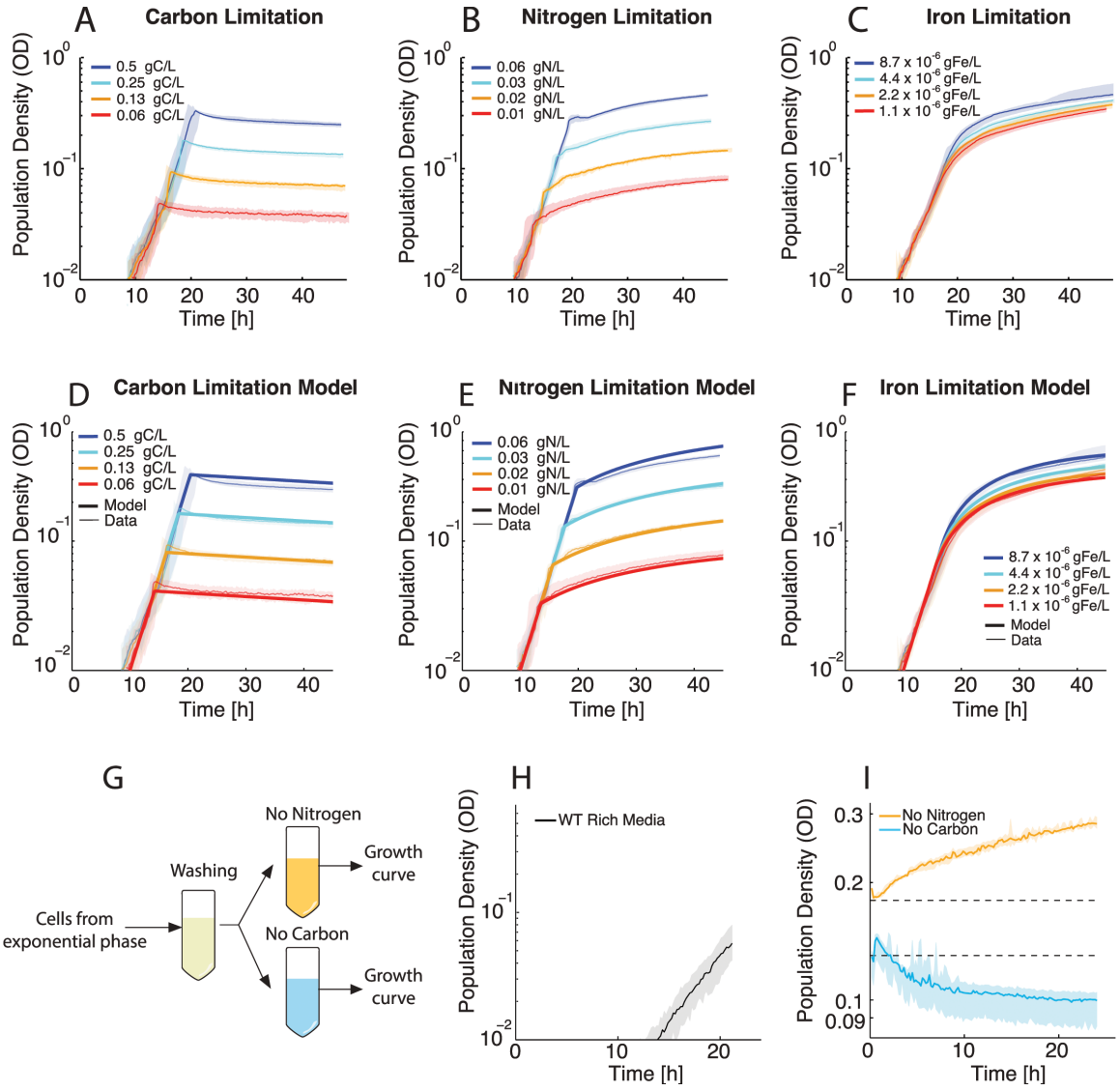
A
Carbon Limitation
0.5 gC/L
0.25 gC/L
0.13 gC/L
0.06 gC/L
Population Density (OD)
Time [h]
B
Nitrogen Limitation
0.06 gN/L
0.03 gN/L
0.02 gN/L
0.01 gN/L
C
Iron Limitation
8.7 x 10-6 gFe/L
4.4 x 10-6 gFe/L
2.2 x 10-6 gFe/L
1.1 x 10-6 gFe/L
D
Carbon Limitation Model
Model
Data
E
Nitrogen Limitation Model
F
Iron Limitation Model
G
No Nitrogen
Washing
Growth curve
Cells from exponential phase
No Carbon
H
WT Rich Media
I
No Nitrogen
No Carbon

## Table 2.1 Biological and Technical Replicates

| Experiment | Carbon Limitation | Nitrogen Limitation | Iron Limitation | Nutrient Depletion | Quorum Sensing |
|---|---|---|---|---|---|
| Replicate Wells for displayed experiment | 6 | 12 | 6 | 6 | 6 |
| Biological Replicates | 3 | 3 | 3 | 4 | 3 |

## Table 2.2 Lag Phases

| Growth Curve | Lag Phase [hours] |
|---|---|
| **Carbon Limitation** | |
| 0.50 gC/L | 4.4228 |
| 0.25 gC/L | 3.9737 |
| 0.125 gC/L | 3.6973 |
| 0.063 gC/L | 3.0001 |
| **Nitrogen Limitation** | |
| 0.0625 gN/L | 3.1000 |
| 0.0312 gN/L | 4.3812 |
| 0.0156 gN/L | 2.6570 |
| 0.0078 gN/L | 3.2814 |
| **Iron Limitation (Supplemented Concentration)** | |
| $6.981 * 10^{-5}$ gFe/L | 2.7400 |
| $3.490 * 10^{-5}$ gFe/L | 2.6322 |
| $1.745 * 10^{-5}$ gFe/L | 2.6269 |
| $8.726 * 10^{-6}$ gFe/L | 3.2804 |
| $4.362 * 10^{-6}$ gFe/L | 3.1083 |
| $2.181 * 10^{-6}$ gFe/L | 3.5053 |
| $1.089 * 10^{-6}$ gFe/L | 4.5329 |
| 0 gFe/L | 4.6104 |
| **Quorum Sensing** | |
| 4 X | 6.5532 |
| 2 X | 6.4149 |
| 1 X | 6.4797 |
| ½ X | 6.2006 |
| ¼ X | 5.4931 |
| 0 | 4.1117 |

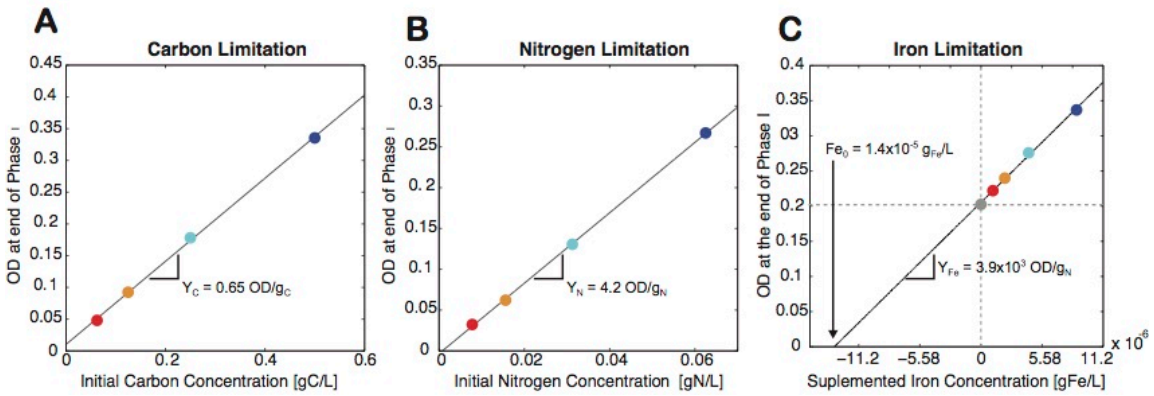


**Figure 2.5 Nutrient Yields**

All data is taken from the growth curves shown in Fig 2.4A–2.4C. A-B Note that the line intersects close to 0 OD and 0 initial concentration for both nitrogen and carbon indicating that trace quantities of these nutrients are not present in the media. (A) Yield of OD per gC/L in the media. The constant slope indicates a constant yield for carbon. Blue 0.5 gC/L, light blue 0.25 gC/L, orange 0.125 gC/L, red 0.0625 gC/L. (B) Yield of OD per gN/L in the media. The constant slope indicates a constant yield for nitrogen. Blue 0.0625 gN/L, light blue 0.0313 gN/L, orange 0.0156 gN/L, red 0.0078 gN/L. (C) Yield of OD per gFe/L supplemented to the in the media. The grey point represents the yield for growth on trace iron alone with no iron supplemented to the media. Absolute value of the point where the regression intersects the X-axis is the trace iron concentration. Supplemented iron concentrations: Blue 8.712 x 10–6 gFe/L, light blue 4.356 x 10–6 gFe/L, orange 2.178 x 10–6 gFe/L, red 4.356 x 10–6 gFe/L, gray 0.0 gFe/L. For all panels: yield of OD produced is determined from the end of phase I by hand for all points shown and the black line represents a linear regression for the data.

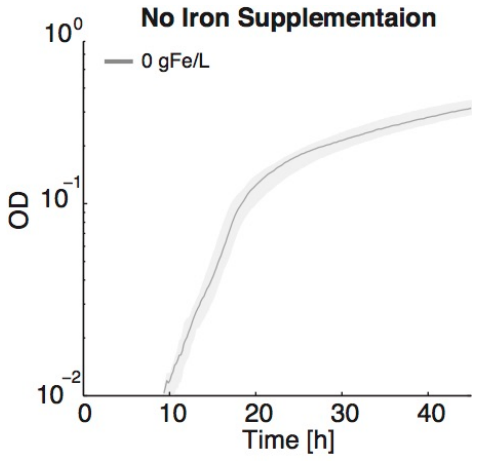


**Figure 2.6 Growth with no iron supplementation**

The population was grown in media with 3.0 gC/L and 0.5 gN/L with no iron added to the media. As predicted from the yield calculations in Fig 2.5C the population is able to grow and sustain exponential growth at the same growth rate as the populations supplemented with iron. The population also reaches the OD predicted by the calculated amount of trace FIg 2.5C.

## Mathematical Model Suggests Growth with Internal Nutrient Pools

In order to investigate how the nutrient levels experienced by cells influence their growth, we created a mathematical model of *P. aeruginosa* growth kinetics. Using the data from the experiments described above where we manipulated the media composition such that carbon, nitrogen, or iron become limiting, we were able to construct a kinetic model based on mass conservation, where biomass production is a function of these three nutrients. Central to this model was the calculation of the yields of biomass produced (in units of OD) per amount of carbon ($Y_C$), nitrogen ($Y_N$) and iron ($Y_{Fe}$) consumed (Fig 2.5). One benefit of this properly calibrated model is the calculation nutrient levels at any given time in the growth curve, which could not be directly measured with our assay.

Bacterial growth limitation due to depletion of an essential nutrient is commonly modeled using Monod kinetics, which requires two parameters: μmax the maximum specific growth rate, and $K_s$, the half-saturation constant [40,41]. In all of our nutrient limitations and titrations we observe the same $\mu_{max}$ in phase I independently of the initial nutrient concentrations. In order to satisfy this constraint, a Monod model would need to have a $K_s$ value for each nutrient that is significantly below our lowest titration value ($K_s$<<0.063 gC/L, $K_s$<<0.0078 gN/L and $K_S$<<1.4 x $10^{-5}$ gFe/L for carbon, nitrogen and iron respectively). In a Monod model, such a low $K_s$ will give a very sharp transition from maximal growth to practically no growth. For carbon limitation we do observe this sharp transition behavior. This behavior is somewhat unexpected as the population might be predicted to slow in growth rate as carbon becomes increasingly scarce. This suggests that the half saturation constant value for carbon is indeed $K_s$<<0.063 gC/L and in order to measure its actual value we would need to monitor population density at OD values below the detection limit of our growth curve assay (OD = 0.01). Therefore, we instead model carbon (C) consumption as a step function with a constant yield $Y_C$ (Fig 2.5A and Eq (2)). This model recapitulates the growth behavior observed in carbon limitation media (Fig 2.4D).

Nitrogen and iron limitation growth curves, on the other hand, are inconsistent with a Monod model even with a Ks value below the lowest titration concentration. Although there is a sharp transition in nitrogen limitation from phase I to phase II, the sustained growth in phase II is incompatible with a Monod model. A Monod model with a low $K_s$ also cannot explain the gradual slowdown in growth rate observed in iron limitation. There are a few possible explanations for the observed curvature in the nitrogen and iron limitations that we can exclude based on the data. Firstly, consistent phase II behavior across titrations excludes the possibility of a toxic product accumulating, as the populations with higher cell densities are not more severely affected. For nitrogen, the

yield calculations predict no contaminating trace nitrogen amounts (Fig 2.5B). The possibility of a contaminating trace nitrogen that is used only in phase II is also eliminated as this would result in the populations with lower cell densities growing much more than the populations with higher cell densities for a given amount of trace nitrogen, and instead phase II behavior is consistent across the titrations.

The nutrient source for phase II growth in nitrogen and iron limitation must scale with population density and is independent of the starting nutrient concentration. A model that fits these criteria is one where the transition from phases I to II represents a switch in cellular metabolism from growth on extracellular nitrogen or iron (upon complete depletion of the limiting nutrient from the media) to intracellular nitrogen or iron [42]. Such growth behavior has been observed before in the yeast *Saccharomyces cerevisiae*. *S. cerevisiae* could grow in the absence of extracellular nitrogen by using nitrogen-rich intracellular biopolymers, presumably protein, and decreasing the nitrogen-to-carbon ratio of its biomass composition [43].

To determine if a model of *P. aeruginosa* utilizing internal nutrient pools for growth, like *S.cerevisiae*, could explain the observed behavior, we created a mathematical model to account for an internal nitrogen pool, internal iron pool, and trace iron. In this model, the cells consume extracellular nutrients to produce biomass and maintain homeostatic levels of intracellular nutrient pools while growing exponentially ($N_i$, $Fe_i$) (Eq (3) and (5)). When the nitrogen or iron in the media is fully depleted, the cells switch to growth on the intracellular pool of the depleted nutrient, which then gradually decreases over time as the cells grow (Eq (4) and (6)). Because we cannot directly measure the size of the internal pool of nitrogen or iron, we normalize it by the size of the pool during balanced growth; both $N_i$, and $Fe_i$ are dimensionless. Each cell enters phase II with $N_i$ or $Fe_i = 1$ and this internal pool is then depleted for cell growth and diluted through cell division.

The current growth rate of the population, μ(t), is dependent on the fraction of the internal pool in each cell. As the internal pool is depleted, growth slows from $\mu_{max}$ (Eq (7)).

The kinetics of biomass (X) (Eq (1)), growth and nutrient consumption of our different limiting nutrients are therefore given by:

$$\frac{dX}{dt} = \begin{cases} \mu(t)\,X & \text{if } C > 0 \\ (\mu(t) - k_d)X & \text{if } C = 0 \end{cases} \quad (1$$

$$\frac{dC}{dt} = -\frac{1}{Y_C}\mu(t)X \qquad \text{if } C > 0 \quad (2$$

$$\frac{dN}{dt} = \begin{cases} -\frac{1}{Y_N}\mu(t)\,X & \text{if } N > 0 \\ 0 & \text{if } N = 0 \end{cases} \quad (3$$

$$\frac{dN_i}{dt} = \begin{cases} -\left(\frac{1}{Y_N} + N_i\right)\mu(t) & \text{if } N = 0 \text{ and } N_i > 0 \\ 0 & \text{if } N > 0 \end{cases} \quad (4$$

$$\frac{dFe}{dt} = \begin{cases} -\frac{1}{Y_N}\mu(t)\,X & \text{if } Fe > 0 \\ 0 & \text{if } Fe = 0 \end{cases} \quad (5$$

$$\frac{dFe_i}{dt} = \begin{cases} -\left(\frac{1}{Y_{Fe_i}} + N_i\right)\mu(t) & \text{if } Fe = 0 \text{ and } Fe_i > 0 \\ 0 & \text{if } Fe > 0 \end{cases} \quad (6$$

where μ(t) is the current specific growth rate. Nitrogen and iron use the same internal nutrient pool model.

We find that in addition to accounting for trace iron in the media and internal nutrient pools of nitrogen and iron, we also must postulate that the maximum growth rate while

using internal nitrogen is lower than μmax here termed $\mu_{max}'$. This postulation is required to explain the sharp transition from phase I to phase II observed in nitrogen limitation (Fig 2.4B). As the transition in iron limitation is more gradual, this postulation is not required for growth on internal iron and thus we do not assume a switch from $\mu_{max}$ to an alternative value ($\mu_{max}'$) in iron limitation. Using this model, we are able to capture the dynamics observed in the experimental data (Fig 2.4D–2.4F). The equation set that determines μ(t) for the different nutrient conditions is given below

$$\begin{aligned} \mu(t) &= \mu_{max} && for\ C, N\ and\ Fe > 0 \\ \mu(t) &= 0 && for\ C = 0 \\ \mu(t) &= \mu_{max} \times Fe_i && for\ Fe \\ \mu(t) &= \mu_{max}' \times N_i && for\ N = 0 \end{aligned} \qquad (7$$

**Nutrient Depletion Experiment Supports Model with Internal Nutrient Pools**

To test our internal nutrient model experimentally, we designed a nutrient depletion experiment (Fig 2.4G). The experiment was only performed for carbon and nitrogen as trace iron prevents the depletion experiment for iron. Cells were grown to exponential phase in rich synthetic media (Fig 2.4H) and then harvested while still in balanced growth, washed, and separately inoculated in media lacking either carbon or nitrogen. As predicted by our model, the cells in media lacking nitrogen were able to grow and increase in population density (Fig 2.4I) whereas in the absence of carbon, the population transitioned immediately to phase III and population density started to decrease (Fig 2.4I), supporting our model that total carbon depletion causes transition to phase III. These results are consistent with the model for phase II of nitrogen limitation and phase III of carbon limitation. We were unable to perform this experiment for iron limitation in the same manner due to the fact that medium without supplemented iron contains trace

amounts of this nutrient (Fig 2.5C). Nonetheless, the model with an internal iron pool is still able to describe the observed growth behavior in iron limitation (Fig 2.4F).

In summary, we developed a model of *P. aeruginosa* kinetics that successfully captures the observed growth dynamics. In total, the model has eight free parameters, which we were able to parameterize using growth curve experiments to derive the nutrient yields, $Y_C$, $Y_N$, and $Y_{Fe}$, as well as kinetic parameters (Fig 2.7 and Table 2.3). We find that for carbon limitation, a Monod model (where growth slows with decreasing concentration of the limiting nutrient) with a very low $K_s$ can explain the data, leading to a very sharp transition from exponential growth to no growth with virtually no slow down due to decreasing availability of carbon in the media (Fig 2.4D). The growth model also reveals that growth behavior in both nitrogen and iron limitation, under these conditions, is incompatible with an explanation using a Monod model. However, the behavior observed in these limiting conditions can be explained using a model of intracellular nutrient pools (Fig 2.4E and 2.4F), which is experimentally supported for nitrogen limitation (Fig 2.4I). A model using these intracellular nutrient pools is required to accurately capture bacterial growth dynamics and recapitulate the observed growth rate. This phenomenological model can be used to constrain the mechanisms of *rhlAB* expression responses we observe in nutrient limitations.

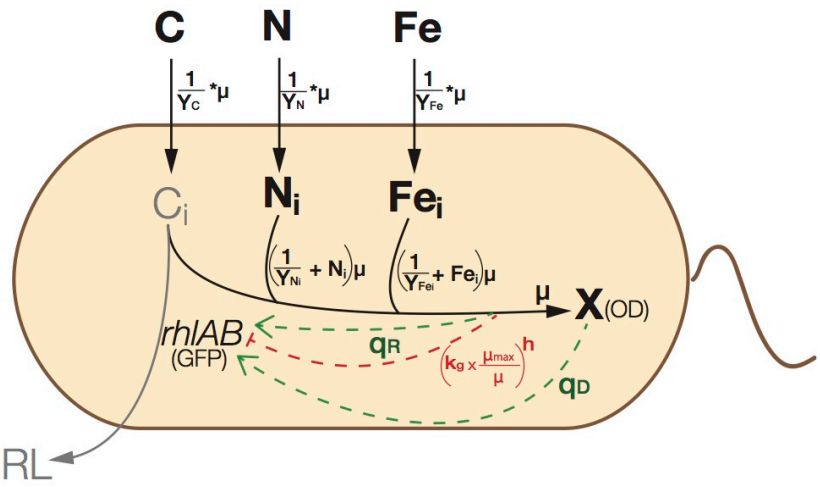


**Figure 2.7 Schematic of mathematical model of bacterial growth and *rhlAB* promoter activity.**

Schematic summarizing the growth model where carbon, nitrogen and iron are taken up into the cell and used to produce biomass. Intracellular pools of nitrogen and iron are used for growth when these nutrients are depleted from the extracellular environment. The three nutrients in the model (C, N, Fe) each have their own yield, which determines how much biomass (X) can be produced per gram of each nutrient. The intracellular pools of nitrogen and iron also have yields to determine what fraction of the intracellular pool is needed to produce a unit of biomass (X). The three components of the rhlAB promoter activity model are also summarized here. Density dependent regulation is scaled by qD, induction by limited growth (calculated from the growth model) is scaled by qR, and shut down of promoter activity when growth becomes extremely limited is determined by kg and the hill coefficient h. Note that the for simplicity the displayed *rhlAB* promoter activity components have been simplified such that qR and $\left(k_g \times \frac{\mu_{max}}{\mu}\right)^h$ represent $q_R \left(\frac{\mu_{max}(\prime)}{\mu} - 1\right)$ and $\frac{1}{1+\left(k_g \times \frac{\mu_{max}}{\mu}\right)^h}$ respectively. Together the *rhlAB* promoter activity components result in density dependent promoter activity during phase I, limited growth induced promoter activity during phase II, and an eventual shut down of promoter activity during prolonged phase II growth. Also note that C, N and Fe can all be experimentally manipulated and that X and rhlAB activity are measured experimentally using OD and GFP respectively. State variables, C, N, Fe, Ni, Fei, and X, are shown in bold. Components not explicitly modeled, Ci (intracellular carbon) and RL (rhamnolipids), are shown in gray.

**Table 2.3 Table of kinetic parameters**

| Parameter | Units | Represents | Value in displayed fit |
|---|---|---|---|
| $\mu_{max}$ | $h^{-1}$ | Maximum growth rate when N>0 | 0.3341 |
| $Y_C$ | OD/gC | Yield for carbon | 0.6516 |
| $k_d$ | $h^{-1}$ | decay when C=0 | 0.0062 |
| $Y_N$ | OD/gN | Yield for nitrogen | 4.1627 |
| $\mu_{max}'$ | $h^{-1}$ | Maximum growth rate when N = 0 | 0.0616 |
| $Y_{Ni}$ | OD/$N_i$ | Yield for internal nitrogen | 2.0011 |
| $Y_{Fe}$ | OD/gFe | Yield for iron | $3.8952 * 10^3$ |
| $Y_{Fei}$ | OD/$I_i$ | Yield for internal iron | 4.9892 |
| $q_D$ | GFP/OD | Density dependent scaling factor | $1.8542 * 10^4$ |
| $q_{RN}$ | GFP | Nitrogen starvation upregulation scaling factor | $7.4541 * 10^3$ |
| $k_{gN}$ | - | Fraction of $\mu_{max}$ in nitrogen starvation when down regulation begins | 0.1667 |
| $h_N$ | - | Hill coefficient nitrogen starvation down regulation | 5.8725 |
| $q_{RFe}$ | GFP | Iron starvation upregulation scaling factor | $8.5933 * 10^3$ |
| $k_{gFe}$ | - | Fraction of $\mu_{max}$ in iron starvation when down regulation begins | 0.3293 |
| $h_{Fe}$ | - | Hill coefficient iron starvation down regulation | 4.9892 |

## *rhlAB* Promoter Response to Nutrient Limitation and Population Density

Rhamnolipid production is a dynamic process and changes in *rhlAB* expression coincide with transitions between growth phases, which are difficult to capture experimentally. Our growth model provides us with an understanding of the conditions cells experience throughout growth and the growth rate response to changes in the nutrient environment. We can use this understanding to interpret the expression response of *rhlAB* under these conditions. Our measurements of GFP driven by the *rhlAB* promoter (Fig 2.8A–2.8C) were taken simultaneously with the population density measurements (Fig 2.4A–2.4C) in the different limiting nutrient conditions. Using GFP (Fig 2.8A–2.8C) and OD

measurements (Fig 2.4A–2.4C), we calculated the promoter activity for *rhlAB* throughout the time series (Fig 2.8D–2.8F), with compensation for GFP dilution by cell division (see Promoter Activity Calculation). Note that promoter activity fluctuates more at the early time points because there is more noise at low OD measurements due to technical limitations of the equipment. We use our mathematical model of growth to systematically identify when the population exits phase I (exponential phase). In Fig 2.8, expression during phase I is shown in solid lines while expression that occurs after phase I (phase II or III) is shown in dashed lines. Our study and model of growth behavior in this media revealed that entry into phase II or III indicates starvation by the limiting nutrient, therefore promoter activity that occurs after phase I occurs during nutrient starvation.

**Figure 2.8 *rhlAB* promoter activity during different phases of growth in nutrient limitation batch culture**.

GFP and promoter activity data are from the same growth curves shown in Fig 2.4. Phase I GFP data and promoter activity are shown in solid lines while data corresponding to phase II or III are shown in dashed lines. Phases were determined by the mathematical model for bacterial growth discussed in the text. (A) Population *rhlAB* (GFP) expression in carbon limitation media. Expression only occurs during phase I. (B) Population *rhlAB* (GFP) expression in nitrogen limitation media. Expression occurs during both phase I and phase II. (C) Population *rhlAB* (GFP) expression in iron limitation media. Expression occurs during phase I, but the majority of GFP production occurs during phase II. Iron limitation hits the saturation for GFP in our conditions ~ $6.0923 \times 10^4$ Arbitrary fluorescence units. D-F $P_{rhlAB}$ activity (see Promoter Activity Calculation) from growth curves in different limitation media. (D) In carbon limitation growth curves *rhlAB* promoter activity occurs during phase I and drops to zero during phase III for all titrations. (E) In nitrogen limitation growth curves promoter activity occurs during phase I and is sustained during phase II for all titrations after an initial decrease at the end of phase I. (F) In iron limitation growth curves promoter activity occurs during phase I and increases at the onset of phase II for all titrations. G-I *rhlAB* promoter activity from limitation growth curves plotted against population density (OD). (G) Promoter activity from carbon limitation growth curves increases with density during phase I. (H) Promoter activity from nitrogen limitation increases with population density during phase I and shows consistent qualitative behavior in phase II at different population densities. I. Promoter activity in iron limitation growth curves also increases with population density during phase I and shows consistent qualitative behavior in phase II at different population densities. Median data is shown in lines with the full range of technical replicates indicated by shaded area.

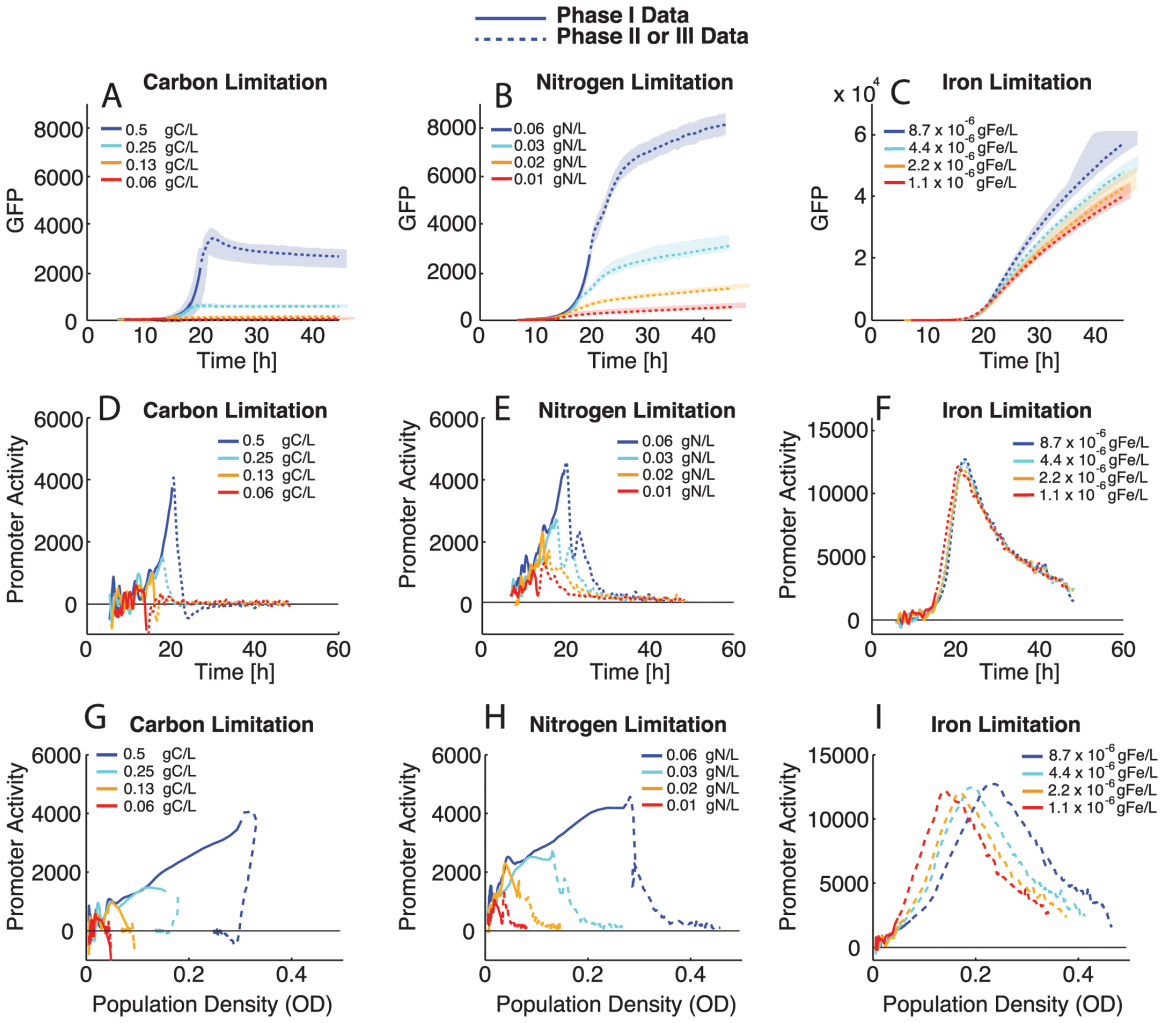
Phase I Data
Phase II or III Data
A
Carbon Limitation
0.5 gC/L
0.25 gC/L
0.13 gC/L
0.06 gC/L
GFP
Time [h]
B
Nitrogen Limitation
0.06 gN/L
0.03 gN/L
0.02 gN/L
0.01 gN/L
C
Iron Limitation
x 10^4
8.7 x 10^-6 gFe/L
4.4 x 10^-6 gFe/L
2.2 x 10^-6 gFe/L
1.1 x 10^-6 gFe/L
D
Promoter Activity
E
F
G
Population Density (OD)
H
I

Previous work suggests that *rhlAB* expression occurs exclusively when carbon is in excess [23,36,44]. However, we unexpectedly observe appreciable *rhlAB* expression and promoter activity in carbon-limited media (Fig 2.8A and 2.8D and 2.8G). Expression in carbon-limited media occurs during phase I and promoter activity drops to zero when the population enters phase III. (The negative promoter activity values computed in carbon limitation media experiments (Fig 2.8D) are artifacts caused by a rapid increase in OD consistently occurring immediately before carbon starvation, coinciding with a shut off of *rhlAB* expression and beginning decay in the GFP signal.)

It is interesting that promoter activity increases throughout phase I, as it could be expected that there would be a constant level of expression during balanced growth and promoter activity would equilibrate quickly. However, increasing promoter activity during phase I is observed in all three limitation conditions (Fig 2.8D–2.8F, solid lines). This phase I promoter activity could be due to the fact that even during exponential growth there is carbon available in excess of what is needed for biomass production, and this carbon can be dedicated to rhamnolipid synthesis. The promoter activity in phase I increases with population density in all conditions suggesting that this expression is density dependent (Fig 2.8G–2.8I). By overlaying phase I of all conditions and plotting against population density we confirm a consistent slope across all conditions, suggesting that the mechanism driving the density dependent expression is the same in all three limitation conditions (Fig 2.9A).

In nitrogen limited media there is not a complete shutdown of expression after phase I. Instead, population level GFP continues to increase in phase II (Fig 2.8B). The promoter activity drops, but is sustained, with a second peak of activity occurring before tapering off to near zero (Fig 2.8E). In contrast, *rhlAB* promoter activity during phase II of iron limitation rapidly increases without an initial drop when the population enters phase II.

Promoter activity of *rhlAB* decreases over time, but never reaches zero in our iron limitation condition (Fig 2.8F). The level of promoter activity reached in iron limitation is much higher than that in nitrogen limitation when the highest titrations are compared directly (Fig 2.9B). We also observe that even in nitrogen and iron starvation when promoter activity is sustained or induced, activity eventually shuts down, most likely due to the prolonged starvation experienced by the cell.

Similar behavior is observed for all titrations within each limiting media across a wide range of population densities (Fig 2.8G–2.8I). Therefore the limiting nutrient and the duration of starvation appear to be the main drivers of qualitative promoter behavior: shut down of activity in carbon starvation, sustained activity in nitrogen starvation, and induction of activity in iron limitation (Fig 2.9B). Although the qualitative behavior is determined by the limiting nutrient, a closer examination of promoter activity during nitrogen starvation reveals that populations with a higher density have higher *rhlAB* promoter activity even during starvation (Fig 2.9C). This suggests that the cells continue to use density-dependent information to modulate the dynamics of *rhlAB* promoter activity in nitrogen limitation.

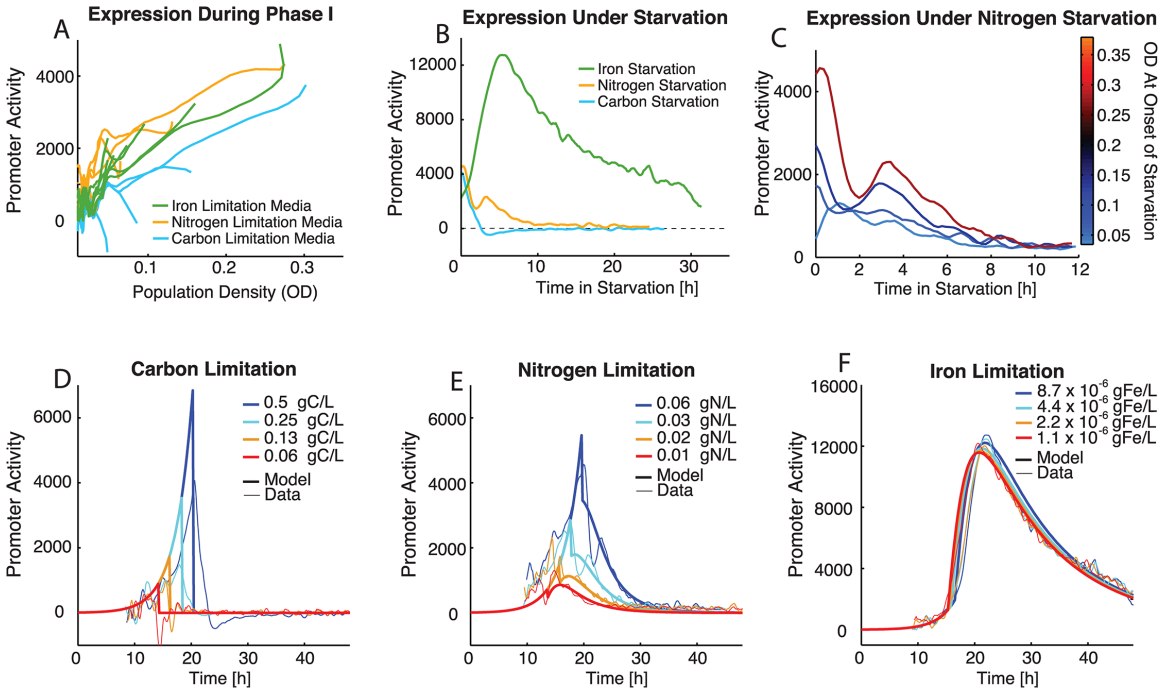


**Figure 2.9 Quantitative analysis of rhlAB promoter dynamics and mathematical model of cooperation.**

(A) Median of experimental data *rhlAB* promoter activity from phase I growth in different limitation media plotted against population density (OD). A similar slope is observed for all limitation media suggesting a consistent relationship between population density and *rhlAB* promoter activity. (B) Median *rhlAB* promoter activity during growth under nutrient starvation over time. *rhlAB* promoter activity increases in iron starvation, is sustained in nitrogen starvation and is shutdown in carbon starvation. The mathematical model of growth systematically determined the start of starvation. Iron starvation initial condition 8.7 x $10^{-6}$ gFe/L, nitrogen starvation initial condition 0.6 gN/ L, carbon starvation initial condition 0.5 gC/L, all shown in Fig 2.8D–2.8F. (C) Median *rhlAB* promoter activity from phase II of nitrogen limited populations (Fig 2.8E). Populations with higher density at the onset of starvation have higher *rhlAB* promoter activity during nitrogen starvation. D-F Mathematical model of *rhlAB* promoter activity compared to experimental data. The model is shown in thick lines and median experimental data is shown in thin lines. A model integrating nutrient starvation and population density is able to capture the many aspects of *rhlAB* promoter activity during periods of balanced and limited growth. (D) Carbon limitation media. (E) Nitrogen limitation media. (F) Iron limitation media.

**Phenomenological Model of the Cellular Decision to Cooperate**

To determine if our current understanding of the *rhlAB* promoter response was sufficient to explain the observed dynamics, we derived a mathematical expression of $P_{rhlAB}$-*gfp* promoter activity. The model contains three components. The first component implements the density-dependent up-regulation observed during balanced growth (Fig 2.9A). The second component implements the observation from here, and in previous work, that *rhlAB* is expressed under nutrient starvation when growth is limited, but not halted (Fig 2.9B, nitrogen and iron starvation) [23,36]. Since promoter activity under starvation is also a function of population density (Fig 2.9C), we use an additive model to describe the integration of population density and nutrient starvation induction. The third component implements a decrease in promoter activity that is observed under prolonged starvation by either nitrogen or iron (Fig 2.9B). Prolonged starvation shutdown is implemented using Hill kinetics.

Our mathematical model of bacterial growth predicts not only nutrient levels over time, but also the effect of these nutrient levels on growth rate. With an accurate prediction of μ(t), from the growth model, and an understanding of the nutrient environment the cells experience in phases II and III, we are able to use growth rate as an indicator of cell starvation. Therefore, expression under starvation is implemented by induction when μ(t) falls below μmax ($\mu_{max}$' for nitrogen starvation). Promoter activity only occurs when carbon has not been depleted in the media. By using μ(t) as an indicator of starvation, rather than absolute nutrient values, our model remains flexible and can be adapted to multiple limitations of these nutrients or additional limiting nutrients. Two variables are required for converting the expression to GFP units and scaling the different components. The variable $q_D$ is used to scale the density dependent activity component and is the same

value for all nutrient conditions. The variable $q_R$ is used to scale the starvation induced promoter activity. Consistent with our observations that expression under nutrient starvation depends on the limiting nutrient (Fig 2.9B), different values of $q_R$ are required to achieve the observed levels of activity in nitrogen or iron limitation ($q_{RN}$ and $q_{RFe}$ respectively)

Activity during prolonged starvation shuts down progressively when μ(t) has decreased further and falls below a threshold fraction of μmax define here as $k_g$. We find again that the limiting nutrient has a great effect on promoter activity and to implement the appropriate shutdown in both nitrogen and iron limitation the values for $k_g$ and h must be adjusted for each limitation ($k_{gN}$, $h_N$ and $k_{gFe}$, $h_{Fe}$ respectively). Although we must adjust for the different starvation conditions of nitrogen and iron, a parameterized three-component model of *rhlAB* expression (Eq (8)) is able to recapitulate the observed expression dynamics under our different nutrient limitations (Fig 2.9D–2.9F).

$$P_{rhlAB} = \left(q_D X + q_R \left(\frac{\mu_{max}(\prime)}{\mu} - 1\right)\right) \times \frac{1}{1+\left(k_g \times \frac{\mu_{max}}{\mu}\right)^h} \qquad (8$$

Although it is perhaps at first unsatisfying that the fitted parameters must be changed to account for behavior in both nitrogen and iron starvation, this ultimately supports that the internal state of the cell, which drives *rhlAB* promoter activity, is significantly different in these two conditions. By eye it is not clear if the growth rate and population size differences could be sufficient to explain the different behavior in the two starvation conditions. However, even by taking the observable differences into account we found no model or single parameter set that could sufficiently explain promoter activity in both starvation conditions simultaneously.

We find that this model is capable of capturing the observed dynamics and indicates that the metabolic signal for expression is potentially at different levels during nitrogen and iron starvation or that downstream regulation is different in these two limitations. The use of μ(t) from our growth model functions as an indicator of starvation and accurately predicts the response of the *rhlAB* promoter to nutrient starvation. Importantly, both density-dependent regulation and metabolic regulation are required in the model as non-digital regulatory components to recapitulate the observed expression dynamics in all nutrient conditions.

**Experimental Test of the Role of Quorum Sensing**

Previous work has shown that quorum sensing is required for *rhlAB* expression, however our observation of a gradual increase in *rhlAB* promoter activity as population density increases (Fig 2.9A) suggests a more nuanced role for quorum sensing in *rhlAB* expression. To confirm that quorum sensing does mediate the density-dependent component of *rhlAB* expression and to explore the effect of perceived density on *rhlAB* promoter activity, we utilized a quorum sensing mutant that does not produce the *lasI/lasR* nor *rhlI/rhlR* system autoinducers $C_{12}$HSL (*N*-(3-oxododecanoyl)-L-homoserine lactone) and $C_4$HSL (*N*-butyryl-L-homoserine lactone), respectively and we manipulated the levels of autoinducers in the medium. This strain (PA14 Δ*lasI* Δ*rhlI* *attB*::$P_{rhlAB}$-*gfp*) has the same $P_{rhlAB}$-*gfp* reporter as our wild-type strain (Fig 2.10A).

We first performed an extensive test of *rhlAB* induction across a wide range of autoinducer concentrations by varying the concentrations of each autoinducer independently (Fig 2.11). The data revealed that although one autoinducer can compensate for a lack of the other, this requires very high levels of that single autoinducer, which are likely not biologically relevant. We also observed that when both

autoinducers are increased in concentration, but kept in the same proportion, there is a consistent increase in *rhlAB* expression. We proceeded with a fixed 1:5 ratio of $C_{12}$HSL to $C_4$HSL used previously [36]. To isolate the density-dependent component of expression, the Δ*lasI*Δ*rhlI* strain was grown in carbon-limited media complemented with different concentrations of C12HSL and C4HSL kept at a 1:5 ratio (Fig 2.10B).

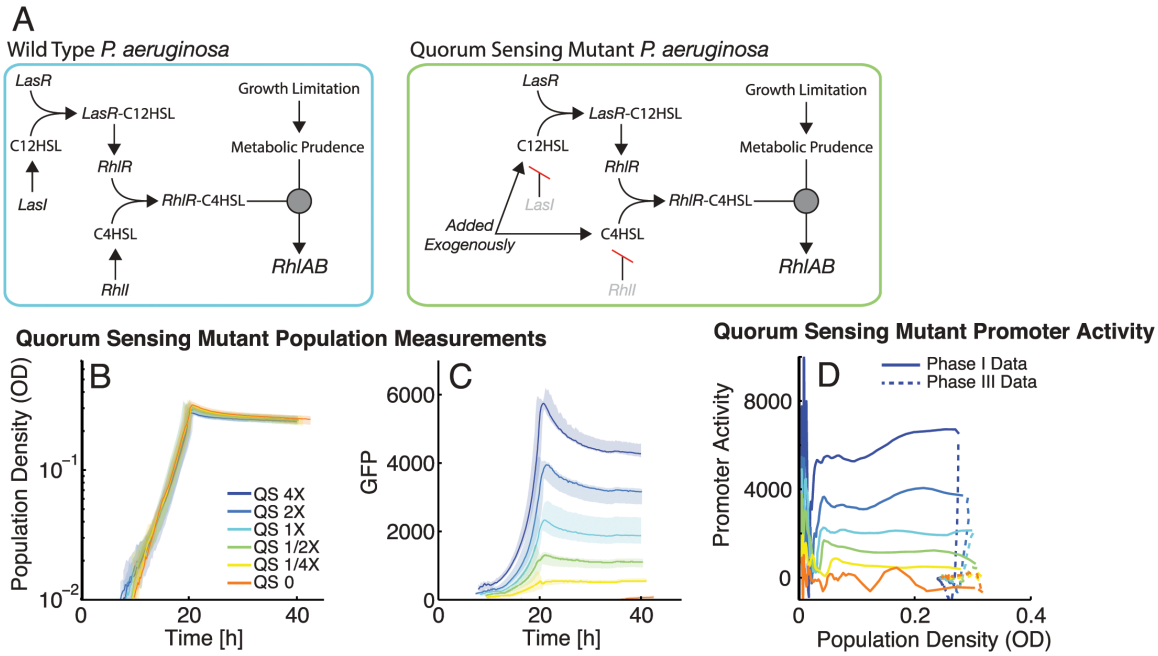


**Figure 2.10 Density-dependent scaling of rhlAB expression is controlled by quorum sensing autoinducers.**

(A) Quorum sensing regulatory cascade in P. aeruginosa WT and in the quorum-sensing mutant, which lacks the genes encoding LasI and RhlI. Median is shown in thick lines with full range indicated by shaded area. All growth curves are aligned to OD = 0.01 at 10 hours. See Table 2.2 for lag times. (B) Growth of the ΔlasIΔrhlI bacterial populations in carbon limitation media with 0.5 gC/L and different concentrations of auto inducer 1 X = 1 μM C12HSL and 5 μM C4HSL. 1X is estimated to be physiological and has recovered the WT level of rhamnolipid production in previous work [19]. (C) GFP expression for each population. Populations that received higher levels of autoinducer express higher levels of GFP. (D) $P_{rhlAB}$ activity in different concentrations of autoinducer plotted against population density. Activity holds constant during phase I and rapidly shuts off at the onset of phase III. Phase I is shown in solid lines and phase III in dashed lines.

Higher total levels of *rhlAB* expression were observed with higher concentrations of quorum sensing signal (Fig 2.10C). Importantly, promoter activity of *rhlAB* became constitutive during phase I (exponential growth) confirming that quorum sensing modulates expression during that phase (Fig 2.10D). In contrast to promoter activity of the wild-type PA14 strain (WT) during exponential growth, phase I promoter activity in the mutant is decoupled from population density (Fig 2.10D, compared with Fig 2.9A). The constitutive level of promoter activity in the mutant scales with the concentration of the autoinducers in the medium, as predicted from the relationship between population density and *rhlAB* promoter activity we observed and modeled in the WT.

We hypothesize that this phase I promoter activity behavior is the result of quorum sensing signals inducing promoter activity when there is a constant level of carbon-rich metabolites present inside the cell during balanced growth in this medium. Because the level of carbon-rich metabolites is constant, promoter activity is modulated only by changes in population density, sensed by quorum sensing signals. Quorum sensing regulation of *rhlAB* is confirmed here to not be a digital switch, but instead produces a graded *rhlAB* expression response. Also, the shutdown of *rhlAB* promoter activity due to carbon depletion occurs even in the presence of high levels of quorum sensing autoinducers (Fig 2.10D) demonstrating that carbon starvation is capable of overriding the quorum-sensing regulated induction. Using this mutant strain we were also able to confirm that quorum sensing signals scale *rhlAB* promoter activity during starvation by nitrogen or iron (Fig 2.12).

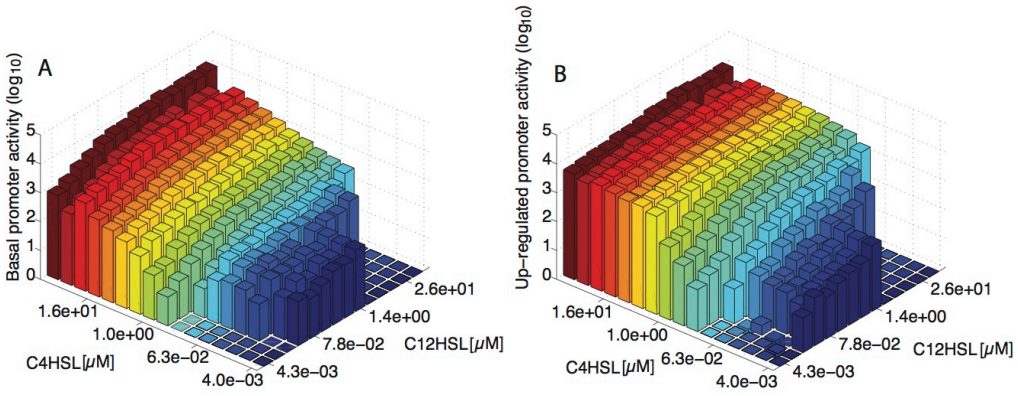


**Figure 2.11 Effect of quorum sensing concentration on *rhlAB* expression.**

(A) Basal rhlAB expression by GFP from the PrhlAB-gfp construct with varying levels of C4HSL and HSL autoinducers in synthetic media. Increasing levels of autoinducers result in increased levels of basal promoter activity. Higher levels of one signal do not directly compensate for low levels of the other. (B) Maximual rhlAB expression by GFP from the PrhlAB-gfp construct with varying levels of C4HSL and HSL autoinducers. Maximal level of expression also increases with increasing levels of autoinducers and again there is not a direct compensation of one for the other. All Cultures were grown in Synthetic media with 3.0 gC/L, 0.5 gN/L and no iron supplementation.

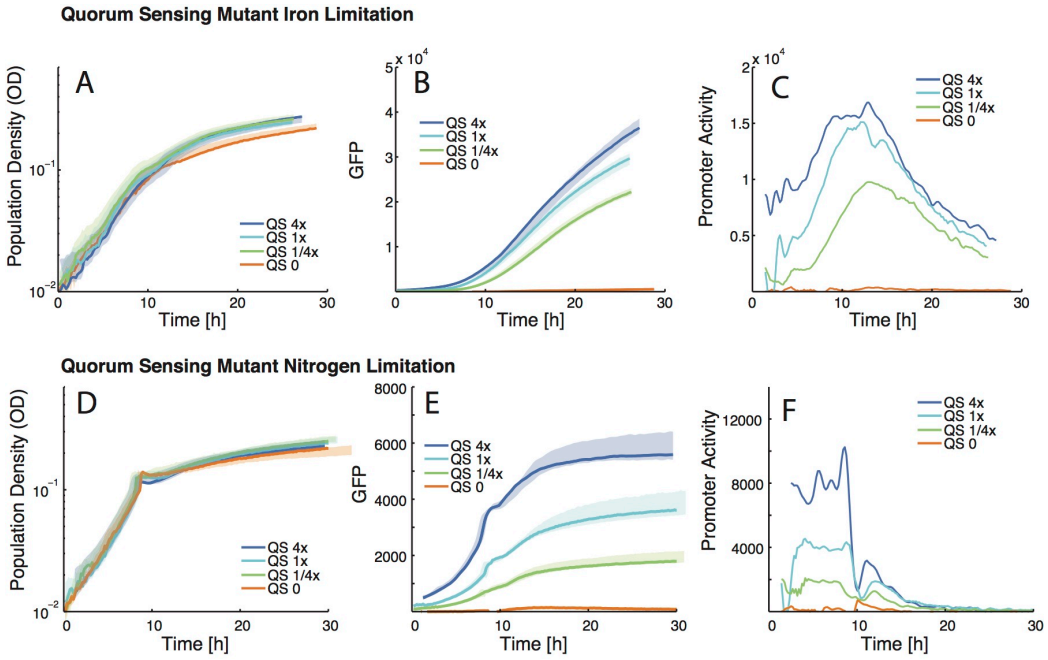


**Figure 2.12 Quorum sensing scales *rhlAB* promoter activity during iron and nitrogen starvation.**

(A) Growth of populations in iron limitation media (0 gFe/L supplemented iron) at different concentrations of quorum sensing signals 1 X = 1 µM C12HSL and 5 µM C4HSL. Growth is similar in different quorum sensing concentrations (B) GFP production in iron limiting media in different concentrations of quorum sensing signals. Higher levels of signal result in higher levels of expression. (C) Promoter activity in iron limitation media in different concentrations of quorum sensing signals. Promoter activity during balanced growth (~0-6h) and promoter activity during starvation (~6-30h) are both scaled by the level of quorum sensing signals. (D) Growth of populations in nitrogen limitation media (0.03 gN/L) at different concentrations of quorum sensing signals 1 X = 1 µM C12HSL and 5 µM C4HSL. Growth is similar in different quorum sensing concentrations (E) GFP production in nitrogen limiting media in different concentrations of quorum sensing signals. Higher levels of signal result in higher levels of GFP expression. (F) Promoter activity in nitrogen limitation media in different concentrations of quorum sensing signals. Promoter activity during balanced growth (~0-10h) and promoter activity during starvation (~10-30h) are both scaled by the level of quorum sensing signals.

**Swarming Cooperation in Nutrient Limitation**

We were able to identify the differential responses of the *rhlAB* promoter to different nutrient limitations and population densities in our liquid culture system. To test the effects of the identified *rhlAB* promoter responses on swarming cooperation, we grew swarming colonies of the Δ*lasI*Δ*rhlI* quorum sensing null strain in different media conditions. Unlike in liquid culture experiments, the media used in swarming assays has to be a complex media where casamino acids serve as the carbon and nitrogen source. In our liquid culture system, we found iron limitation to be a potent inducer of *rhlAB* activity. To test if the integration of quorum sensing signals and iron limitation is required for swarming colony formation we tested several conditions with and without iron limitation and with and without quorum sensing signals. Without quorum sensing signals, the colony is unable to swarm regardless of whether iron is limiting (Fig 2.13A and 2.13B). As predicted from our liquid culture experiments and mathematical models, if a population has quorum sensing signals but lacks iron limitation, the colony does not have normally branching and does not travel far from the inoculation site (Fig 2.13C). This confirms that the significant induction of *rhlAB* promoter activity we observe under iron limitation in our liquid culture system is also key for rhamnolipid production in swarming colonies. Only when a population is provided with both quorum-sensing signals and iron limitation does successful swarming occur (Fig 2.13D). Swarming behavior in these four conditions supports our liquid culture data; significant production of rhamnolipids requires both quorum sensing signals and iron limitation. The observation that iron starvation facilitates swarming cooperation is consistent with our experiments showing that iron starvation induces higher *rhlAB* promoter activity than nitrogen starvation or quorum sensing signals alone (Fig 2.8F) and with previous reports [45,46]. Given these data the induction of *rhlAB* expression in swarming colonies (Fig 2.1D) is likely induced by iron limitation. We also tested the effect of nitrogen limitation,

iron limitation, and additional quorum sensing signals on the WT. We found again that iron limitation is necessary for successful swarming while nitrogen limitation and additional quorum sensing signals only moderately affect swarming colony morphology (Fig 2.14).

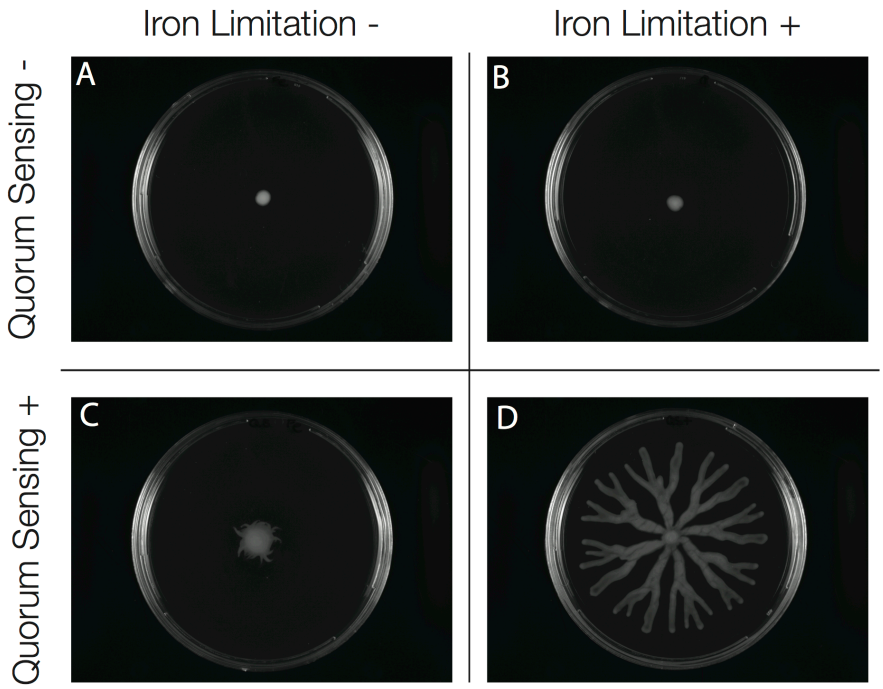


**Figure 2.13 Quorum sensing signals and iron limitation are required for swarming colony formation.**

Quorum sensing signals and iron were supplemented in the agar swarming plates. Quorum sensing signals were supplemented at 1 μM C12HSL and 5 μM C4HSL. Iron was supplemented at $2.79*10^{-4}$ gFe/L by addition of iron(II) sulfate. All swarms were done using the ΔlasIΔrhlI strain (A) Populations that do not receive quorum sensing signals and are not in iron limiting conditions fail to swarm. (B) Populations that do not receive quorum sensing signals and have iron limiting conditions fail to swarm. (C) Populations that receive quorum sensing signals, but are not in iron limiting conditions do not swarm far from the inoculation site and do not form branching tendrils. This demonstrates the key role of iron limitation in rhamnolipid production and swarming colony formation (D) Populations that receive quorum sensing signals and have iron limiting conditions exhibit WT swarming colony morphology with branched tendrils that extend to the edges of the plate.

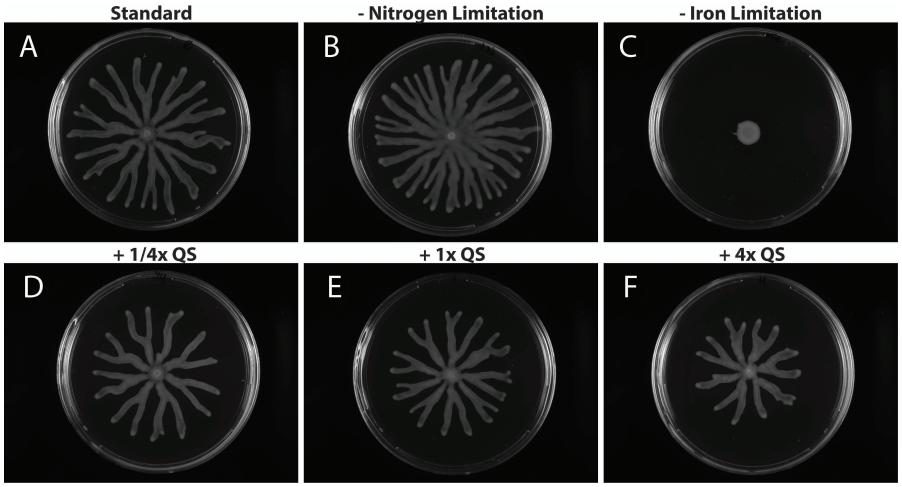


**Figure 2.14 Effects of Quorum sensing signals and nutrient concentrations on swarming colony formation.**

(A) WT *P. aeruginosa* swarming colony morphology in standard media. (B) Branching morphology is affected when additional nitrogen is added to the media (0.5 gN/L by ammonium sulfate). This could be due to decreased overall rhamnolipid production (C) Swarming cooperation is prevented by the addition of iron to the media ($2.79*10^{-4}$ gFe/L by iron(II) sulfate). Lack of iron limitation reduces overall rhamnolipid production preventing the colony from swarming. D-F The coverage of WT swarming colonies is reduced with increasing concentrations of quorum sensing signals added to the media (QS 1x = 1 μM C12HSL and 5 μM C4HSL). This could be due to overproduction of rhmanolipids or over production of other quorum sensing regulated secreted products such as exopolysaccharides.

## Discussion

Here we investigated the molecular circuitry underlying the regulation of genes required for a model multicellular trait, swarming in *P. aeruginosa*. We performed this analysis using a combination of quantitative growth curve experiments and mathematical models. Swarming requires cooperation between cells and the production and secretion of rhamnolipids [32]. Expression of the *rhlAB* operon results in expression of the rate-limiting enzyme for rhamnolipid synthesis and commits the cell to cooperation [31,38]. We carried out liquid batch culture growth experiments in shaken microtiter plates, which allows for a high-throughput investigation of gene expression during periods of changing

nutrient conditions and cell densities [47]. Shaken liquid-culture neglects the spatial gradients of rhamnolipids, quorum sensing signals and nutrients that may occur in swarming colonies [48,49]. In turn, the conditions experienced by cells can be more precisely manipulated in liquid culture allowing us to build a quantitative picture of how metabolic prudence and quorum sensing are integrated into the cellular decision to cooperate.

Our data and mathematical model support previous metabolic prudence models where the expression of *rhlAB* is triggered by excess carbon. During balanced growth internal levels of carbon-rich metabolites are constant and *rhlAB* promoter activity increases proportionally to population density (quorum sensing signals). Since the population maintains the same growth rate in spite of increasing *rhlAB* promoter activity, the uptake rate of carbon would be predicted to also increase, to compensate for the increasing demand of rhamnolipid synthesis. This suggests that the rate of carbon uptake is not limiting the growth rate during balanced growth and that even in exponential growth cells can increase carbon uptake to allow for rhamnolipid synthesis.

When carbon is fully depleted, *rhlAB* expression stops abruptly, potentially to reduce the demand on intracellular carbon-rich metabolites when the lack of carbon has become growth limiting. When extracellular iron is depleted, growth slows and *rhlAB* expression increases. We predict that the decreased growth rate reduces the demand for carbon in biomass production, leading to excess carbon-rich metabolites, which in turn trigger *rhlAB* expression. Growth also slows during nitrogen starvation, which should also decrease the demand for carbon in biomass production. However, cells can actively decrease carbon uptake due to nitrogen starvation [50], which would balance the decreased demand for carbon in biomass production. In support of this balancing of supply and demand we observe that the expression of *rhlAB* during nitrogen starvation is

sustained at a low level, but does not increase. Also in support of nitrogen starvation actively decreasing carbon uptake more significantly than iron starvation, our mathematical model reveals that maximum growth rate must undergo a dramatic decrease in nitrogen starvation, but not in iron starvation.

Quorum sensing regulates multicellular traits in natural and synthetic bacterial systems, but it is not sufficient for robustness against cheating [3,18–20]. Promoter activity of *rhlAB* during exponential growth and non-carbon nutrient starvation scales with population density, supporting that quorum sensing signals do not act as a checkpoint, but instead continually modulate promoter activity and the decision to cooperate through swarming. Our results demonstrate that these two regulatory mechanisms are continually integrated throughout the entire period of expression and may allow cells to adapt to fluctuations in nutrient conditions and population concentration. The ability to respond to changing population density after the decision to express *rhlAB* has been made could play a role in maintaining an individual's fitness while cooperating in a mixed population [37]. Furthermore, metabolic prudence was recently demonstrated as a regulatory mechanism in multiple other secreted products of *P. aeruginosa*[23], suggesting that integration of population density and nutrient environment information may be a more widespread regulatory strategy.

Taken together our data suggests that rhamnolipid synthesis is regulated by feed-forward supply-driven activation, similar to the coupling of end-product inhibition and supply-driven activation reported to regulate amino acid pools in *E. coli* [51]. To ensure maintenance of intracellular carbon rich metabolites, the uptake rate of carbon is in turn regulated using a feedback end-product inhibition (Fig 2.15). The data presented here supports that quorum sensing is continually integrated into the decision to express *rhlAB* and that the cell is capable of maintaining a constant rate of biomass

production even while expressing *rhlAB* during exponential phase. The latter observation suggests that the cell can increase the uptake of carbon during balanced growth to compensate for the production of rhamnolipids.

Our analysis provides new insights into metabolic prudence, but many details of its molecular implementation remain to be discovered. For example, what is (are) the molecule(s) that indicates that intracellular carbon is in excess? Which proteins detect these metabolic signals and how do they interact with quorum sensing regulation at the molecular level? Answering these and other questions will improve our knowledge of rhamnolipid synthesis by *P.aeruginosa* with implications for medicine and industry. Rhamnolipids have the power to disperse infectious biofilms of *P. aeruginosa* and other bacteria, and could thus be used in medical applications [52,53]. They also have commercial value as biodegradable surfactants [54,55]. Beyond *P. aeruginosa*, metabolic prudence emerges as a design principle to stabilize cooperation in multicellular groups. Like other design principles of biology [56] metabolic prudence may be applied to synthetic biology where quorum sensing modules are already used to regulate population level traits [57,58].

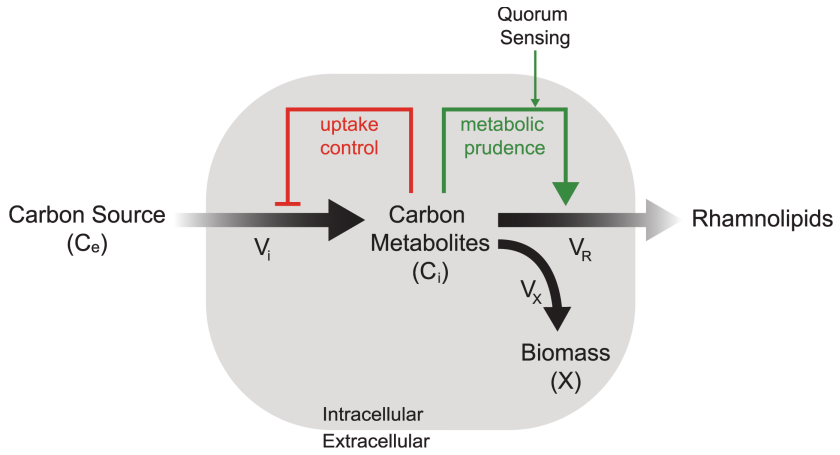


**Figure 2.15 Conceptual model of cooperation by rhamnolipid secretion.**

Conceptual feed-forward supply-driven model of growth and *rhlAB* expression in *P. aeruginosa*. A slowdown in growth would lead to buildup of intracellular carbon metabolites. This buildup would trigger the expression of genes, in this case rhlAB, which would convert carbon metabolites into secreted rhamnolipids that can benefit the cell and the population. By only expressing rhlAB when there is a buildup of metabolites the cell never decreases the rate of biomass production, $V_X$.

## Materials and Methods

All chemicals were obtained from Fisher Scientific (Waltham, MA) unless otherwise specified.

### Single Cell Gene Expression

Cells of the P*rhlAB-gfp* reporter were taken from a growth curve in a 96 well plate using the growth curve synchronization method described previously [59]. Cells were taken from the 96 well plate wells and mounted on agar pads of low melt agar (approximately 1.75% agar) with no nutrients. Cells were imaged for bright-field, GFP, and DsRed. A ratio of GFP to DsRed was used to determine expression level of *rhlAB* by GFP.

Cells of the P*rhlAB-gfp* reporter were taken from a growth curve in a 96 well plate using the growth curve synchronization method described previously [59]. Cells were taken from the 96 well plate wells and mounted on agar pads of low melt agar (approximately 1.75% agar) with no nutrients. Cells were imaged for bright-field, GFP, and DsRed. A ratio of GFP to DsRed was used to determine expression level of *rhlAB* by GFP.

**Correction of Autofluoresence in the gfp Signal**

To correct for autofluorescence in the GFP signal, we measured the fluorescence of the unlabeled PA14 strain, which lacks the PrhlAB-gfp reporter, in numerous experiments across multiple days and a range of conditions, and performed a linear regression on the logarithm of these data (S1A Fig). We found the OD data (OD600) to be a good predictor of the autofluorescence. The fit of the autofluorescence (AF) is then a function of the OD600 of the form:

$$AF = e^{(a+b\times\log(OD_{600}))}$$

We found a correlation coefficient r2 = 0.97 using all data points that were OD600>0.01. Using this function, we estimated the amount of autofluorescence in our reporter strains by using the OD600. We then subtracted the calculated autofluorescence value from the total GFP signal to obtain a corrected GFP (S1B Fig).

**Synthetic Growth Media**

All synthetic media utilized glycerol as the sole carbon source, ammonium sulfate as the sole nitrogen source and Fe(II) sulfate (Acros Organics, Geel, Belgium) for iron supplementation. Base media contains 64 g/L of Na2HPO4.7H2O, 15 g/L of KH2PO4, 2.5 g/L of NaCl, 1 mM of MgCl2, 0.1 mM of CaCl2 and carbon, nitrogen and iron

concentrations depending on the limiting nutrient. Carbon limitation media: 0.5 gN/L, 2.79 *10–4 gFe/L, carbon at listed concentration. Nitrogen limitation media: 3.0 gC/L, 2.79 *10–4 gFe/L, nitrogen at concentration listed. Iron limitation media: 3.0 gC/L, 0.5 gN/L, iron at concentration listed.

**Promoter Activity Calculation**

Promoter activity was calculated as the change in population GFP per unit time divided by OD leading to the following expression [40,60]:

$$P_{rhlAB} = \frac{1}{OD}\frac{dGFP}{dt}$$

OD and GFP data are smoothed before calculating promoter activity using the 1-D digital filter using the function filter in Matlab with a window size of 5 timepoints. This calculation accounts for GFP dilution by cell division.

**Time Lapse of Gene Expression in Swarming Colonies**

Swarming motility and GFP expression were monitored at 37°C at 10 min intervals using a custom-made colony visualizer. The images acquired were processed using Matlab to quantify GFP signal and colony density.

**Batch Culture Growth Curves**

Starter cultures are inoculated into 3 mL of LB Miller from glycerol stock and incubated overnight at 37°C with shaking. 1 mL of this LB culture is taken, pelleted at 6000 rpm and re-suspended with 1x PBS. Pelleting and re-suspension in PBS is repeated twice before inoculation into the growth media at an OD600 of 0.0025. All growth curves are performed at 37°C in clear flat-bottom BD Falcon 96 well microtiter plates with 150 µL

of media per well. Measurements were taken using a Tecan M1000 plate reader (Mannedor, Switzerland) every 10 minutes for the duration of the experiment. Quorum sensing autoinducers HSL and C4HSL used to induce *rhlAB* expression were obtained from Sigma-Aldrich, St. Louis, MO. Unless otherwise indicated, all growth curves are aligned to have OD 0.01 occur at 10 hours. The lag time for each growth curves is determined during this analysis and reported in 2.2 Table.

**Mathematical Modeling and Parameter Fitting**

The mathematical model was implemented as a system of ordinary differential equations in Matlab (the Mathworks, Natick, MA) and solved numerically using the ode45 function. Parameter fitting was carried out using the fminbnd function in a step-wise manner. The OD time series were fitted initially, since these data are independent of the GFP time series data. The goal function to be minimized was defined as:\

$$err_{OD} = \sum_{i=1}^{N} \left( log\left(\frac{X_i}{OD_i}\right)\right)$$

where i $\in$ (1, N) represents all the data points used for the fit. The GFP data was fitted by first calculating the promoter activity from the data as explained in the main text followed by fitting with fminbnd to minimize the following function:

$$err_{ODGFP} = \sum_{i=1}^{N} (P_i - p_i)^2$$

where Pi is the promoter activity calculated from the data and pi is the promoter activity predicted by the model. Parameter sensitivity was performed for both the bacterial growth and *rhlAB* expression models and results are reported in Tables 2.4 and 2.5.

**Table 2.4 Parameter sensitivity growth model**

| Variable | $\mu_{max}$ | $Y_C$ | $k_d$ | $Y_N$ | $\mu_{max}'$ | $Y_{Ni}$ | $Y_{Fe}$ | $Y_{Fei}$ |
|---|---|---|---|---|---|---|---|---|
| Units | $h^{-1}$ | OD/gC | $h^{-1}$ | OD/gN | $h^{-1}$ | $OD/N_i$ | OD/gFe | $OD/I_i$ |
| **Fit with all data** | **0.3341** | **0.6516** | **0.0062** | **4.1627** | **0.0616** | **2.0011** | **$3.8952 * 10^3$** | **4.9892** |
| Highest parameter value fitted with 2/3 data | 0.3464 | 0.6611 | 0.0061 | 4.2644 | 0.0614 | 2.0492 | $3.6548 * 10^3$ | 5.1533 |
| Lowest parameter value fitted with with 2/3 data | 0.3243 | 0.6387 | 0.0059 | 4.1799 | 0.0601 | 1.9234 | $3.9305 * 10^3$ | 5.2690 |

**Table 2.5 Parameter sensitivity *rhlAB* expression model**

| Variable | $q_D$ | $q_{RN}$ | $k_{gN}$ | $h_N$ | $q_{RFe}$ | $k_{gFe}$ | $h_{Fe}$ |
|---|---|---|---|---|---|---|---|
| Units | GFP/OD | GFP | - | - | GFP | - | - |
| **Fit with all data** | **$1.8542 * 10^4$** | **$7.4541 * 10^3$** | **0.1667** | **5.8725** | **$8.5933 * 10^3$** | **0.3293** | **1.9158** |
| Highest parameter value fitted with 4 replicates each | $1.9005 * 10^4$ | $9.4672 * 10^3$ | 0.1765 | 5.7399 | $8.2950 * 10^3$ | 0.3193 | 1.9554 |
| Lowest parameter fitted with with 4 replicates each | $1.7595 * 10^4$ | $6.2586 * 10^3$ | 0.1662 | 5.2734 | $7.1706 * 10^3$ | 0.2926 | 1.9274 |

## Nutrient Depletion Experiment

Starter cultures and inoculation were performed as in Batch Culture Growth curves. Cells were grown to exponential phase in media with 3.0 gC/L, 0.5 gN/L and 2.79 *10–4 gFe/L in 88 wells of a 96 well plate. All wells were harvested and the cells were pelleted and washed with PBS as in Batch culture growth curves. The harvested cells were then split and re-suspended either 1.2 mL of media without nitrogen (3.0 gC/L, 2.79 *10–4 gFe/L) or 1.2 mL media without carbon (0.5 gN/L, 2.79 *10–4 gFe/L) and grown in a 96 well plate in a Tecan M1000 plate reader as described in Batch Culture Growth curves.

**P. aeruginosa Swarming Colonies**

Swarming assays were performed as previously described [36]. Nitrogen was supplemented with ammonium sulfate at 0.5gN/L. Iron was supplemented using iron(II) sulfate at 2.79*10–4 gFe/L. Quorums sensing autoinducers were added at the listed concentrations from liquid stock solutions.

## References


1. Xavier JB (2011) Social interaction in synthetic and natural microbial communities. Molecular Systems Biology 7.
2. Nadell CD, Bucci V, Drescher K, Levin SA, Bassler BL, et al. (2013) Cutting through the complexity of cell collectives. Proc Biol Sci 280: 20122770. doi: 10.1098/rspb.2012.2770 PMID: 23363630
3. Chuang JS, Rivoire O, Leibler S (2009) Simpson's paradox in a synthetic microbial system. Science 323: 272–275. doi: 10.1126/science.1166739 PMID: 19131632
4. Griffin AS, West SA, Buckling A (2004) Cooperation and competition in pathogenic bacteria. Nature 430: 1024–1027. PMID: 15329720
5. Gore J, Youk H, van Oudenaarden A (2009) Snowdrift game dynamics and facultative cheating in yeast. Nature 459: 253–256. doi: 10.1038/nature07921 PMID: 19349960
6. Momeni B, Waite AJ, Shou W (2013) Spatial self-organization favors heterotypic cooperation over cheating. Elife 2: e00960. doi: 10.7554/eLife.00960 PMID: 24220506
7. Drescher K, Nadell Carey D, Stone Howard A, Wingreen Ned S, Bassler Bonnie L Solutions to the Pub- lic Goods Dilemma in Bacterial Biofilms. Current Biology 24: 50–55. doi: 10.1016/j.cub.2013.10.030 PMID: 24332540
8. Perkins TJ, Swain PS (2009) Strategies for cellular decision-making. Mol Syst Biol 5: 326. doi: 10. 1038/msb.2009.83 PMID: 19920811
9. Waters CM, Bassler BL (2005) Quorum sensing- cell-to-cell communication in bacteria. Annu Rev Cell Dev Biol 21: 319–346. PMID: 16212498

10. Fuqua WC WS, Greenberg EP (1994) Quorum Sensing in Bacteria- the LuxR-LuxI Family of Cell Den- sity-Responsive Transcriptional Regulators. Journal of Bacteriology 176: 269–275. PMID: 8288518

11. Pai A, You L (2009) Optimal tuning of bacterial sensing potential. Mol Syst Biol 5: 286. doi: 10.1038/ msb.2009.43 PMID: 19584835

12. Davies DG, Parsek MR, Pearson JP, Iglewski BH, Costerton JW, et al. (1998) The involvement of cell- to-cell signals in the development of a bacterial biofilm. Science 280: 295–298. PMID: 9535661

13. O'Loughlin CT, Miller LC, Siryaporn A, Drescher K, Semmelhack MF, et al. (2013) A quorum-sensing in- hibitor blocks Pseudomonas aeruginosa virulence and biofilm formation. Proc Natl Acad Sci U S A 110: 17981–17986. doi: 10.1073/pnas.1316981110 PMID: 24143808

14. Miller Melissa B., Skorupski Karen, Lenz Derrick H., Taylor Ronald K., Bassler BL (2009) Parallel Quo- rum Sensing Systems Converge to Regulate Virulence in Vibrio cholerae. Cell 110: 303–314.

15. Lewenza S, Conway B, Greenberg EP, Sokol PA (1999) Quorum Sensing in Burkholderia cepacia- Identification of the LuxRI Homologs CepRI. Journal of Bacteriology 181: 748–756. PMID: 9922236

16. Zhu J, Miller MB, Vance RE, Dziejman M, Bassler BL, et al. (2002) Quorum-sensing regulators control virulence gene expression in Vibrio cholerae. Proc Natl Acad Sci U S A 99: 3129–3134. PMID: 11854465

17. Schuster M, Sexton DJ, Diggle SP, Greenberg EP (2013) Acyl-homoserine lactone quorum sensing: from evolution to application. Annu Rev Microbiol 67: 43–63. doi: 10.1146/annurev-micro-092412- 155635 PMID: 23682605

18. Anand Paia YT, and You Lingchong (2012) Optimality and robustness in quorum sensing (QS)- mediat- ed regulation of a costly public good enzyme. PNAS 109: 19810–19815. doi: 10.1073/pnas. 1211072109 PMID: 23144221

19. Sandoz KM, Mitzimberg SM, Schuster M (2007) Social cheating in Pseudomonas aeruginosa quorum sensing. Proc Natl Acad Sci U S A 104: 15876–15881. PMID: 17898171

20. Diggle SP, Griffin AS, Campbell GS, West SA (2007) Cooperation and conflict in quorum-sensing bac- terial populations. Nature 450: 411–414. PMID: 18004383

21. Whooley MA OCJ, McLoughlin AJ (1983) Effect of substrate on the regulation of exoprotease produc- tion by Pseudomonas aeruginosa ATCC 10145. Journal of General Microbiology 129: 981–988. PMID: 6411860

22. Guerra-Santos L, Käppeli O, Fiechter A (1984) Pseudomonas aeruginosa biosurfactant production in continuous culture with glucose as carbon source. Appl Environ Microbiol 48: 301–305. PMID: 6435520

23. Mellbye B, Schuster M (2014) Physiological Framework for the Regulation of Quorum Sensing-Depen- dent Public Goods in Pseudomonas aeruginosa. J Bacteriol 196: 1155–1164. doi: 10.1128/JB.01223- 13 PMID: 24375105

24. Blehert DS, Palmer RJ, Xavier JB, Almeida JS, Kolenbrander PE (2003) Autoinducer 2 Production by Streptococcus gordonii DL1 and the Biofilm Phenotype of a luxS Mutant Are Influenced by Nutritional Conditions. Journal of Bacteriology 185: 4851–4860. PMID: 12897005

25. Lazazzera BA (2000) Quorum sensing and starvation- signals for entry into stationary phase. Current Opinion in Microbiology 3: 177–182. PMID: 10744996

26. Lee J, Wu J, Deng Y, Wang J, Wang C, et al. (2013) A cell-cell communication signal integrates quorum sensing and stress response. Nat Chem Biol 9: 339–343. doi: 10.1038/nchembio.1225 PMID: 23542643

27. Dandekar AA, Chugani S, Greenberg EP (2012) Bacterial quorum sensing and metabolic incentives to cooperate. Science 338: 264–266. doi: 10.1126/science.1227289 PMID: 23066081

28. Gupta R, Schuster M (2013) Negative regulation of bacterial quorum sensing tunes public goods coop- eration. ISME J 7: 2159–2168. doi: 10.1038/ismej.2013.109 PMID: 23823496

29. Deforet M, van Ditmarsch D, Carmona-Fontaine C, Xavier JB (2014) Hyperswarming adaptations in a bacterium improve collective motility without enhancing single cell motility. Soft Matter 10: 2405–2413. doi: 10.1039/c3sm53127a PMID: 24622509

30. Kearns DB (2010) A field guide to bacterial swarming motility. Nat Rev Microbiol 8: 634–644. doi: 10. 1038/nrmicro2405 PMID: 20694026

31. Deziel E, Lepine F, Milot S, Villemur R (2003) rhlA is required for the production of a novel biosurfactant promoting swarming motility in Pseudomonas aeruginosa: 3-(3-hydroxyalkanoyloxy)alkanoic acids (HAAs), the precursors of rhamnolipids. Microbiology 149: 2005–2013. PMID: 12904540

32. Caiazza NC, Shanks RM, O'Toole GA (2005) Rhamnolipids modulate swarming motility patterns of Pseudomonas aeruginosa. J Bacteriol 187: 7351–7361. PMID: 16237018

33. van Ditmarsch D, Boyle KE, Sakhtah H, Oyler JE, Nadell CD, et al. (2013) Convergent evolution of hyperswarming leads to impaired biofilm formation in

pathogenic bacteria. Cell Rep 4: 697–708. doi: 10.1016/j.celrep.2013.07.026 PMID: 23954787

34. Latifi A, Foglino M, Tanaka K, Williams P, Lazdunski A (1996) A hierarchical quorum-sensing cascade in Pseudomonas aeruginosa links the transcriptional activators LasR and RhIR (VsmR) to expression of the stationary-phase sigma factor RpoS. Mol Microbiol 21: 1137–1146. PMID: 8898383

35. Pesci EC, Pearson JP, Seed PC, Iglewski BH (1997) Regulation of las and rhl quorum sensing in Pseu- domonas aeruginosa. J Bacteriol 179: 3127–3132. PMID: 9150205

36. Xavier JB, Kim W, Foster KR (2011) A molecular mechanism that stabilizes cooperative secretions in Pseudomonas aeruginosa. Mol Microbiol 79: 166–179. doi: 10.1111/j.1365-2958.2010.07436.x PMID: 21166901

37. de Vargas Roditi L, Boyle KE, Xavier JB (2013) Multilevel selection analysis of a microbial social trait. Mol Syst Biol 9: 684. doi: 10.1038/msb.2013.42 PMID: 23959025

38. Zhu K, Rock CO (2008) RhlA converts beta-hydroxyacyl-acyl carrier protein intermediates in fatty acid synthesis to the beta-hydroxydecanoyl-beta-hydroxydecanoate component of rhamnolipids in Pseudo- monas aeruginosa. J Bacteriol 190: 3147–3154. doi: 10.1128/JB.00080-08 PMID: 18326581

39. Lequette Y, Greenberg EP (2005) Timing and localization of rhamnolipid synthesis gene expression in Pseudomonas aeruginosa biofilms. J Bacteriol 187: 37–44. PMID: 15601686

40. Anat Bren YH, Dekel Erez, Koster Daniel and Alon Uri (2013) The last generation of bacterial growth in limiting nutrient. BMC Systems Biology 7.

41. Monod J (1949) The Growth of Bacterial Cultures. Annu Rev Microbiol 3: 371.

42. Straight JV, Ramkrishna D (1994) Cybernetic Modeling and Regulation of Metabolic Pathways. Growth on Complementary Nutrients. Biotechnology Progress 10: 574–587.

43. Brauer MJ, Yuan J, Bennett BD, Lu W, Kimball E, et al. (2006) Conservation of the metabolomic re- sponse to starvation across two divergent microbes. Proc Natl Acad Sci U S A 103: 19302–19307. PMID: 17159141

44. Guerra-Santos L, Kappeli O, Fiechter A (1984) Pseudomonas aeruginosa Biosurfactant Production in Continuous Culture with Glucose as Carbon Source. Applied and Environmental Microbiology 48: 301–305. PMID: 6435520

45. Glick R, Gilmour C, Tremblay J, Satanower S, Avidan O, et al. (2010) Increase in rhamnolipid synthesis under iron-limiting conditions influences surface motility

and biofilm formation in Pseudomonas aerugi- nosa. J Bacteriol 192: 2973–2980. doi: 10.1128/JB.01601-09 PMID: 20154129

46. Schmidberger A, Henkel M, Hausmann R, Schwartz T (2014) Influence of ferric iron on gene expres- sion and rhamnolipid synthesis during batch cultivation of Pseudomonas aeruginosa PAO1. Appl Microbiol Biotechnol 98: 6725–6737. doi: 10.1007/s00253-014-5747-y PMID: 24752844

47. Afroz T, Biliouris K, Kaznessis Y, Beisel CL (2014) Bacterial sugar utilization gives rise to distinct sin- gle-cell behaviours. Mol Microbiol 93: 1093–1103. doi: 10.1111/mmi.12695 PMID: 24976172

48. Deng P, de Vargas Roditi L, van Ditmarsch D, Xavier JB (2014) The ecological basis of morphogenesis: branching patterns in swarming colonies of bacteria. New J Phys 16: 015006–015006. PMID: 24587694

49. Morris JD, Hewitt JL, Wolfe LG, Kamatkar NG, Chapman SM, et al. (2011) Imaging and analysis of Pseudomonas aeruginosa swarming and rhamnolipid production. Appl Environ Microbiol 77: 8310– 8317. doi: 10.1128/AEM.06644-11 PMID: 21984238

50. Doucette CD, Schwab DJ, Wingreen NS, Rabinowitz JD (2011) alpha-Ketoglutarate coordinates car- bon and nitrogen utilization via enzyme I inhibition. Nat Chem Biol 7: 894–901. doi: 10.1038/nchembio. 685 PMID: 22002719

51. Scott M, Klumpp S, Mateescu EM, Hwa T (2014) Emergence of robust growth laws from optimal regula- tion of ribosome synthesis. Mol Syst Biol 10: 747. doi: 10.15252/msb.20145379 PMID: 25149558

52. Boyle KE, Heilmann S, van Ditmarsch D, Xavier JB (2013) Exploiting social evolution in biofilms. Curr Opin Microbiol 16: 207–212. doi: 10.1016/j.mib.2013.01.003 PMID: 23357558

53. Boles BR, Thoendel M, Singh PK (2005) Rhamnolipids mediate detachment of Pseudomonas aerugi- nosa from biofilms. Mol Microbiol 57: 1210–1223. PMID: 16101996

54. Pornsunthorntawee O, Wongpanit P, Rujiravanit R (2010) Rhamnolipid biosurfactants: production and their potential in environmental biotechnology. Adv Exp Med Biol 672: 211–221. PMID: 20545285

55. Muller MM, Kugler JH, Henkel M, Gerlitzki M, Hormann B, et al. (2012) Rhamnolipids—next generation surfactants? J Biotechnol 162: 366–380. doi: 10.1016/j.jbiotec.2012.05.022 PMID: 22728388

56. Alon U (2006) An introduction to systems biology: design principles of biological circuits: CRC press.

57. Pai A, Srimani JK, Tanouchi Y, You L (2013) Generic Metric to Quantify Quorum Sensing Activation Dy- namics. ACS Synth Biol 3: 220–227. doi: 10.1021/sb400069w PMID: 24011134

58. Hong SH, Hegde M, Kim J, Wang X, Jayaraman A, et al. (2012) Synthetic quorum-sensing circuit to control consortial biofilm formation and dispersal in a microfluidic device. Nat Commun 3: 613. doi: 10. 1038/ncomms1616 PMID: 22215088

59. van Ditmarsch D, Xavier JB (2011) High-resolution time series of Pseudomonas aeruginosa gene ex- pression and rhamnolipid secretion through growth curve synchronization. BMC Microbiol 11: 140. doi: 10.1186/1471-2180-11-140 PMID: 21682889

60. Ronen M, Rosenberg R, Shraiman BI, Alon U (2002) Assigning numbers to the arrows: parameterizing a gene regulation network by using accurate expression kinetics. Proc Natl Acad Sci U S A 99: 10555– 10560. PMID: 12145321

# Chapter 3 - Investigating The Link Between Intracellular Metabolism and the Evolution of Stable Cooperation

Kerry E. Boyle, Hilary T. Monaco, Maxime Deforet, Zhe Wang, Kyu Rhee, Joao Xavier

## Abstract

Here we investigate how metabolism influences social behavior and, ultimately, the evolution of cooperative behavior in a tractable model system, swarming in the bacterium *Pseudomonas aeruginosa*. We perturb the natural ability of cells to cooperate at a low cost to their fitness by deleting a key metabolic regulator, the gene *cbrA*, producing a highly altruistic strain that we can monitor using metabolomics. Evolutionary experiments in swarming colonies reveal that the D*cbrA* altruistic strain is rapidly invaded by two distinct types of mutants that reduce the fitness cost of cooperation through metabolome rearrangement. The most frequent class has mutations in *crc* and a metabolome that resembles the wild-type, but remains altruistic and vulnerable to invasion. The second, less frequent, class has mutations in *hfq* and cooperates at a low cost similar to the wild-type, yet has a surprisingly distinct metabolome. Thus, cells lacking a key regulatory gene can recover stable multicellular cooperation via an alternative metabolic state.

## Introduction

How can individuals behave cooperatively when it seems detrimental to their own fitness? Cooperation is key concept in biology, and central to the evolution from unicellular to multicellular life [1]. Although we know the importance of cooperative behavior, the mechanisms that allow it to evolve and remain stable largely remain a puzzle. Cooperation plays a large role in the microbial world where most species secrete substances such as quorum sensing signals, extracellular polymers and nutrient scavenging molecules that enable multicellular communities where microbes can achieve strength in numbers [2, 3] [4-6]. Hamilton's famous kin selection theory [7] explains that a cooperative action can be favored when its benefit to the recipient ($b$) multiplied by the relatedness between the cooperator and the recipient ($r$) exceeds the cost to the actor ($c$):

*br>c*.

There are many examples showing that cooperation can be favored when relatedness is high [8], but most microbial communities such as the human microbiome are highly diverse [9]. How can cooperation evolve and remain stable in such communities?

Microbial cooperative secretions are public goods produced by an individual that can benefit others in the community, irrespective of who produces them [10]. The metabolic burden of synthetizing and secreting public good molecules can impose a fitness cost on the cell. Cooperation can be stabilized through the cellular regulatory mechanism *metabolic prudence*, which reduces the metabolic burden by delaying expression of public good synthesis genes to times when the cell has excess metabolites [11]. Swarming, a form of multicellular migration in the bacterial pathogen *Pseudomonas aeruginosa*, requires the production of massive amounts of carbon rich surfactants called rhamnolipids [12, 13]. Secreted rhamnolipids, like other public goods, are shared with surrounding individuals and therefore could be exploited by non-producers such as mutants lacking the rhamnolipid synthesis gene *rhlA*. *P. aeruginosa* uses metabolic prudence to delay expression of the rhamnolipid synthesis operon *rhlAB* to times when it has excess carbon, which happens in carbon rich environments when other nutrients like nitrogen or iron are depleted before carbon [11, 14]. Furthermore, Regulation of *rhlAB* expression integrates metabolic prudence with quorum sensing signals to ensure that cells cooperate only when they are in a large population [15]. Engineered strains of *P. aeruginosa* that express *rhlAB* constitutively are incapable of metabolic prudence and pay a high fitness cost for swarming cooperation, and can only be favored when relatedness is very high [16]. The regulation of *rhlAB* expression by metabolic prudence is key to reduce the cost of swarming cooperation and make it stable even when relatedness is low.

Metabolic prudence explains how microbes stabilize cooperative secretions [17], but its function appears to rely on the balances of intracellular metabolites and the surrounding nutrient environment such as carbon and nitrogen sources [15]. What happens to cooperation after mutations disrupt intracellular metabolite levels? We combine experimental evolution [18] with the power of metabolomics [19] to address this question. We construct a strain lacking a metabolic regulation gene, *cbrA*, known to affect carbon and nitrogen utilization [20] and nutrient uptake [21, 22] and we follow changes in the metabolome of this strain as it recovers the ability to cooperate during evolutionary experiments. The Δ*cbrA* strain overexpress an essential gene for rhamnolipid production, *rhlA* [23] and over-cooperates with a huge cost to its fitness. We follow the evolution of this altruistic strain through repeated rounds of swarming and observe a rapid takeover by new mutants with compensatory mutations downstream of *cbrA*. We find two mutually exclusive mutations leading to distinct social behaviors and internal metabolomes. Early mutations in the gene *crc* allow strains to recover an internal metabolic state similar to the wild-type but are not evolutionarily stable. Later emerging mutants in *hfq* recover wild-type social behavior but have a significantly different internal metabolic state. Our results provide a new link between the metabolome and social behavior, highlighting the importance of intracellular metabolism in the evolution of stable cooperation.

## Results

### Construction of an altruistic strain with disrupted metabolic regulation

We constructed a Δ*cbrA* strain of *Pseudomonas aeruginosa* PA14. This strain is unable to swarm even though it overexpresses the rhamnolipid operon *rhlAB*, maintains the necessary flagella machinery to swarm and is capable of swimming as well as biofilm formation but is incapable to swarm (Fig 1A&B Fig S1B&C). Δ*cbrA* grows slower in rich media and other carbon sources such as glycerol (Fig 3.1C, Fig 3.2A), which is in

line with previous literature [24]. CbrA is part of a two-component system with CbrB. Although a signal for the CbrA/B system is presently unknown, current literature supports that the system regulates catabolic repression involving downstream proteins that include Hfq and Crc [25, 26]. The Δ*cbrA* strain acts as an altruist helping the Δ*rhlA*, a strain incapable of producing its own rhamnolipids, to swarm. When the Δ*rhlA* strain is placed on a colony adjacent to Δ*cbrA* the Δ*rhlA* strain is able to utilize the rhamnolipids produced by the Δ*cbrA* strain while the Δ*cbrA* strain is unable to swarm (Fig 3.1D). The altruism shown by Δ*cbrA* is in striking contrast to the wild-type, which is mutualistic [7] and is able to swarm successfully even as it helps the Δ*rhlA* strain causing both strains to benefit from the rhamnolipids produced by the wild-type.

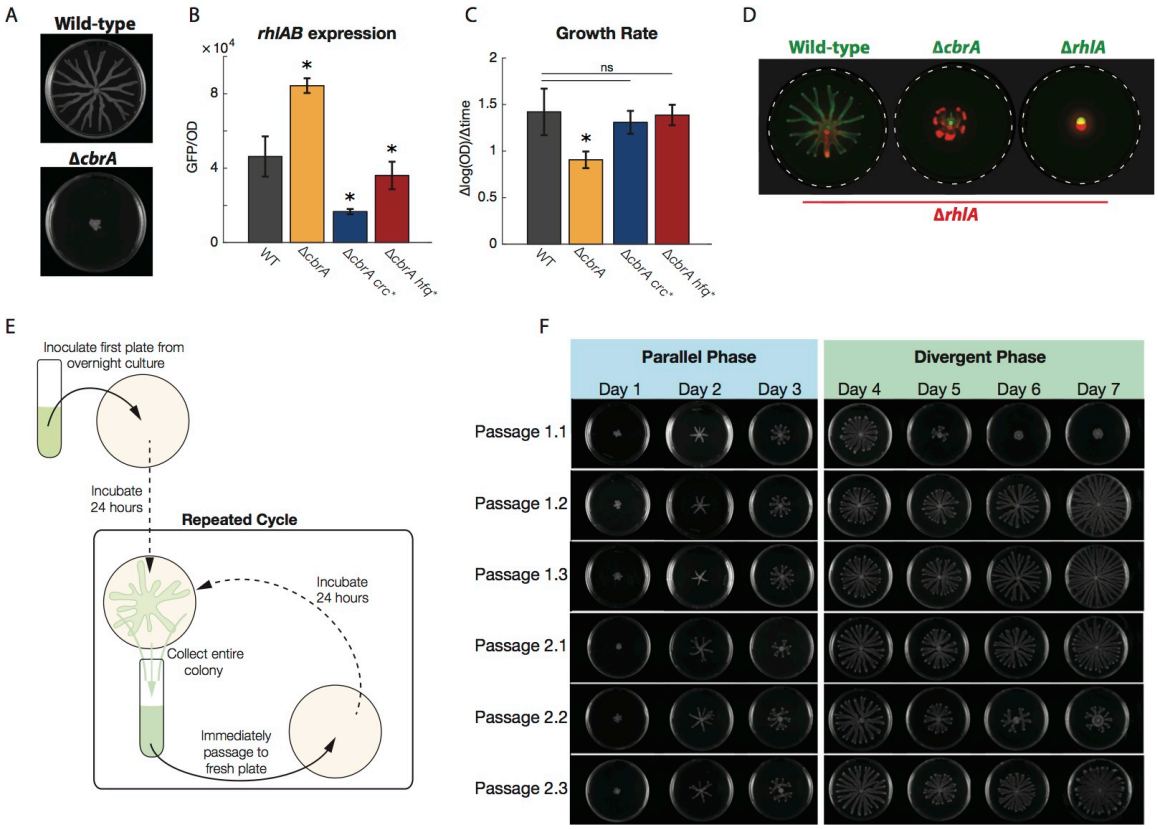


**Figure 3.1 Δ*cbrA* behavior and experimental evolution**

(A) Wild-type and Δ*cbrA* swarming colonies. Wild-type is capable of forming a successful swarming colony while Δ*cbrA* is unable to swarm. (B) *rhlAB* expression measured from the $P_{rhlAB}$-gfp promoter (methods). Δ*cbrA* over expresses *rhlAB* while Δ*cbrA crc** (1.3-1) and Δ*cbrA hfq* (1.2-1) under express *rhlAB* with Δ*cbrA crc** expressing less than Δ*cbrA hfq**. Data shown is from 3 biological replicates. (C) Exponential growth rate of strains in minimal media with the same nutrient concentration as swarming plates. Δ*cbrA* grows significantly slower than the wild-type while Δ*cbrA crc** and Δ*cbrA hfq** are not significantly different from wild-type. Data shown is from 3 biological replicates. (D) Co-inoculated swarming plates showing cheating of Δ*rhlA* (methods). Δ*rhlA* is capable of using the rhamnolipis produced by other strains to swarm. The wild-type benefits the Δ*rhlA* strain by enabling movement to nutrient rich parts of the plate while still swarming successful itself. The Δ*cbrA* strain performs poorly at swarming, but the Δ*rhlA* strain receives a significant benefit and is able to swarming using the rhamnolipids Δ*cbrA* produces. Δ*rhlA* does not benefit from being inoculated near Δ*rhlA* as no rhamnolipids are produced. (E) Experimental evolution experimental design (methods). (F) Results of the experimental evolution. Passages 1.1-1.3 are from one biological replite while 2.1-2.3 are from a second biological replicate. The first three days of the experiment are consistent and termed the parallel stage. Days 4-7 show divergence in swarming phenotype and are termed the divergent phase. (pvalue for significance <= 0.05)

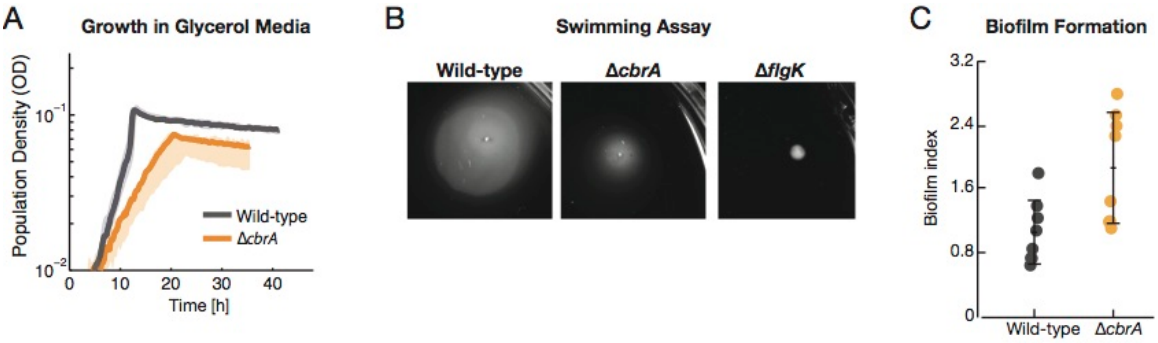


**Figure 3.2 Growth, swimming and biofilm formation of Δ*cbrA* strain**

(A) Growth of wild-type and Δ*cbrA* in glycerol synthetic media with 0.5gC/L, 0.5gN/L and 5µm iron. The Δ*cbrA* strain has a significant growth defect compared to wild-type. (B) Swimming assay in soft agar petri dishes. The wild-type, Δ*cbrA* are capable of swimming while Δ*flgK* cannot. (C) Biofilm formation. The Δ*cbrA* strain is not deficient in biofilm production compared to wild-type.

**Experimental evolution days 1-3: Parallel phase**

We used a Δ*cbrA* strain with a *PrhlAB-gfp* reporter fusion to initiate an experimental evolution in swarming plates (Fig 1 E&F)(methods). We started six independent lineages, all of which recovered the ability to swarm within the first three days. These first days of the experimental evolution (day 1-3) were remarkably reproducible and this was termed the 'parallel phase'. In contrast, there was a large variability in the later days (4-7) with some populations sustaining successful swarming and others experiencing a complete loss of swarming. This later stage was termed the 'divergent phase'.

To determine what happened in the parallel phase we first investigated hard agar colony morphologies of each population. The Δ*cbrA* strain makes very small compact colonies on minimal media agar plates (methods). We found large colony variants as early as day 1 of our experimental evolution in all of the populations, indicating that compensatory mutations had occurred (Fig 3.3A inset). Large colony variants rapidly took over all of the populations within the first few days, and by day 4 the small colonies were

completely extinct (Fig 3.3A). We sequenced the whole genome of a large colony variant and found a mutation in the gene *crc*, which encodes for a protein in the down-stream signaling pathway of CbrA/CbrB [25, 26]. Targeted sequencing of *crc* in 53 random isolates taken from across all of the passages from day 3 populations revealed that 43 (>80%) of isolates had *crc* mutations. The mutations include frameshifts, large deletions, stop codons and non-synonymous substitutions, that likely cause loss of Crc function (Fig 3.3C). The frequency of these variants and the speed at which they invaded all populations indicates that loss of Crc function improves fitness in the *cbrA* background. Although a representative Δ*cbrA crc** strain (1.3-1 Fig 3.4A) recovers exponential growth rate back to wild-type levels, (Fig 3.1C) it swarms less than the wild-type PA14 (Fig 3.5A and Fig 3.5A 1.3-1) and *rhlAB* expression is approximately half of its wild-type level (Fig 3.1B). The growth rate difference likely explains its competitive advantage against the Δ*cbrA* ancestor. The Δ*cbrA crc** mutant phenocopies a Δ*crc* strain in swarming colony morphology, *rhlAB* expression, and exponential growth rate (Fig 3.4A-C). This supports that Crc is critical for the functional downstream signaling of the CbrA/CbrB system in these conditions.

The parallel phase was characterized by a rapid emergence of Δ*cbrA crc** strains which have faster growth rates than Δ*cbrA*. However, we still observe further changes in all populations at day 4, and particularly drastic divergence in the late stages of the experiment. This suggests that additional or alternative mutations increase competitive fitness in swarming colonies over Δ*cbrA crc**.

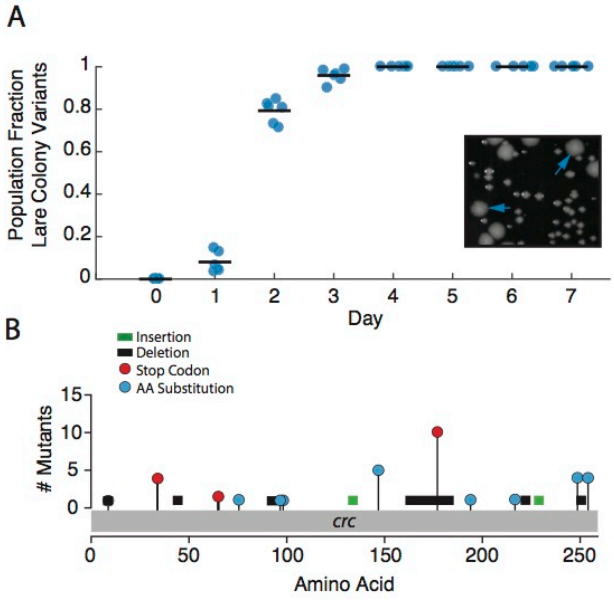


**Figure 3.3 Parallel phase analysis**

(A) Large colony variants take over all of the populations with similar dynamics. Starting at day 1 large colony variants in the Δ*cbrA* background (blue arrows in inset) start to appear and rapidly take over each population. (B) Mutations found in *crc* from 53 randomly selected isolates across all day 3 populations. More than 80% of randomly isolated colonies had mutations in *crc* and these mutations were diverse and frequently predicted loss of function mutations.

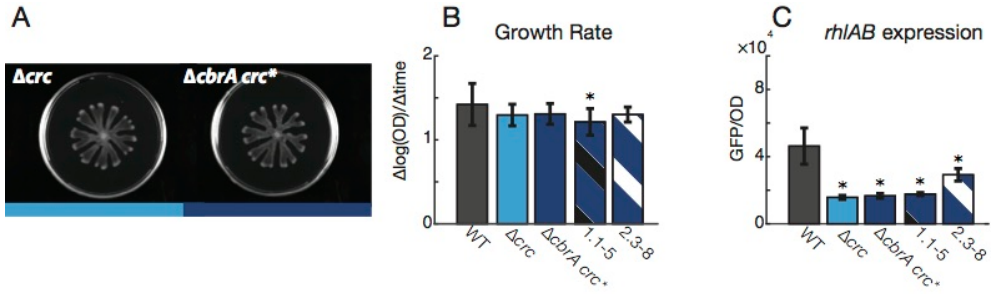


**Figure 3.4 Comparison of wild-type Δ*crc* and Δ*cbrA crc** strains**

(A) Swarms of Δ*crc* and Δ*cbrA crc**. The swarming phenotype of Δ*cbrA crc** closely resembles that of Δ*crc*. (B) Exponential growth rate of wild-type (same data as Fig 1C), Δ*cbrA crc** (same data as Fig 1C), Δ*crc*, 1.1-5 and 2.3-8. The Δ*crc* strain has a growth rate not significantly different from Δ*cbrA crc** and wild-type. 1.1-5 has a slower exponential growth rate than wild-type and 2.3-8 has a growth rate not significantly different from wild-type. (C) *rhlAB* expression of wild-type, Δ*cbrA crc**(same data as Fig 1B), Δ*crc* (same data as Fig 1B), 1.1-5 and 2.3-8. All mutant strains under express compared to wild-type. Δ*cbrA crc** has an expression level not significantly different from Δ*crc* (pvalue for significance <= 0.05).

**Experimental evolution days 4-7: Divergent phase**

The experimental populations show divergent evolution after day 3. We compared the clonal diversity of all populations in the final day (day 7) by randomly picking eight isolates from each and conducting a battery of phenotypic assays in liquid culture (Fig 3.5A)(methods). We then determined the number of phenotypic groups using hierarchical clustering and calculated a diversity score for each day 7 population (Fig 3.5B, Fig 3.6A)(methods). Passage 1.1 has extremely low diversity suggesting that a single clone dominates this passage by day 7. In contrast passages 1.3 and 2.1 have high diversity scores revealing the coexistence of multiple clones at day 7 (Fig 3.6A). The other populations fall between these two extremes of single clone dominance and population diversity.

Guided by the liquid culture phenotypic assays and diversity scores, we selected a total of twenty isolates for whole genome sequencing (Fig 3.6A). The twenty sequenced isolates span a wide range of swarming phenotypes from wild-type-like to complete lack of swarming. To capture the variance within each population more clones were selected for sequencing from the most diverse populations. We picked disproportionally more clones from population 2.2 as the shape of the swarming colony suggested that this population was undergoing a domination by non-swarming strains and we aimed to get a good representation of the strains driving these dynamics. Whole genome sequencing revealed that every strain accumulated an additional mutation in the Δ*cbrA* background (Fig 3.6B). However, all of the isolates fell into two mutually exclusive mutation types with mutations in either the promoter or coding region of two genes downstream of *cbrA*: *hfq* or *crc* (Fig 3.6B).

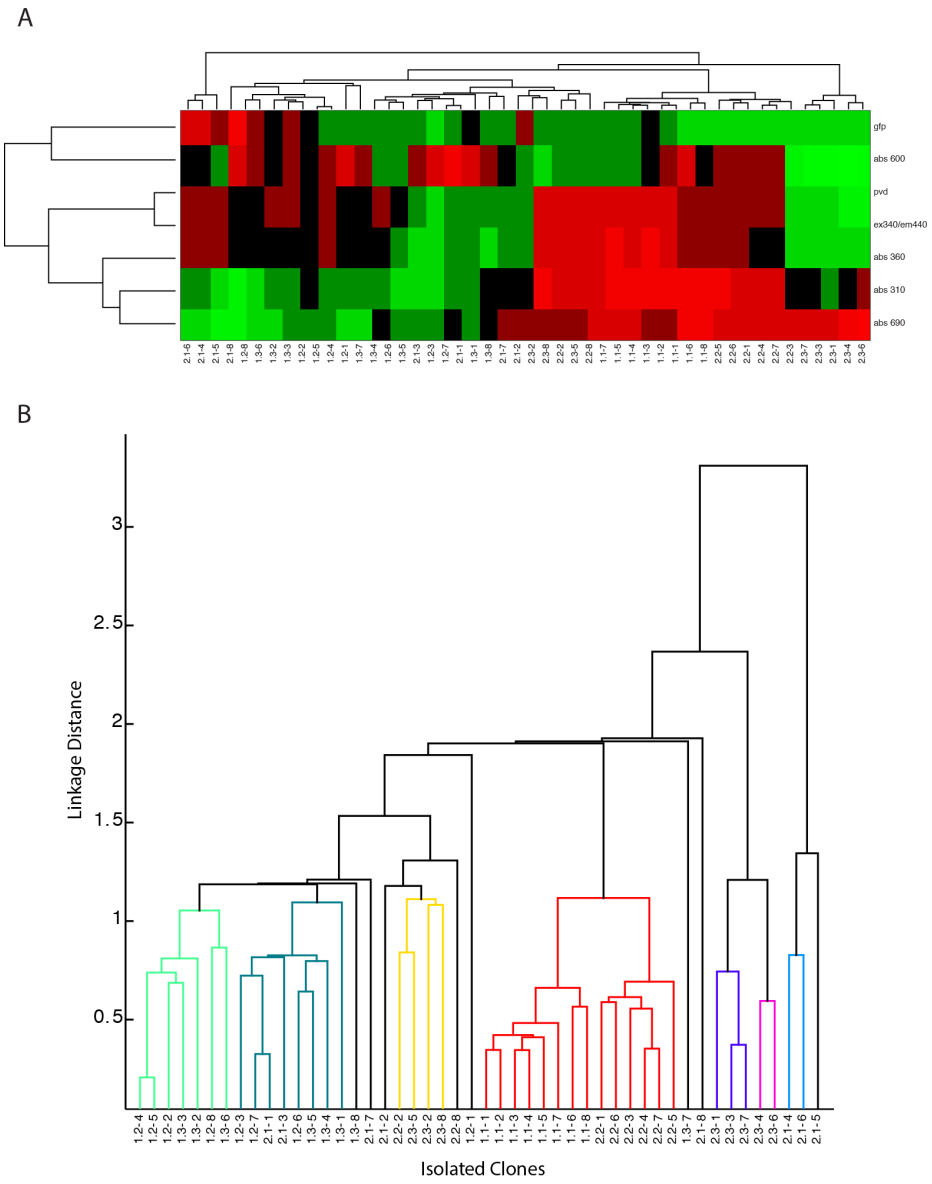


**Figure 3.5 Liquid culture assays and dendogram**

(A) Unsupervised clustering of the liquid culture absorbance and fluorescence assay results. The isolated clones from some populations are tightly clustered together (1.1) while other populations have clones in multiple clusters (1.3 & 2.1). (B) Dendogram calculated from the liquid culture phenotypes. The clusters used to calculate the diversity score for each population (Fig 3A) are indicated by different colors.

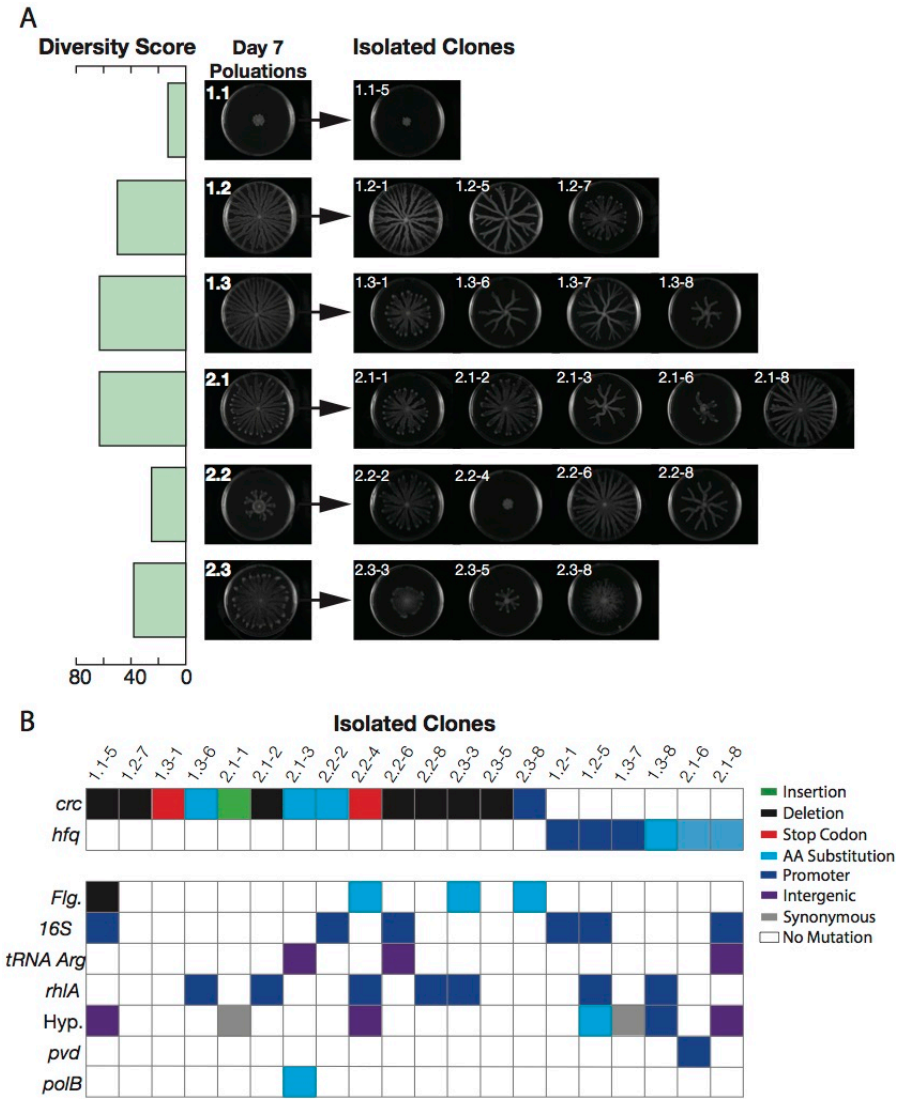


**Figure 3.6 Divergent phase analysis**

(A) Day 7 populations have a range of clonal diversity. Diversity scores are based on the number of predicted clones in each population based on a samples of 8 isolated clones from each population (methods). The day 7 population from passage 1.1 is predicted to have only one clone present while day 7 populations from passages 1.3 and 2.1 have significant diversity. Twenty individual clones were isolated from the day 7 populations (Isolated Clones). A range of swarming phenotypes including non-swarming are observed in the isolated clones. (B) Summary of mutations found in the 20 isolated clones from whole genome sequencing. All clones either had a mutation in the gene or promoter of *crc* or *hfq*. Other mutations were also found in a number of genes including flagella regulation genes. Mutations are fully detailed in Table 3.1.

Similar to the large colony variants found in the parallel phase of the experiment, the majority of the new mutations found in *crc* are likely loss of function mutations. In contrast, none of the mutations affecting *hfq* are obvious loss of function mutations (Fig 3.6A and Table 3.1). A representative Δ*cbrA hfq** strain (1.2-1 Fig 3.5A) shows a wild-type growth rate suggesting that mutations in *hfq* confer a growth recovery similar to *crc* mutations (Fig 3.1B). Crc and Hfq are predicted to act together in the downstream signaling of the CbrA/B [26]. The consistent growth rate recovery associated with a mutation in either of the genes supports that altering this regulatory step in the downstream signaling partially corrects metabolic deregulations caused by the Δ*cbrA* deletion. Compared to the Δ*cbrA crc** strain, the *rhlAB* activity of the Δ*cbrA hfq** strain is more similar to the level expressed by the wild-type (Fig 3.1A). This strain also has increased swarming motility suggesting that *hfq* mutations affect both the social behavior and the internal metabolome differently than *crc* mutations.

## Table 3.1 List of mutations in evolved isolates

| Strain | Position | Mutation | Annotation | Gene | Description of mutation location |
|---|---|---|---|---|---|
| **1.1-5** | 732,660 | G→A | intergenic (+114/-435) | *tyrZ* → / → *PA14_08570* | tyrosyl-tRNA synthetase 2/16S ribosomal RNA |
| | 3,645,629 | (T)9→8 | intergenic (+60/-198) | *PA14_40860* → / → *PA14_40880* | putative sterol carrier protein/putative aminoglycoside phosphotransferase |
| | 4,458,707 | Δ1 bp | coding (840/1422 nt) | *fleR* ← | two-component response regulator |
| | 6,275,314 | Δ2 bpcoding | (275-276/780 nt) | *crc* → | catabolite repression control protein |
| **1.2-1** | 5,820,047 | C→T | intergenic (-12/+94) | *hfq* ← / ← *miaA* | putative host factor-I protein/delta 2-isopentenylpyrophosphate transferase |
| | 732,660 | G→A | intergenic (+114/-435) | *tyrZ* → / → *PA14_08570* | tyrosyl-tRNA synthetase 2/16S ribosomal RNA |
| **1.2-5** | 5,820,047 | C→T | intergenic (-12/+94) | *hfq* ← / ← *miaA* | putative host factor-I protein/delta 2-isopentenylpyrophosphate transferase |
| | 732,660 | G→A | intergenic (+114/-435) | *tyrZ* → / → *PA14_08570* | tyrosyl-tRNA synthetase 2/16S ribosomal RNA |
| | 1,648,344 | A→G | intergenic (+136/-288) | *dcd* → / → *rhlA* | putative deoxycytidine triphosphate deaminase/rhamnosyltransferase chain A |
| | 2,545,663 | T→C | I527I (ATT→ATC) | *PA14_29390* → | conserved hypothetical protein |
| **1.2-7** | 6,275,182 | Δ1 bp | coding (143/780 nt) | *crc* → | catabolite repression control protein |
| **1.3-1** | 6,275,268 | A→T | K77* (AAA→TAA) | *crc* → | catabolite repression control protein |
| **1.3-6** | 6,275,593 | T→C | L185P (CTC→CCC) | *crc* → | catabolite repression control protein |
| | 1,648,344 | A→G | intergenic (+136/-288) | *dcd* → / → *rhlA* | putative deoxycytidine triphosphate deaminase/rhamnosyltransferase chain A |
| **1.3-7** | 2,545,663 | T→C | I527I (ATT→ATC) | *PA14_29390* → | conserved hypothetical protein |
| | 5,820,094 | G→C | intergenic (-59/+47) | *hfq* ← / ← *miaA* | putative host factor-I protein/delta 2-isopentenylpyrophosphate transferase |
| **1.3-8** | 5,819,890 | G→C | T49S (ACC→AGC) | *hfq* ← | putative host factor-I protein |
| | 1,648,588 | A→C | intergenic (+380/-44) | *dcd* → / → *rhlA* | putative deoxycytidine triphosphate deaminase/rhamnosyltransferase chain A |
| | 3,645,629 | (T)9→8 | intergenic (+60/-198) | *PA14_40860* → / → *PA14_40880* | putative sterol carrier protein/putative aminoglycoside phosphotransferase |
| **2.1-1** | 6,275,443 | +A | coding (404/780 nt) | *crc* → | catabolite repression control protein |
| | 2,545,633 | T→C | H517H (CAT→CAC) | *PA14_29390* → | conserved hypothetical protein |
| | 2,545,663 | T→C | I527I (ATT→ATC) | *PA14_29390* → | conserved hypothetical protein |

## Table 3.2 (continued)

| | | | | | |
|---|---|---|---|---|---|
| **2.1-2** | 6,275,529 | Δ60 bp | coding (490-549/780 nt) | *crc* → | catabolite repression control protein |
| | 1,648,344 | A→G | intergenic (+136/-288) | *dcd* → / → *rhlA* | putative deoxycytidine triphosphate deaminase/rhamnosyltransferase chain A |
| **2.1-3** | 6,275,604 | G→A | D189N (GAC→AAC) | *crc* → | catabolite repression control protein |
| | 3,577,158 | T→C | M117V (ATG→GTG) | *polB* ← | DNA polymerase II |
| | 4,659,831 | Δ1 bp | intergenic (+71/+31) | *PA14_52530* → / ← *PA14_52540* | probable transcriptional regulator/tRNA-Arg |
| **2.1-6** | 5,819,846 | G→C | P64A (CCG→GCG) | *hfq* ← | putative host factor-I protein |
| | 2,910,713 | C→A | intergenic (-96/-548) | *pvdS* ← / → *pvdG* | sigma factor PvdS/PvdG |
| **2.1-8** | 5,819,840 | G→A | R66C (CGT→TGT) | *hfq* ← | putative host factor-I protein |
| | 732,660 | G→A | intergenic (+114/-435) | *tyrZ* → / → *PA14_08570* | tyrosyl-tRNA synthetase 2/16S ribosomal RNA |
| | 1,441,862 | ©6→5 | intergenic (+32/+11) | *PA14_16820* → / ← *PA14_16830* | putative efflux transmembrane protein/conserved hypothetical protein |
| | 3,673,534 | T→C | intergenic (+83/+15) | *fabI* → / ← *ppiD* | NADH-dependent enoyl-ACP reductase/putative peptidyl-prolyl cis-trans isomerase D |
| | 3,673,536 | T→C | intergenic (+85/+13) | *fabI* → / ← *ppiD* | NADH-dependent enoyl-ACP reductase/putative peptidyl-prolyl cis-trans isomerase D |
| | 4,659,831 | Δ1 bp | intergenic (+71/+31) | *PA14_52530* → / ← *PA14_52540* | probable transcriptional regulator/tRNA-Arg |
| **2.2-2** | 6,275,479 | G→A | G147D (GGC→GAC) | *crc* → | catabolite repression control protein |
| | 732,660 | G→A | intergenic (+114/-435) | *tyrZ* → / → *PA14_08570* | tyrosyl-tRNA synthetase 2/16S ribosomal RNA |
| **2.2-4** | 6,275,139 | C→T | Q34* (CAG→TAG) | *crc* → | catabolite repression control protein |
| | 4,461,536 | A→C | V270G (GTC→GGC) | *fleQ* ← | transcriptional regulator FleQ |
| | 1,648,588 | A→C | intergenic (+380/-44) | *dcd* → / → *rhlA* | putative deoxycytidine triphosphate deaminase/rhamnosyltransferase chain A |
| | 3,645,629 | (T)9→8 | intergenic (+60/-198) | *PA14_40860* → / → *PA14_40880* | putative sterol carrier protein/putative aminoglycoside phosphotransferase |
| **2.2-6** | 6,275,757 | Δ9 bp | coding (718-726/780 nt) | *crc* → | catabolite repression control protein |
| | 732,660 | G→A | intergenic (+114/-435) | *tyrZ* → / → *PA14_08570* | tyrosyl-tRNA synthetase 2/16S ribosomal RNA |
| | 4,659,831 | Δ1 bp | intergenic (+71/+31) | *PA14_52530* → / ← *PA14_52540* | probable transcriptional regulator/tRNA-Arg |

## Table 3.2 (continued)

| | | | | | |
|---|---|---|---|---|---|
| **2.2-8** | 6,275,757 | Δ9 bp | coding (718-726/780 nt) | *crc* → | catabolite repression control protein |
| | 1,648,344 | A→G | intergenic (+136/-288) | *dcd* → / → *rhlA* | putative deoxycytidine triphosphate deaminase/rhamnosyltransferase chain A |
| **2.3-3** | 6,275,529 | Δ60 bp | coding (490-549/780 nt) | *crc* → | catabolite repression control protein |
| | 4,060,176 | G→A | S28L (TCG→TTG) | *fleN* ← | flagellar synthesis regulator FleN |
| | 1,648,588 | A→C | intergenic (+380/-44) | *dcd* → / → *rhlA* | putative deoxycytidine triphosphate deaminase/rhamnosyltransferase chain A |
| | 1,648,631 | G→A | intergenic (+423/-1) | *dcd* → / → *rhlA* | putative deoxycytidine triphosphate deaminase/rhamnosyltransferase chain A |
| **2.3-5** | 6,275,529 | Δ60 bp | coding (490-549/780 nt) | *crc* → | catabolite repression control protein |
| **2.3-8** | 6,275,007 | T→C | intergenic (-48/-33) | *pyrE* ← / → *crc* | orotate phosphoribosyltransferase/catabolite repression control protein |
| | 4,059,726 | A→C | V178G (GTC→GGC) | *fleN* ← | flagellar synthesis regulator FleN |

**Social Behavior changes in the divergent phase**

We developed a quantitative assay to compare the social behaviors of our strains. In classic sociobiology, social behaviors can be classified according to the two parameters: the fitness effect on the actor and the fitness effect on the recipient [7]. Classic social behaviors fall into four basic categories: selfish, spiteful, altruistic, and mutualistic (Fig 3.7A). Inspired by this classification, we use the Δ*rhlA* strain labeled with DsRedExpress as a recipient strain, we mix it together with a GFP-labeled actor strain that we want to investigate and we spot the mix on a standard swarming plate. The resulting swarm after 24 h is then analyzed to determine the number and frequency for each strain. The benefit for the recipient is quantified by the final number of the Δ*rhlA-DsRedExpress* cells mixed with the GFP labeled actor comparing the numbers that would have been obtained if it would be mixed only with a GFP labeled Δ*rhlA* non-cooperator. The cost for the actor is quantified by the decrease in its frequency within the mixed population. To demonstrate the validity of this approach we first analyzed data from previous experiments using Δ*rhlA* as the recipient and a constitutive cooperator as the actor [16]. The constitutive cooperator, the inducible strain $P_{BAD}$-*rhlAB*, expresses rhamnolipids based on the amount of L-arabinose inducer present in the media, with more L-arabinose inducing higher levels of expression [11]. Higher levels of expression make the $P_{BAD}$-*rhlAB* strain less fit and benefit the Δ*rhlA* strain more [16]. As expected, our method of quantifying costs and benefits confirms that increasing amounts of L-arabinose makes the $P_{BAD}$-*rhlAB* overexpress rhamnolipids and increases the level of altruistic behavior in a concentration dependent manner (Fig 3.7A).

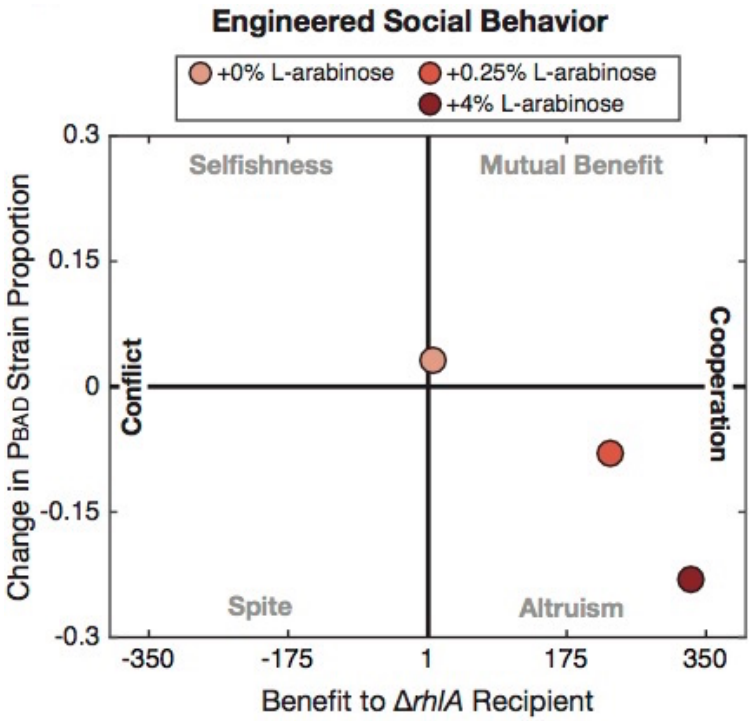


**Figure 3.7 Engineered altruism with inducible *rhlAB* expression**

(A) Social behavior assay was performed with $P_{BAD}$-*rhlAB* at multiple L-arabinose concentrations. With no L-arabinose added to the media the $P_{BAD}$-*rhlAB* strain is slightly mutualistic. Increasing levels of L-arabinose cause the $P_{BAD}$-*rhlAB* strain to behave more altruistically.

We then quantified the social behavior of the wild-type, Δ*cbrA*, Δ*cbrA crc**, and Δ*cbrA hfq** strains using our quantitative social behavior assay (Fig 3.8A). The wild-type falls into the mutualistic quadrant, because it helps the Δ*rhA* strain reach a higher cell number than it does when alone and has a mild increase in its own frequency, a feature observed previously [16]. The Δ*cbrA* strain, as expected, behaves as an extreme altruist. When mixed with Δ*cbrA*, the Δ*rhlA* non-cooperator reaches a much higher cell number than it does when it is alone and the Δ*cbrA* strain has a significant fitness cost. The ΔcbrA *crc** strain is less altruistic than Δ*cbrA,* but remains in the altruistic quadrant. On the other hand, the Δ*cbrA hfq** strain falls in the mutualistic quadrant with a mutualistic behavior very similar to the wild-type. The distinct social behaviors of the Δ*cbrA crc** and the

Δ*cbrA hfq** strains are particularly intriguing because the exponential growth rates of both of these strains are not significantly different from the WT (Fig 3.1C), and yet the Δ*cbrA crc** strain is less fit in a swarming colony, suggesting that its phenotypic differences are only revealed in a social context.

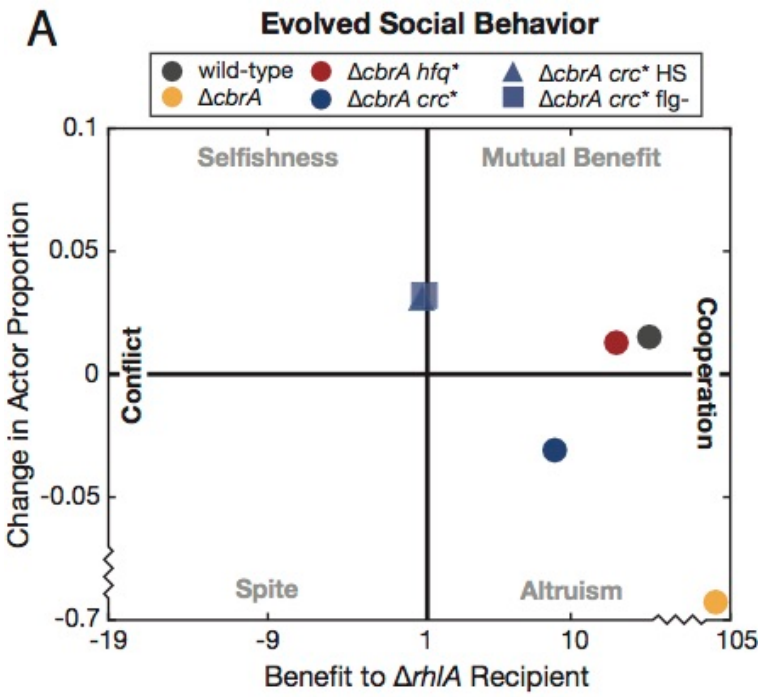


**Figure 3.8 Social behavior in isolated clones**

(A) Social behavior assay was performed with wild-type, Δ*cbrA,* Δ*cbrA crc** (1.3-1), Δ*cbrA hfq** (1.2-1), Δ*cbrA crc** HS (hyperswarmer) (2.3-8) and Δ*cbrA crc** flg- (flagella-less) (1.1-5) (methods). The wild-type and Δ*cbrA hfq** strains both show a mutualistic social phenotype while Δ*cbrA* and Δ*cbrA crc** strains are altruistic and their behavior is not predicted to be evolutionarily stable. Both Δ*cbrA crc** HS and Δ*cbrA crc** flg- show slightly selfish behavior.

**Stable cooperation achieved via an alternative metabolomic state**

To determine if the wild-type like behavior of the Δ*cbrA hfq** strain (Fig 3.1B&C Fig 3.7A) was due to a recovery of wild-type metabolism and to shed new light on the regulation of cooperation through metabolic prudence we compared the metabolomes of four strains: wild-type, Δ*cbrA,* Δ*rhlA,* Δ*cbrA crc** and Δ*cbrA hfq** strains (methods). Interstingly, we saw that the metabolome of the Δ*rhlA* strain very closely resembles the wild-type (Fig 3.9A and Figure 3.10). This suggests that complete removal of a cell's ability to produce rhamnolipids causes no significant disruption to the steady state levels of many key metabolites. This interesting finding is in agreement with previous work demonstrating that *rhlAB* expression dynamics are unchanged in the Δ*rhlA* strain compared to the wild-type [27]. It also supports a proposed feed-forward supply-driven model by which *P. aeruginosa* can maintain homeostatic levels of its metabolites independently of whether or not it produces rhamnolipids [15].

**Figure 3.9 Evolved isolates have distinct metabolic profiles**

(A) Unsupervised clustering of metabolites that have significant differences between strains by ANOVA with multiple hypothesis correction using an alpha of 0.01 and an n of 142. Sample numbers 1-3 indicate one biological replicate and sample numbers 4-6 indicate the second biological replicate. The Δ*rhlA* strain very closely resembles the wild-type and the Δ*cbrA crc** strain also has a metabolome very similar to wild-type. The Δ*cbrA* strain has a metabolome very distinct from the wild-type where multiple pathways appear to be disrupted. The Δ*cbrA hfq** strain most closely resembles the Δ*cbrA* strain, but has a distinct metabolic profile. (B) Fold change of metabolites in Δ*cbrA,* Δ*cbrA crc** and Δ*cbrA hfq** strains compared to wild-type. Multiple metabolites were found at high levels in the Δ*cbrA* strain and return to wild-type levels in Δ*cbrA crc** and Δ*cbrA hfq** strains. A number of metabolites are also found a low levels in Δ*cbrA* and return to normal levels in the Δ*cbrA crc** strain, but remain low in the Δ*cbrA hfq** strain. Metabolites shown were significantly altered in one of the mutant strains by ANOVA with multiple hypothesis correction using an alpha of 0.01 and an n of 145.

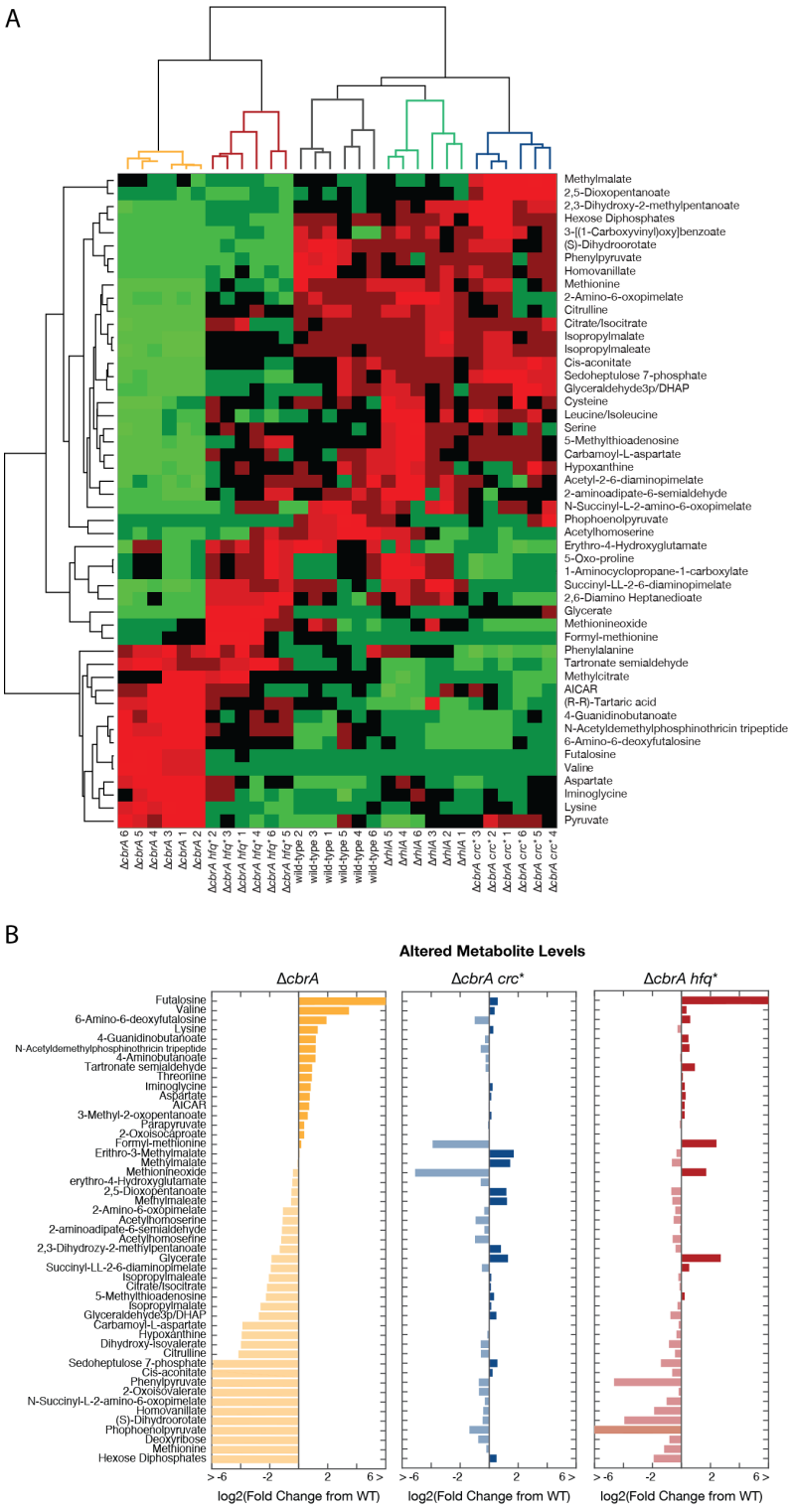
A
Methylmalate
2,5-Dioxopentanoate
2,3-Dihydroxy-2-methylpentanoate
Hexose Diphosphates
3-[(1-Carboxyvinyl)oxy]benzoate
(S)-Dihydroorotate
Phenylpyruvate
Homovanillate
Methionine
2-Amino-6-oxopimelate
Citrulline
Citrate/Isocitrate
Isopropylmalate
Isopropylmaleate
Cis-aconitate
Sedoheptulose 7-phosphate
Glyceraldehyde3p/DHAP
Cysteine
Leucine/Isoleucine
Serine
5-Methylthioadenosine
Carbamoyl-L-aspartate
Hypoxanthine
Acetyl-2-6-diaminopimelate
2-aminoadipate-6-semialdehyde
N-Succinyl-L-2-amino-6-oxopimelate
Phophoenolpyruvate
Acetylhomoserine
Erythro-4-Hydroxyglutamate
5-Oxo-proline
1-Aminocyclopropane-1-carboxylate
Succinyl-LL-2-6-diaminopimelate
2,6-Diamino Heptanedioate
Glycerate
Methionineoxide
Formyl-methionine
Phenylalanine
Tartronate semialdehyde
Methylcitrate
AICAR
(R-R)-Tartaric acid
4-Guanidinobutanoate
N-Acetyldemethylphosphinothricin tripeptide
6-Amino-6-deoxyfutalosine
Futalosine
Valine
Aspartate
Iminoglycine
Lysine
Pyruvate
ΔcbrA 6
ΔcbrA 5
ΔcbrA 4
ΔcbrA 3
ΔcbrA 1
ΔcbrA 2
ΔcbrA hfq* 2
ΔcbrA hfq* 3
ΔcbrA hfq* 1
ΔcbrA hfq* 4
ΔcbrA hfq* 6
ΔcbrA hfq* 5
wild-type 2
wild-type 3
wild-type 1
wild-type 5
wild-type 4
wild-type 6
ΔmlrA 5
ΔmlrA 4
ΔmlrA 6
ΔmlrA 3
ΔmlrA 2
ΔmlrA 1
ΔcbrA crc* 3
ΔcbrA crc* 2
ΔcbrA crc* 1
ΔcbrA crc* 6
ΔcbrA crc* 5
ΔcbrA crc* 4
B
Altered Metabolite Levels
ΔcbrA
ΔcbrA crc*
ΔcbrA hfq*
Futalosine
Valine
6-Amino-6-deoxyfutalosine
Lysine
4-Guanidinobutanoate
N-Acetyldemethylphosphinothricin tripeptide
4-Aminobutanoate
Tartronate semialdehyde
Threonine
Iminoglycine
Aspartate
AICAR
3-Methyl-2-oxopentanoate
Parapyruvate
2-Oxoisocaproate
Formyl-methionine
Erithro-3-Methylmalate
Methylmalate
Methionineoxide
erythro-4-Hydroxyglutamate
2,5-Dioxopentanoate
Methylmaleate
2-Amino-6-oxopimelate
Acetylhomoserine
2-aminoadipate-6-semialdehyde
Acetylhomoserine
2,3-Dihydrozy-2-methylpentanoate
Glycerate
Succinyl-LL-2-6-diaminopimelate
Isopropylmaleate
Citrate/Isocitrate
5-Methylthioadenosine
Isopropylmalate
Glyceraldehyde3p/DHAP
Carbamoyl-L-aspartate
Hypoxanthine
Dihydroxy-Isovalerate
Citrulline
Sedoheptulose 7-phosphate
Cis-aconitate
Phenylpyruvate
2-Oxoisovalerate
N-Succinyl-L-2-amino-6-oxopimelate
Homovanillate
(S)-Dihydroorotate
Phophoenolpyruvate
Deoxyribose
Methionine
Hexose Diphosphates
> -6
-2
2
6 >
log2(Fold Change from WT)

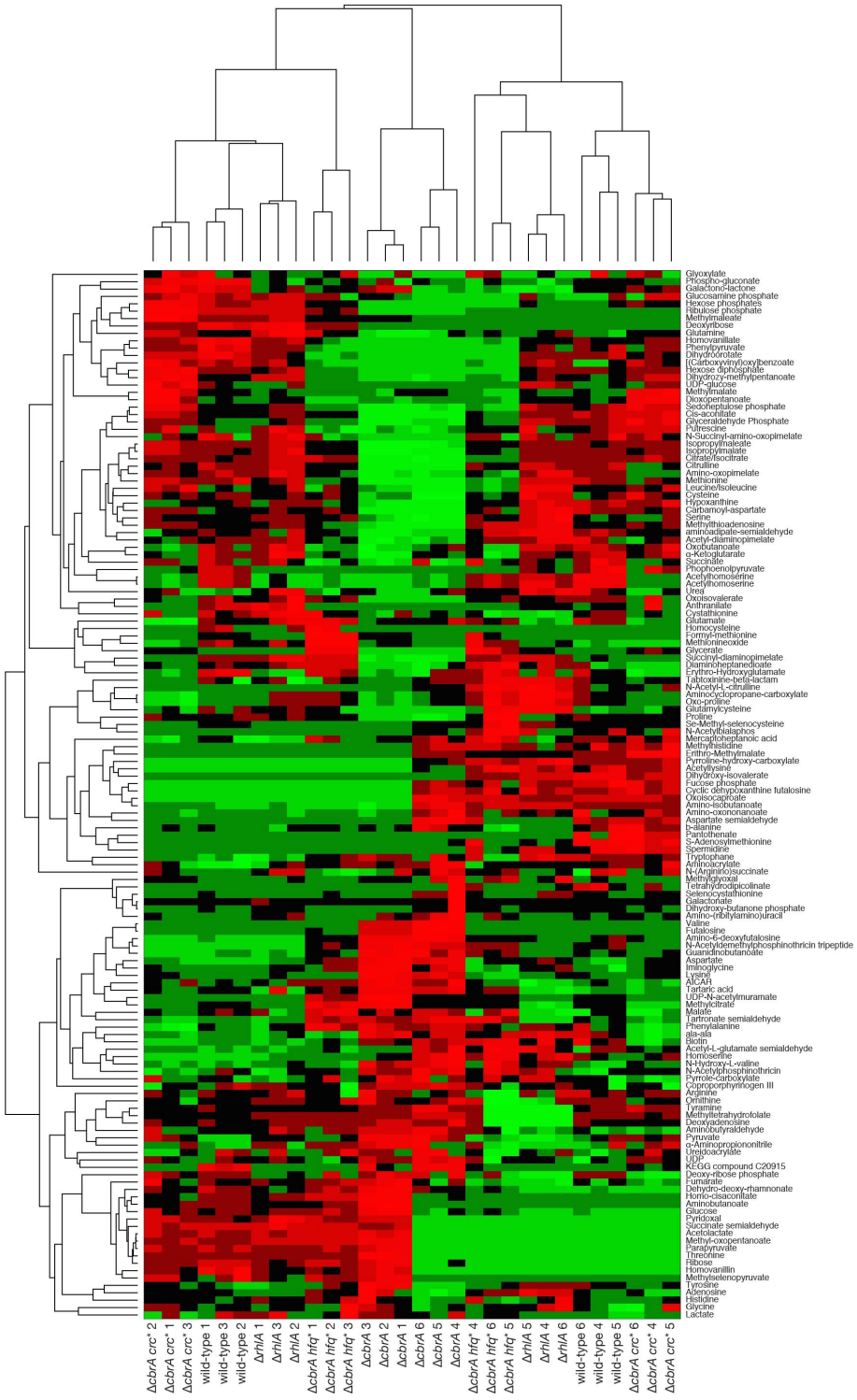


**Figure 3.10 Clustering of all metabolites**
Unsupervised clustering of strains using all measured metabolites from the targeted analysis (n = 142).

The metabolome of the Δ*cbrA* strain is, as expected, significantly altered compared to the wild-type (Fig. 3.9A). The many metabolites perturbed in the in the Δ*cbrA* strain participate in diverse pathways including amino acid synthesis and central carbon metabolism, for example: Methionine and citrate are at low levels while valine and lysine are particularly high (Fig. 3.9B). As we had suspected, most of the metabolites disrupted in the Δ*cbrA* strain returned to wild-type levels in Δ*cbrA crc** and Δ*cbrA hfq** strains, including the amino acids valine, lysine and methionine. Quite surprisingly we find that the metabolome of the Δ*cbrA crc** strain is more similar to the wild-type than the Δ*cbrA hfq** strain is (Fig 3.9A). Several metabolites that are found at lower levels in Δ*cbrA* compared to wild-type are also at lower levels in Δ*cbrA hfq**, while many of these have returned wild-type levels in the Δ*cbrA crc** strain (Fig 3.9B). This result is the opposite of what would have been predicted from the phenotypes we tested, including the social behavior assay, where the Δ*cbrA hfq** is more similar to the wild-type. Taken together our metabolic data suggests that the Δ*cbrA crc** strain has returned to a metabolic state more similar to the wild-type, but that this does not confer the same social behavior. In contrast the Δ*cbrA hfq** strain has a distinct metabolic profile, but shows a decreased cost of cooperation and a mutualistic social phenotype that can stabilize swarming cooperation.

**Mutants with altered flagella number emerge in sub-optimal cooperator**

Although the Δ*cbrA crc** strain shows recovery of the wild-type growth rate, its altruistic phenotype suggests that it may still be susceptible to invasion by fitter cheater strains. In fact, we identified two additional mutations emerging on the Δ*cbrA crc** background in isolates 1.1-5, 2.2-4, 2.3-3 and 2.3-8. Interestingly, strains 1.1-5 and 2.2-4 invaded the population even though they are incapable of swarming on their own (Fig 3.4A). These

strains have mutations in the flagella related genes *fleR* and *fleQ* respectively (Fig 3.4B Table 3.1). Closer examination revealed that these strains can outcompete other swarming strains by physically blocking competitors from swarming (Fig 3.11A). Interestingly, strains 2.3-3 and 2.3-8 are resistant to this blocking behavior. These isolates, 2.3-3 and 2.3-8, also have mutations in flagella related genes, but in this case both mutations are in *fleN*. Mutations in *fleN* have been previously shown to produce hyperswarmers [28]. Microscopy imaging revealed that 1.1-5 and 2.2-4 lack flagella while 2.3-3 and 2.3-8 have multiple flagella (*Pseudomonas aeruginosa* is normally mono-flagellated) (Fig 3.11B). These *fleN* mutant strains are capable of resisting smothering, potentially by piercing through the blockade produced by the strains lacking flagella.

Quantification of social behavior of the non-flagellated strain 1.1-5 and the multi-flagellated strain 2.3-8 reveals that both types of strains, non-flagellated and multi-flagellalted, are less cooperative and, therefore, more selfish (Fig 3.8B). These strains increase in numbers when mixed with the Δ*rhlA* strain and do so without benefiting the recipient strain. This selfish advantage is not simply due to a faster growth rate as 1.1-5 grows slower than the wild-type and 2.3-8 grows at the same rate (Fig 3.5B). Rather the additional mutations altering flagella number convey a fitness advantage in the Δ*cbrA crc** background by affecting the physical interactions between the bacteria in swarming colonies. Importantly, although both strains have reached the same fitness and social behavior, one strain remains a successful swarmer while the other prevents any swarming from occurring. To confirm that flagella-less cells can indeed block swarming colonies and that multi-flagellated cells can be resistant to blocking, we carried out competitions in the wild-type background. We used a Δ*flgK* mutant as a model non-flagellated strain and a *fleN* mutated hyperswarmer [28] as a model multi-flagellated strain (Fig 3.11C). The experiments confirmed that the mono-flagellated wild-type cells suffer the effects of

blocking when mixed with a Δ*flgK* strain at a frequency of 5:1 (Δ*flgK*:wild-type) or less. However, multi-flagellated hyperswarmers can resist blocking down to a frequency of 100:1 (Δ*flgK*:hyperswarmer) (Fig 3.11C).

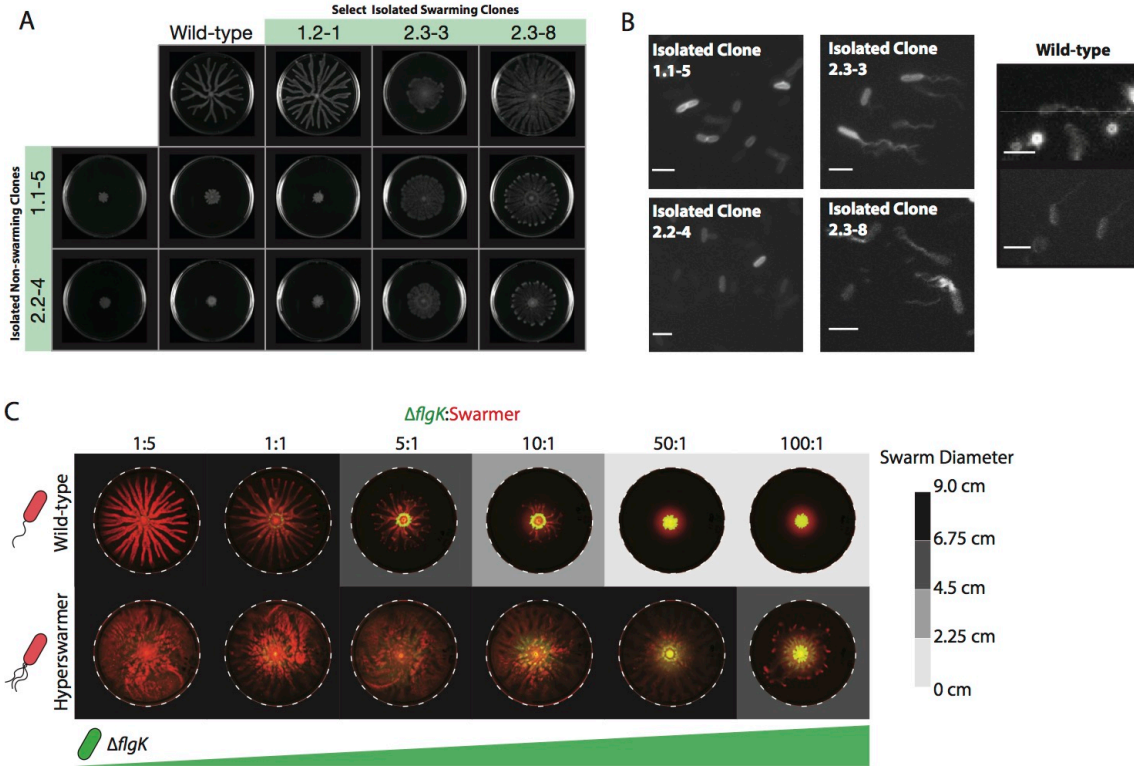


**Figure 3.11 The effect of flagella number on swarming morphology**

(A) Swarms of individual strains and swarms from mixed inoculation. When 1.1-5 or 2.2-4 were mixed with wild-type or 1.2-1 and inoculated onto a swarming plate the swarm is smothered and unable to spread across the plate. Isolated clones 2.3-3 and 2.3-8 are resistant to smothering and are capable of swarming even when mixed with 1.1-5 and 2.2-4. (B) Microscopy images of isolated clones and wild-type. Isolated clones 1.1-5 and 2.2-4 do not have any observed flagella while 2.3-3 and 2.3-8 have instances of multiple flagella. The wild-type is mono-flagellated. Scale bars are 5μM (C) Mixed swarms of fluorescently labeled wild-type, wild-type background hyperswarmer [28] and Δ*flgK*. The wild-type begins to decrease in swarming radius at 5:1 Δ*flgK*:wild-type while the hyperswarmer only decreases in swarming radius at 1000:1 Δ*flgK*:hyperswarmer.

## Discussion

Bacteria have diverse social lives and their many social behaviors constitute ideal experimental systems to investigate the intricate links between social evolution and molecular mechanism. Here we used swarming in *Pseudomonas aeruginosa*, a remarkable cooperative behavior, to investigate for the first time the recovery of stable cooperation at a metabolic level by combining experimental evolution and metabolomics. Previous evolutionary experiments with *P. aeruginosa* swarming had shown remarkably reproducible evolution of hypwerswarmer mutants [28]. Those experiments started with wild-type bacteria that are already capable of metabolic prudence and therefore inform little about the link between metabolism and the evolution of cooperation. Here we took a different approach by starting evolutionary experiments with the carbon catabolite repression mutant Δ*cbrA*, an altruistic strain that is incapable of swarming on its own even though it over-cooperates to such a degree that cooperation has a major cost to fitness.

Our results reveal that swarming cooperation can indeed recover from a major perturbation, the genetic deletion of *cbrA*, but the recovery is not always stable. Δ*cbrA crc** mutants initially invade the experimental populations because loss of function mutations in *crc* are very common and advantageous in the Δ*cbrA* background. These Δ*cbrA crc** strains rearrange their metabolome relative to the Δ*cbrA* perturbed state to a state that closely resembles the wild-type. Despite the wild-type similarities (Fig 3.1B and Fig 3.9A) the Δ*cbrA crc** strain still behaves as an altruist and therefore can easily be invaded by selfish strains with mutations that affect flagella number (Fig 3.8B). In contrast, mutations in *hfq* or its promoter recover wild-type growth rate and cooperative at a low cost to individual fitness (Fig 3.1B&C).

The metabolomics analysis of the Δ*rhlA* strain was also informative as it allowed confirmation of previous hypotheses about metabolic prudence for the first time. Previous work investigating metabolic prudence and the regulation of *rhlAB* suggested that when the rhamnolipid production pathway is removed the cell is able to compensate for this lack of carbon secretion in a way that does not effect growth or *rhlAB* expression, potentially by decreasing uptake of carbon [15, 27]. The metabolomics of wild-type, Δ*cbrA*, Δ*cbrA crc**, and Δ*cbrA hfq** strains together with the phenotypic data suggest that in the Δ*cbrA* background it is possible to regain a metabolic state similar to the wild-type, but that this is not the most advantageous state evolutionarily. The Δ*cbrA* strain has a significantly altered metabolism and the slowed growth and overexpression of *rhlAB* are likely consequences of this disrupted metabolome. Multiple pathways are disrupted in the Δ*cbrA* strain compared to wild-type including the citric acid cycle, glycolysis and many amino acid pathways, with particularly high levels of valine and low levels of methionine being found in Δ*cbrA*. Although the CbrA/CbrB system has been known to influence metabolism and carbon usage from several previous studies [21, 22, 29], here we confirm this regulatory role from a systems-level view. Interestingly, many of the disruptions seen in the Δ*cbrA* strain are not present in the Δ*cbrA crc** mutant which has an internal metabolome that very closely resembles the wild-type with a few exceptions, namely methylmalate and 2-5 Dioxopentanoate that are only metabolites detected at significantly higher levels in Δ*cbrA crc** (Fig 3.9 A&B). Although Δ*cbrA crc** has a metabolome similar to the wild-type it behaves more altruistically and therefore remains vulnerable to invasion by selfish strains. The Δ*cbrA hfq** strain is mutualistic like the wild-type, but has a very distinct metabolome (Fig 3.8A, Fig 3.9A). A number of metabolites are found at lower levels in both Δ*cbrA hfq** and Δ*cbrA* including hexose diphosphates, [(Carboxyvinyl)oxy]benzoate, dihydroorotate, phenylpyruvate, homovanillate and methionine (Fig 3.9A&B). A few metabolites are also only found at high levels in Δ*cbrA hfq** and Δ*cbrA* such as tartronate semialdehyde, methylcitrate and

AICAR (Fig 3.9 A&B). It is possible that one of these metabolites that is either maintained at a low or high level in the Δ*cbrA hfq** and Δ*cbrA* strains plays a role in controling *rhlAB* expression and explains the higher levels of rhamnolipid synthesis in Δ*cbrA hfq** compared to the Δ*cbrA crc**. It should be noted, however, that we are comparing steady state metabolite levels and not metabolite fluxes. This allows us to observe wide disruptions of the metabolomic state, but does not inform us how the actual metabolic fluxes are perturbed. Overall, our results suggest that the Δ*cbrA hfq** strain has a metabolic state that allows it to behave socially like the wild-type even though it lacks CbrA. Our data supports that, at least in social behavior, it is not always advantageous to return to the pre-perturbation metabolic state after a key regulatory element has been removed. In this study we found that organisms can recover stable cooperation in the absence of a key metabolic regulator by achieving a distinct metabolomic state.

High relatedness can stabilize constitutive cooperative secretions like rhamnolipids [16], however, factors like environmental mixing, horizontal gene transfer and high mutation rates make maintaining high relatedness a significant challenge for microbial cooperation. There are examples of mechanisms that increase relatedness by keeping a lineage spatially segregated such as physical aggregation, colony sectoring and certain secreted products that work similarly to kin recognition [30-36]. However, these fairly rudimentary methods do not guarantee that a bacterial cooperator will only interact with relatives in the long term. Reducing the cost of cooperation, on the other hand, can stabilize cooperative traits without a need for maintaining high relatedness. This study reveals that the metabolic state of the cell is a key determinant of stable cooperation. Further steps in identifying molecular mechanisms that regulate prudent expression of public good genes by unicellular organisms will shed new light on the fascinating problem of the evolution of multicellular cooperation.

## Materials and Methods

All primers are from IDT unless otherwise stated.

All chemical reagents are from Fisher Scientific unless otherwise stated.

### Deletion of *cbrA*

Primers:

UpCbrAFwd GGGGACAAG

TTTGTACAAAAAAGCAGGCTACAGCTGGAATATCGCTTCGTCG

UpCbrARev CGCCTTCTCGCTGGTGATCCGTCAGCATCGCGCTGGCTC

DownCbrAFwd GATCACCAGCGAGAAGGCG

DownCbrARev

GGGGACCACTTTGTACAAGAAAGCTGGGTACAGCTCGGATTCGATCAGGG

CbrAPCRFwd AAGCATGAGGGAAGCGGCAT

CbrAPCRRev AACAACATGTCGAAGGAGGG

CbrASeqFwd CCTCATCGTGGTCACTTTC

CbrASeqRev ATTCAGCTCTCTCGACGTGC

Milli-Q-Water-resuspended stocks of oligonucleotides (100 μM) were stored at −20°C. Stock solutions were diluted tenfold to a working concentration. Regions of homology outside of a cbrA of interest were created using the following primers: Upstream region: UpCbrAFwd and UpCbrARev, Downstream region: DownCbrAFwd and DownCbrARev. The deletion construct was obtained through splicing overlap extension (SOE) PCR, followed by Gateway cloning (Life Technologies, Grand Island, NY) before integration of the suicide plasmid into the P. aeruginosa genome. SOEing was done using UpCbrAFwd and DownCbrARev. The deletion yielded a scarred deletion encoding a 27aa peptide. Integration of the suicide plasmid into the genome of P. aeruginosa was

verified with primers CbrAPCRFwd and CbrAPCRRev. The clones of interest that were obtained after sucrose counter-selection were verified through PCR followed by sequencing using CbrAPCRFwd, CbrAPCRRev, CbrASeqFwd and CbrASeqRev.

**Media**

Minimal media nutrient composition is used in liquid minimal media and the media in swarming plates. Minimal medium for swarming plate and liquid culture assays: 800 ml of Milipore water, 200 ml of 5X minimal salts buffer, 1 ml of 1 M magnesium sulphate, 0.1 ml of calcium sulphate, 25 ml of 200 g/L solution of casamino acids (Bacto TM from BD, Sparks, MD). 5X stock minimal salts buffer: 12 g of Na2HPO4 (anhydrous), 15 of KH2PO4 (anhydrous) and 2.5 g of NaCl into 1L water. Synthetic media for liquid culture: 800 ml of Milipore water, 200 ml of 5X minimal salts buffer, 1 ml of 1 M magnesium sulphate, 0.1 ml of calcium sulphate with stated concentrations of carbon (glycerol), nitrogen (ammonium sulphate) and iron at 5μM (iron III sulphate). 6.25% agar was used for hard agar plates, and 1.857% agar for swarming plates.

**Swarming Assay**

Swarming assays were performed as described previously [11]. Swarming assays were performed using minimal media 1.875% agar plates. Strains were grown in 3mL LB overnight cultures at 37C. 1mL of each strains was washed 2X with PBS and 2uL of the final suspension was used to inoculate a swarming plate. Plates were incubated at 37C for 24 hours. For co-inoculated swarms, where swarming plates are inoculated with two strains that are not well mixed, 2μL of the cell suspension for each strain are spotted onto the agar plate at a distance of <2mm apart.

**Imaging Swarming Colonies**

Swarming colonies were imaged using a Typhoon 9400 (GE Healthcare) for fluorescent labels and a Chemidoc gel doc imager (Bio Rad) for non-fluorescent still images.

**Growth Rate**

Growth curves were performed as reported previously [27] in the media stated. Cultures were started at an OD of 0.0025. Exponential growth rates were calculated from the first 10 time points occurring after the culture had reached an OD of 0.01 on Tecan plate reader.

***rhlAB* expression**

*rhlAB* expression was measured using a $P_{rhlAB}$-*gfp* promoter [37]. Measurements reported are expression from 24 hours of growth in minimal media.

**Biofilm Index**

Biofilm formation was assessed using a crystal violet assay in a 96 well plate as described previously [38] with some adaptions. Biofilm index is the ratio of attached cells to free cells in the media.

**Experimental Evolution**

Experimental evolution was performed as described previously [28]. To initiate the experimental evolution the Δ*cbrA* $P_{rhlAB}$-*gfp* strain was inoculated in 3mL of LB and incubated overnight at 37C. 1mL of overnight culture was washed 2X with PBS and 2 uL of the final suspension was used to initiate each of 3 replicates on swarming minimal media agar plates. Each of the swarms grown after 24 hours was then washed from the plate into a volume of 3mL 1X PBS. 2uL of this cell suspension were then used to inoculate a fresh swarming plate, which was then incubated for 24 hours at 37C. The

washing and inoculation of a fresh plate was repeated for each day of the experimental evolution.

**Liquid Culture Measurements**

Strains were inoculated into 3mL of LB and incubated overnight at 37˚C. 1mL of overnight culture was washed twice with 1mL PBS and then inoculated into minimal media at an OD of 0.0025 in a 96 well plate 150µL per well. The plates were shaken and incubated at 37˚C for 24 hours. Absorbance, and excitations and emissions were measured using a Tecan plate reader (Tecan). Absorbance measurements were done at 600nm, 690nm, and 310nm. GFP was measured using an excitation 488nm of and an emission of 452nm. Pyoverdine (pvd) was measured using an excitation of 405nm and an emission of 465nm. An excitation of 340nm and an emission of 440nm was also measured.

**Diversity Score**

Liquid culture measurements for each strain were used to generate a dendogram. A linkage distance cutoff of 1.12 was used to set the number of clusters present. The diversity score was then calculated for each population by the following formula:
*(number of clusters represented in population / 8 ) * 100*
Yielding a maximum possible score of 100 and a minimum possible score of 12.5.

**Whole genome sequencing**

Genomic DNA extraction was performed using Wizard Genomic DNA Purification Kit (Promega). Genomes were sequenced at the New York Genome center with 2 X 125bp HiSeq with coverage of 50X. Mutations were determined using breseq [39].

**Social Behavior Assay**

Strains were grown and washed according to the swarming assay protocol above. Before inoculation Δ*rhlA* $P_{A1/04/03}$-DsRed was mixed with the actor strain at a ratio of 1:25 Δ*rhlA*:actor. 2µL of the mixed cell suspension were used to inoculate the swarming plate. After 24 hours of incubation the swarms were washed and the cells collected in 3mL 1XPBS. The collected cellular suspension was used for colony forming unit plating on hard agar minimal media plates. Colony forming units (CFU) were used to determine the ratio and total number of cells for each strain. The benefit to the actor is calculated by the following equation: *(Starting actor fraction) – (Final actor fraction)*. The fraction of the actor strain is determined by: *(number of actor cells / total cells observed)*. The number of cells is determined by CFU count. The benefit to the DsRedExpress labeled Δ*rhlA* recipient is calculated by: *(*Δ*rhlA total cell number when mixed with actor/* Δ*rhlA total cell number when mixed with GFP labled* Δ*rhlA)*

**Metabolite Extraction**

Strains were grown to exponential phase in synthetic media with 3.0 gC/L (glycerol) 0.5gN/L (ammonium sulfate) and 5µM iron (iron III sulfate). Bacteria were loaded onto 0.20µm nylon membranes (Millipore) using a vacuum apparatus. Bacteria laden filters were immediately transferred to pre-warmed hard agar plates with a media composition identical to the synthetic liquid media. Filters on hard agar plates were incubated at 37˚C for 2.5 hours. Filters were then transferred to 35mm polystyrene dishes (Falcon) with 1mL 2:2:1 acetonitrile:methanol:water quenching buffer on dry ice. Filters were incubated for 15 minutes on ice and cells were removed from filters by scraping. Quenching buffer containing cell lysate was then transferred to 1.5mL micro-centrifuge tubes (eppendorf) on ice and centrifuged at 16000rcf for 10 minutes at 4˚C. Supernatant was then transferred to a fresh tube and stored at -80C.

**Metabolomics Analysis**

LC-MS based metabolomic profiling was utilized to report the metabolic landscapes of the wild-type and genetic modified *Pseudomonas aeruginosa*. As shown previously [40], extracted metabolites were separated on a Cogent Diamond Hydride type C column (MicroSolv). The mobile phase comprises solvent A (dd$H_2O$ with 0.2% formic acid) and solvent B (acetonitrile with 0.2% formic acid). The gradient used was as listed below: 0–2 min, 85% B; 3–5 min, 80% B; 6–7 min, 75%; 8–9 min, 70% B; 10–11.1 min, 50% B; 11.1–14 min 20% B; 14.1–24 min 5% B followed by a 10 min reequilibration period at 85% B at a flow rate of 0.4 mL/min. Agilent Accurate Mass 6220 TOF coupled to an Agilent 1200LC system was used as the mass spectrometer. The metabolites were identified by accurate-mass matching (mass tolerance < 0.005 Da) and where available retention time matching against chemical standards. Metabolite ion counts were extracted using Profinder 8.0 and Qualitative Analysis 6.0 (Agilent). In order to correct for variation in sample concentration we calculated the scaling factor by fitting a generalized linear model using the fitglm function in Matlab using log as the link function with the following formula in Wilkinson notation:

*peakArea ~ mutant*experiment + metabolite*

This calculates the scaling coefficient under the assumption that majority of metabolites are unchanged across the strains. We selected metabolites that passed multiple hypothesis correction using ANOVA with an alpha of 0.01 and an n of 142.

**Flagella Staining**

Flagella staining was adapted from Darnton [41] performed as reported previously [42]. Cells in exponential in LB liquid media phase are gently washed three times in 1mL 1X PBS (centrifuged at 350 rcf for 10 min). A solution of 10 mg/mL (suspended in dimethyl sulfoxide) Alexa Fluor 488 carboxylic acid, succinimidyl ester (Molecular Probes) was added to the cellular suspension at a ratio of 1:50 (label solution volume : cell suspension volume). Cells were incubated with the label for 90 min at room temperature. Cells were

washed three times in 1X PBS (centrifuged at 350 rcf for 10 min). After washing cells are suspended in 1X PBS to a final OD600 of ~0.1.

## References


1. JM Smith, E.S., *The major transitions in evolution*. 1997: Oxford University Press.
2. Nadell, C.D., et al., *Cutting through the complexity of cell collectives.* Proc Biol Sci, 2013. **280**(1755): p. 20122770.
3. West, S.A., et al., *Social evolution theory for microorganisms.* Nat Rev Microbiol, 2006. **4**(8): p. 597-607.
4. Gore, J., H. Youk, and A. van Oudenaarden, *Snowdrift game dynamics and facultative cheating in yeast.* Nature, 2009. **459**(7244): p. 253-6.
5. Koschwanez, J.H., K.R. Foster, and A.W. Murray, *Improved use of a public good selects for the evolution of undifferentiated multicellularity.* Elife, 2013. **2**: p. e00367.
6. Popat, R., et al., *Collective sensing and collective responses in quorum-sensing bacteria.* J R Soc Interface, 2015. **12**(103).
7. Hamilton, W.D., *The Genetical Evolution of Social Behaviour.* Journal of Theoretical Biology, 1964. **7**: p. 1-16.
8. West, S.A., A.S. Griffin, and A. Gardner, *Evolutionary explanations for cooperation.* Curr Biol, 2007. **17**(16): p. R661-72.
9. Human Microbiome Project, C., *Structure, function and diversity of the healthy human microbiome.* Nature, 2012. **486**(7402): p. 207-14.
10. Xavier, J.B., *Social interaction in synthetic and natural microbial communities.* Mol Syst Biol, 2011. **7**: p. 483.
11. Xavier, J.B., W. Kim, and K.R. Foster, *A molecular mechanism that stabilizes cooperative secretions in Pseudomonas aeruginosa.* Mol Microbiol, 2011. **79**(1): p. 166-79.
12. Rashid, M.H. and A. Kornberg, *Inorganic polyphosphate is needed for swimming, swarming, and twitching motilities of Pseudomonas aeruginosa.* Proc Natl Acad Sci U S A, 2000. **97**(9): p. 4885-90.
13. THILO KOHLER, L.K.C., FRANCISCO BARJA, CHRISTIAN VAN DELDEN, AND JEAN-CLAUDE PECHE`RE, *Swarming of Pseudomonas aeruginosa Is Dependent on*
*Cell-to-Cell Signaling and Requires Flagella and Pili.* Journal Of Bacteriology, 2000. **182**(21).
14. Brett Mellbye, M.S., *Physiological Framework for the Regulation of Quorum Sensing- Dependent Public Goods in Pseudomonas aeruginosa.* Journal Of Bacteriology, 2014. **196**(6): p. 1155-1164.
15. Boyle, K.E., et al., *Integration of Metabolic and Quorum Sensing Signals Governing the Decision to Cooperate in a Bacterial Social Trait.* PLoS Comput Biol, 2015. **11**(5): p. e1004279.

16. de Vargas Roditi, L., K.E. Boyle, and J.B. Xavier, *Multilevel selection analysis of a microbial social trait.* Mol Syst Biol, 2013. **9**: p. 684.
17. Schuster, M., et al., *Acyl-homoserine lactone quorum sensing: from evolution to application.* Annu Rev Microbiol, 2013. **67**: p. 43-63.
18. Tadler, R.E.L.M.R.R.S.C.S.S.C., *Long-Term Experimental Evolution in Escherichia coli. I. Adaptation and Divergence During 2,000 Generations.* The American Naturalist, 1991. **138**(6).
19. Aldridge, B.B. and K.Y. Rhee, *Microbial metabolomics: innovation, application, insight.* Curr Opin Microbiol, 2014. **19**: p. 90-6.
20. Li, W. and C.D. Lu, *Regulation of carbon and nitrogen utilization by CbrAB and NtrBC two-component systems in Pseudomonas aeruginosa.* J Bacteriol, 2007. **189**(15): p. 5413-20.
21. Zhang, X.X., et al., *Role of the Transporter-Like Sensor Kinase CbrA in Histidine Uptake and Signal Transduction.* J Bacteriol, 2015. **197**(17): p. 2867-78.
22. Valentini, M., et al., *Hierarchical management of carbon sources is regulated similarly by the CbrA/B systems in Pseudomonas aeruginosa and Pseudomonas putida.* Microbiology, 2014. **160**(Pt 10): p. 2243-52.
23. Deziel, E., et al., *rhlA is required for the production of a novel biosurfactant promoting swarming motility in Pseudomonas aeruginosa: 3-(3-hydroxyalkanoyloxy)alkanoic acids (HAAs), the precursors of rhamnolipids.* Microbiology, 2003. **149**(Pt 8): p. 2005-13.
24. Takayuki Nishijyo, D.H.a. and Y. Itoh, *The CbrA-CbrB two-component regulatory system controls the utilization of multiple carbon and nitrogen sources in Pseudomonas aeruginosa.* Molecular Microbiology 2001. **40**(4): p. 917-931.
25. Sonnleitner, E. and U. Blasi, *Regulation of Hfq by the RNA CrcZ in Pseudomonas aeruginosa carbon catabolite repression.* PLoS Genet, 2014. **10**(6): p. e1004440.
26. Moreno, R., et al., *The Crc and Hfq proteins of Pseudomonas putida cooperate in catabolite repression and formation of ribonucleic acid complexes with specific target motifs.* Environ Microbiol, 2015. **17**(1): p. 105-18.
27. van Ditmarsch, D.J.o.B.X., *High-resolution time series of Pseudomonas aeruginosa gene expression and rhamnolipid secretion through growth curve synchronization.* BMC Microbiology, 2011. **11**(140).
28. van Ditmarsch, D., et al., *Convergent evolution of hyperswarming leads to impaired biofilm formation in pathogenic bacteria.* Cell Rep, 2013. **4**(4): p. 697-708.
29. Valentini, M. and K. Lapouge, *Catabolite repression in Pseudomonas aeruginosa PAO1 regulates the uptake of C4 -dicarboxylates depending on succinate concentration.* Environ Microbiol, 2013. **15**(6): p. 1707-16.
30. Koschwanez, J.H., K.R. Foster, and A.W. Murray, *Sucrose utilization in budding yeast as a model for the origin of undifferentiated multicellularity.* PLoS Biol, 2011. **9**(8): p. e1001122.
31. Smukalla, S., et al., *FLO1 is a variable green beard gene that drives biofilm-like cooperation in budding yeast.* Cell, 2008. **135**(4): p. 726-37.

32. Nadell, C.D., K.R. Foster, and J.B. Xavier, *Emergence of spatial structure in cell groups and the evolution of cooperation.* PLoS Comput Biol, 2010. **6**(3): p. e1000716.
33. Hallatschek, O., et al., *Genetic drift at expanding frontiers promotes gene segregation.* Proc Natl Acad Sci U S A, 2007. **104**(50): p. 19926-30.
34. Ratcliff, W.C., et al., *Origins of multicellular evolvability in snowflake yeast.* Nat Commun, 2015. **6**: p. 6102.
35. Xavier, J.B. and K.R. Foster, *Cooperation and conflict in microbial biofilms.* Proc Natl Acad Sci U S A, 2007. **104**(3): p. 876-81.
36. Zhang, F., et al., *A Synthetic Quorum Sensing System Reveals a Potential Private Benefit for Public Good Production in a Biofilm.* PLoS One, 2015. **10**(7): p. e0132948.
37. Boles, B.R., M. Thoendel, and P.K. Singh, *Rhamnolipids mediate detachment of Pseudomonas aeruginosa from biofilms.* Mol Microbiol, 2005. **57**(5): p. 1210-23.
38. Kolter, G.A.O.T.a.R., *Initiation of biofilm formation inPseudomonasfluorescensWCS365 proceeds via multiple, convergentsignalling pathways: a genetic analysis.* Molecular Microbiology 1998. **28**(3): p. 449-461.
39. Deatherage, D.E. and J.E. Barrick, *Identification of mutations in laboratory-evolved microbes from next-generation sequencing data using breseq.* Methods Mol Biol, 2014. **1151**: p. 165-88.
40. Rhee, H.E.a.K.Y., *Multifunctional essentiality of succinate metabolism in adaptation to hypoxia in Mycobacterium tuberculosis.* PNAS, 2013 **110**(16): p. 6554-9.
41. Darnton, N.C., et al., *On torque and tumbling in swimming Escherichia coli.* J Bacteriol, 2007. **189**(5): p. 1756-64.
42. Deforet, M., et al., *Hyperswarming adaptations in a bacterium improve collective motility without enhancing single cell motility.* Soft Matter, 2014. **10**(14): p. 2405-13.

# Chapter 4 - Conclusion

**The importance of Computational and Systems Biology to Unveil the Role of Bacteria as Members of Complex Social Communities**

Cooperative behavior plays a key role in bacterial survival in the host and in the environment [1, 2]. Approaches that integrate molecular microbiology, computational systems biology, and sociobiology can increase our understanding of bacterial behavior. Advances in molecular microbiology have increased the experimental tractability of many organisms and parallel advances in sequencing technology now allow us to track genetic changes in bacterial systems with unprecedented precision and depth [3]. Although technological advances allow for detailed high-throughput experiments, these studies generate large amounts of multidimensional data. Systems biology approaches that utilize computational techniques allow us to fully harness the amount of information that can now be gathered from microbial systems [4]. The improved organization and processing of biological data that can be achieved with computational methods will increase the insights we can gain from experiments making use of new technologies, but using computational techniques only as a data management tools falls dramatically short of the true value that these methods can bring to the study of biological problems. Computation models of molecular systems can provide predictive power and generate novel hypotheses that would be difficult or impossible to formulate otherwise. Additionally, computational methods can increase the feasibility of studying complex communities. We have come to realize that bacteria are more frequently members of social communities than freestanding cells. Microbiology can now leverage the wealth of literature and theory developed for understanding social interactions in multicellular organisms. Viewing microbes through the lens of sociobiology can increase our understanding of bacterial behaviors and the molecular architecture of regulatory systems that govern social traits. Studies of microbial social systems can also inform studies of

multicellular organisms and vice versa, increasing our understanding of the fundamental mechanisms that stabilize cooperation at individual and population levels.

The studies in chapters two and three of this thesis take an integrated approach, utilizing computational, molecular and sociobiology methods. Through the use of quantitative wet lab experiments and computational models the regulation that stabilizes cooperation through rhamnolipid production in *P. aeruginosa* was found to involve a continual integration of metabolic and population density signals. The work detailed in chapter three utilized sociobiology theory and molecular techniques to study the recovery of stable rhamnolipid production after significant perturbation to cellular metabolism. Together these studies increase our understanding of the molecular mechanisms that govern cooperative systems, demonstrate the value of integrative approaches in molecular microbiology, and support the significant role that metabolism plays in social behavior.

### *Pseudomonas aeruginosa* Integrates Metabolic and Population Density Information into the Molecular Decision to Cooperate

In chapter 2 I determined that *P. aeruginosa* integrates metabolic signals with quorum sensing information in a non-digital manner in the regulation of rhamnolipid production. Although the induction of the *rhlAB* operon can appear to act like a digital switch in rich media, through careful manipulation of synthetic media the graded response of the *rhlAB* promoter to quorum sensing signals and nutrient starvation became evident. The differing expression of *rhlAB* in iron and nitrogen starvation highlights that differences in the metabolic state of the cell can have a significant effect on the level of cooperative gene expression.

Importantly, the conclusions of this study would not have been possible without the aid of computational techniques. The expression of the *rhlAB* operon was studied over several conditions and across high-resolution time series. The large amount of dynamic, multidimensional data was analyzed and interpreted through a mathematical model of bacterial growth and *rhlAB* expression. The use of mathematical modeling revealed early on in the project that we could not explain *P. aeruginosa* growth in nitrogen and iron starvation through classical bacterial growth dynamics and led us to generate novel hypotheses about the biological processes occurring during these starvation periods. In the analysis of *rhlAB* expression, computation methods were essential to accurately determine the expression dynamics. The ability to precisely account for growth rate and population density and to perform autocorrection on *gfp* measurements enabled the realization that expression occurs during exponential growth and that this expression is due to a graded response to quorum sensing signals. As demonstrated here, computational methods can be used to harness large data sets, increase the tractability of studying complex dynamics systems, and aid in the analysis of subtle behavior that would otherwise evade explanation.

**The Metabolic Basis of Cooperative Trait Stability**

In the third chapter of this thesis the link between metabolism and cooperation was investigated using the *P. aeruginosa* swarming model system. The value of prudently regulating rhamnolipid production in swarming colonies has been well demonstrated [5, 6]. To understand the molecular mechanisms that regulate prudent cooperation, known molecular information was combined with experimental evolution techniques to observe the recovery of stable cooperation after significant metabolic perturbation.

Although bacteria are relatively simple model organisms for study, the benefits of using such a system can outweigh the biological distance between bacteria and more complex multicellular organisms. The genetic tractability and short generation times of bacteria allow for the study of social behavior on evolutionary time scales not yet possible with multicellular organisms. Perhaps more importantly, bacteria offer us the ability to study an organism in its entirety. The links between genes, biochemistry, metabolism and behavior are complex and dynamic. Bacteria offer the ability to measure the entire system and validate hypotheses generated from multicellular systems or theoretical work. In this study the phenotypic behavior of the evolved mutants suggested that Δ*cbrA hfq** mutants had recovered to a state closer to the wild-type than Δ*cbrA crc** mutants. However, by analyzing the metabolome of these strains it was determined that the behavior of the Δ*cbrA hfq** mutant was actually associated with a distinct metabolic state that more closely resembled the Δ*cbrA* ancestor than the wild-type. Here the ability to investigate the entire metabolome of each strain allowed for an objective analysis of the intercellular state associated with different behaviors and greatly influenced the conclusions drawn from this study. Additionally, the genotypes of the mutants of interest were only known due whole genome sequencing. The ability to couple genomics with metabolomics in increasingly high-throughput can allow us to continue to elucidate how changes in the genome translate to changes in the metabolome and ultimately alter how organisms interact with each other through social behavior.

**The Role of Social Behavior in Infections**

Although bacterial communication and social behavior is now known as an important component of virulence and infection [1], sociobiology approaches have yet to be widely applied to infectious pathogens, particularly *in vivo*. The types of social behavior and dynamic interactions between bacteria in an infection are still largely a mystery, however

several examples of bacterial social behavior shaping the dynamics an infection and antibiotic resistance have added to our understanding [7, 8]. Unraveling the types of social interactions that occur within an infection model could lead to novel targets for therapy or new practices for preventing infection. Studying the dynamic systems in an *in vivo* setting presents a considerable challenge. The interactions between bacteria and between bacteria and the host must be taken into account simultaneously and over the course of an infection. Here the application of computation and systems biology techniques can be used to manage the complex data, while sociobiology theory can aid in the explanation and contextualization of observed behaviors.

We also increasingly appreciate the importance of commensal bacteria that colonize multicellular organisms [9]. This has led to viewing certain infections, particularly those in the gut, not as single pathogens invading an organism, but as pathogens expanding or invading an already present and diverse community of microbes. Here the social dynamics between and within species of bacteria could play large roles in determining the course an infection will take. *In vitro* model systems that expand to examine multiple species within a model social system can be used to increase our understanding of bacterial social dynamics in more complex settings. These data can then be leveraged to better understand social behavior of microbes in increasingly complex environments. Systems biology techniques are critical to use in increasingly complex environments, however bringing these methods and a sociobiology approach to infectious systems with single pathogens has the potential to reveal interactions and dynamics that are key to the establishment of infection.

**Metabolism and Social Behavior**

The link between metabolism and social behavior is a complex one because it involves processes at several different timescales [10, 11]. The role of intracellular metabolism in the social behavior of animals raises interesting questions for molecular and sociobiology, but they come with a large degree of complexity. The metabolic processes will differ in different cells types and brain function and energy consumption must also be carefully taken into account. Microbial model systems with simple social behaviors allow us to investigate the link between metabolism and social behavior and discover general principles that bridge genetic, metabolic and social networks. Social behavior and costs of cooperation require the careful management of an individual's resources. This internal management will ultimately reduce to a regulation of the metabolic network within an individual. Using microbes as a model system allows for the study of the entire metabolome as well as the entire genome on evolutionary timescales. Combining bacterial metabolomics studies with social phenotypes that can be precisely manipulated in the lab has the potential to inform us of the metabolic foundation that underlies social interaction in an unprecedented manner.

**References:**


1. Rutherford, S.T. and B.L. Bassler, *Bacterial quorum sensing: its role in virulence and possibilities for its control.* Cold Spring Harb Perspect Med, 2012. **2**(11).
2. West, S.A., et al., *Social evolution theory for microorganisms.* Nat Rev Microbiol, 2006. **4**(8): p. 597-607.
3. Metzker, M.L., *Sequencing technologies - the next generation.* Nat Rev Genet, 2010. **11**(1): p. 31-46.
4. Nathan C. VerBerkmoes, V.J.D., Robert L. Hettich & Jillian F. Banfield, *Systems Biology: Functional analysis of natural microbial consortia using community proteomics.* Nature Review Microbiology, 2009. **7**: p. 196-205.
5. Xavier, J.B., W. Kim, and K.R. Foster, *A molecular mechanism that stabilizes cooperative secretions in Pseudomonas aeruginosa.* Mol Microbiol, 2011. **79**(1): p. 166-79.

6. de Vargas Roditi, L., K.E. Boyle, and J.B. Xavier, *Multilevel selection analysis of a microbial social trait.* Mol Syst Biol, 2013. **9**: p. 684.
7. Lee, H.H., et al., *Bacterial charity work leads to population-wide resistance.* Nature, 2010. **467**(7311): p. 82-5.
8. Ackermann, M., et al., *Self-destructive cooperation mediated by phenotypic noise.* Nature, 2008. **454**(7207): p. 987-90.
9. Cho, I. and M.J. Blaser, *The human microbiome: at the interface of health and disease.* Nat Rev Genet, 2012. **13**(4): p. 260-70.
10. Careau, V. and T. Garland, *Performance, Personality, and Energetics: Correlation, Causation, and Mechanism.* Physiological and Biochemical Zoology, 2012. **85**(6): p. 543-571.
11. Biro, P.A. and J.A. Stamps, *Do consistent individual differences in metabolic rate promote consistent individual differences in behavior?* Trends Ecol Evol, 2010. **25**(11): p. 653-9.